Technical Report Documentation Page

1. Report No.	2. Government Accession No.	3. Recipient's Catalog No.
FHWA/TX-05/0-4418-1		

4. Title and Subtitle	5. Report Date
Bridge Slab Behavior at Expansion Joints	October 2004, Rev. March 2006
	6. Performing Organization Code

7. Author(s)	8. Performing Organization Report No.
Christin J. Coselli, Elizabeth M. Griffith, Jeremy L. Ryan, Oguzhan Bayrak, James O. Jirsa, John E. Breen, and Richard E. Klingner	Research Report 0-4418-1

9. Performing Organization Name and Address	10. Work Unit No. (TRAIS)
Center for Transportation Research The University of Texas at Austin 3208 Red River, Suite 200 Austin, TX 78705-2650	11. Contract or Grant No. Technical Study 0-4418

12. Sponsoring Agency Name and Address	13. Type of Report and Period Covered
Texas Department of Transportation Research and Technology Implementation Office P.O. Box 5080 Austin, TX 78763-5080	Technical Report (9/01-8/04)
	14. Sponsoring Agency Code

15. Supplementary Notes

Project conducted in cooperation with the U.S. Department of Transportation, Federal Highway Administration, and the Texas Department of Transportation.

16. Abstract

The primary objective of this research study was to evaluate the behavior and capacity of the IBTS and alternate 8 in. UTSE (Uniform Thickness Slab End) details at expansion joints, especially on skewed ends of bridge slabs. The two full-scale CIP (cast-in-place) specimens, 0^o and 45^o skews, were constructed to test the effect of skew on the IBTS and UTSE details. Test results showed that at design load levels, skew had no significant effect on the behavior of the two details. All test areas failed in shear, predominantly punching shear. The UTSE details failed at slightly lower load levels than the IBTS detail due to a 2 in. difference in section depth. However, both details had ultimate capacities at loads well above the design load levels.

Another objective of the research study was to develop alternate details and investigate construction issues of those alternate details. Since the UTSE details performed satisfactorily at design and ultimate load levels, an alternate detail using the stay-in-place PC (precast) panels in the end regions was developed and tested. The PCPE (Precast Panel End) details would eliminate special formwork construction and reduce safety concerns associated with such formwork construction at heights. The full-scale PCPE specimen, 0^o skew, was built since panels cannot be easily incorporated in bridge decks with a skewed end. In addition to the behavior and capacity of PCPE details, the effects of armor joints (AJ) and sealed expansion joints (SEJ) on slab ends at design and ultimate loads were investigated. Test results showed that the PCPE details performed similar to the IBTS and UTSE details at design and failure load levels. The PC panel details failed at loads lower than the IBTS details, and the AJ and SEJ increased ultimate capacity by 20 to 25% when compared to PCPE without AJ or SEJ.

17. Key Words	18. Distribution Statement
concrete, bridge, deck, slab, diaphragm, end, punching shear, overhang	No restrictions. This document is available to the public through the National Technical Information Service, Springfield, Virginia 22161.

19. Security Classif. (of report)	20. Security Classif. (of this page)	21. No. of pages	22. Price
Unclassified	Unclassified	101	

Form DOT F 1700.7 (8-72) Reproduction of completed page authorized

BRIDGE SLAB BEHAVIOR AT EXPANSION JOINTS

by

Christin J. Coselli, Elizabeth M. Griffith, Jeremy L. Ryan,
Oguzhan Bayrak, James O. Jirsa, John E. Breen, and Richard E. Klingner

Research Report 0-4418-1

Research Project 0-4418

BRIDGE SLAB BEHAVIOR AT EXPANSION JOINTS

conducted for the

Texas Department of Transportation

in cooperation with the

U.S. Department of Transportation
Federal Highway Administration

by the

CENTER FOR TRANSPORTATION RESEARCH
BUREAU OF ENGINEERING RESEARCH
THE UNIVERSITY OF TEXAS AT AUSTIN

September 2004, Rev. March 2006

Research performed in cooperation with the Texas Department of Transportation and the U.S. Department of Transportation, Federal Highway Administration.

ACKNOWLEDGMENTS

We greatly appreciate the financial support from the Texas Department of Transportation that made this project possible. The support of the project director, Dean Van Landuyt (BRG), program coordinator, David Hohmann (BRG), and monitoring committee member, David McDonnold, is also very much appreciated.

DISCLAIMER

PRODUCTS

Products 0-4418-P1 and 0-4418-P2 are included in this report. They are both found in Section 2.3.1 of this report, pages 10-14.

O. Bayrak

J. O. Jirsa, P.E., Texas #31360

J. E. Breen, P.E., Texas #18479

R. E. Klingner, P.E., Texas #42483

Research Supervisors

TABLE OF CONTENTS

LIST OF FIGURES

LIST OF TABLES

SUMMARY

The primary objective of this research study was to evaluate the behavior and capacity of the IBTS (I-Beam Thickened Slab) and alternate 8 in. UTSE (Uniform Thickness Slab End) details at expansion joints, especially on skewed ends of bridge slabs. The two full-scale CIP (cast-in-place) specimens, 0^o and 45^o skews, were constructed to test the effect of skew on the IBTS and UTSE details. Test results showed that at design load levels, skew had no significant effect on the behavior of the two details. All test areas failed in shear, predominantly punching shear. The UTSE detail failed at slightly lower load levels than the IBTS detail due to a 2 in. difference in section depth. However, both details had ultimate capacities at loads well above the design load levels.

Another objective of the research study was to develop alternate details and investigate construction issues of those alternate details. Since the UTSE detail performed satisfactorily at design and ultimate load levels, an alternate detail using the stay-in-place PC (precast) panels in the end regions was developed and tested. This slab end detail is named as PCPE (Precast Panel End) detail. The use of PC panels in the end regions would eliminate special formwork construction and reduce safety concerns associated with such formwork construction at heights. The full-scale PCPE specimen was built with a 0° skew since panels cannot be easily incorporated in bridge decks with a skewed end. In addition to the behavior and capacity of an end detail with PC panels, the effects of armor (AJ) and sealed expansion joints (SEJ) on slab ends at design and ultimate loads were investigated. Test results showed that slab details with the PCPE details performed similar to the IBTS and UTSE details at design and failure load levels. The PCPE details failed at loads somewhat lower than the IBTS details, and the AJ and SEJ increased ultimate capacity by 20 to 25% when compared to PCPE details without AJ or SEJ.

CHAPTER 1:
INTRODUCTION

1.1 BACKGROUND

The Texas Department of Transportation (TxDOT) currently uses, for most of its bridges, the "IBTS" standard detail for bridge slab ends at expansion joints. That detail, shown in Figures 1.1 and 1.2, has enabled TxDOT to eliminate the use of diaphragms at slab ends by increasing the transverse stiffness at slab ends. Slab ends are stiffened by a 2-in. increase in slab thickness and reduced reinforcement spacing for skewed slabs. The origin of this detail is unknown, but has been used successfully by TxDOT for years. Currently, TxDOT uses a combination of prestressed concrete deck panels as stay-in-place formwork and cast in place concrete topping for the interior portion of bridge decks.

All bridges in Texas are designed according to AASHTO provisions. Currently, the AASHTO Design Tendom (DT) load is typically used in design of bridges. However concerns from trucks operating beyond their legal weight limits and increased truck traffic as a result of the North American Free Trade Agreement (NAFTA) have led many TxDOT districts to increase their design loads by a factor of 1.25. This increased load has been labeled as the "1.25DT" design load.

Prior to this research project, the capacity and behavior of the IBTS slab end detail under applied AASHTO design loads have not been verified by tests. Previous related research had focused on the behavior at interior locations of bridge decks with diaphragms. Tests have indicated that bridge decks fail in punching shear at interior locations at loads that far exceed the design load capacity. This is due to effects of two-way actions and arching action that increase flexural capacity. At deck ends, capacity is not expected to increase as much because the slab is less restrained. The effect of different end details, and in particular the IBTS detail, has not been studied.

The research described here is intended to fill that gap. The research is intended to show how loads are carried at free ends of slab; how skew affects behavior at free ends; how serviceability and capacity are affected by the use of the IBTS detail and the elimination of diaphragms; and how this behavior can be modeled for design purposes. In addition to understanding the behavior of the slab end with the IBTS detail, alternate end details, including a cast-in-place detail with a uniform thickness of 8 in. (UTSE) and a detail including the stay-in-place precast, prestressed concrete panels (PCP), were also developed and investigated.

Most prior bridge deck tests have been performed on scaled specimens, and only rarely on full-scale ones. According to Bazant and Cao (1987), results from scaled specimens may be unconservative. This is because the stress at punching shear failure increases with decreasing specimen size for models of identical proportions with proportional critical perimeters. This so-called "size effect" could result in higher punching-shear capacities for smaller-scale models and is one reason full-scale tests were used in this project. Prior research in cast in place bridge decks and decks with prestressed concrete deck panels focused primarily on the composite action between the panels and the cast in place concrete topping, but not the behavior of the section at slab ends (Buth, et al. 1972). The research described here is intended to evaluate the behavior and capacity of end details at slab ends.

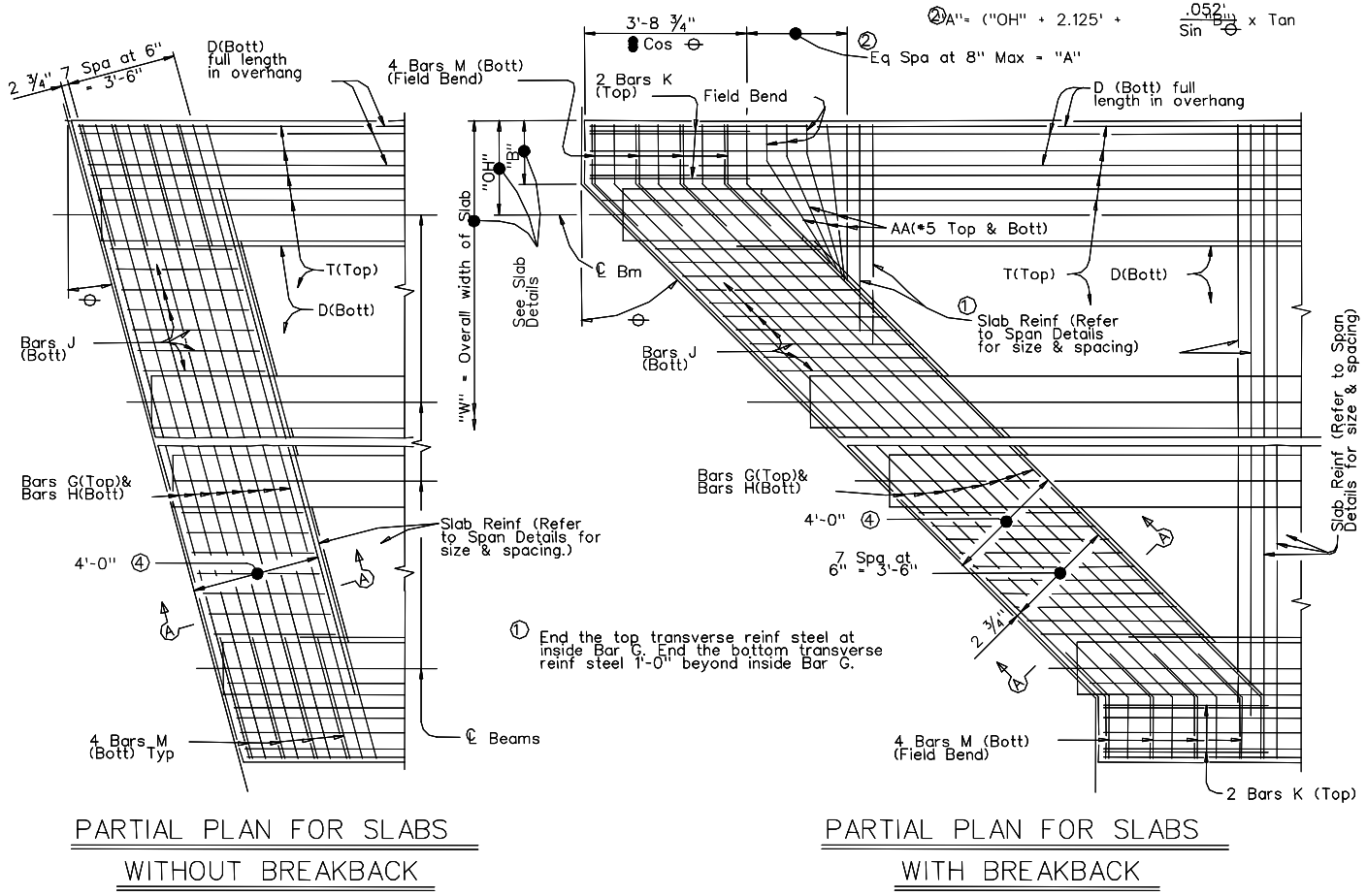

Figure 1.1 IBTS detail: Plan view

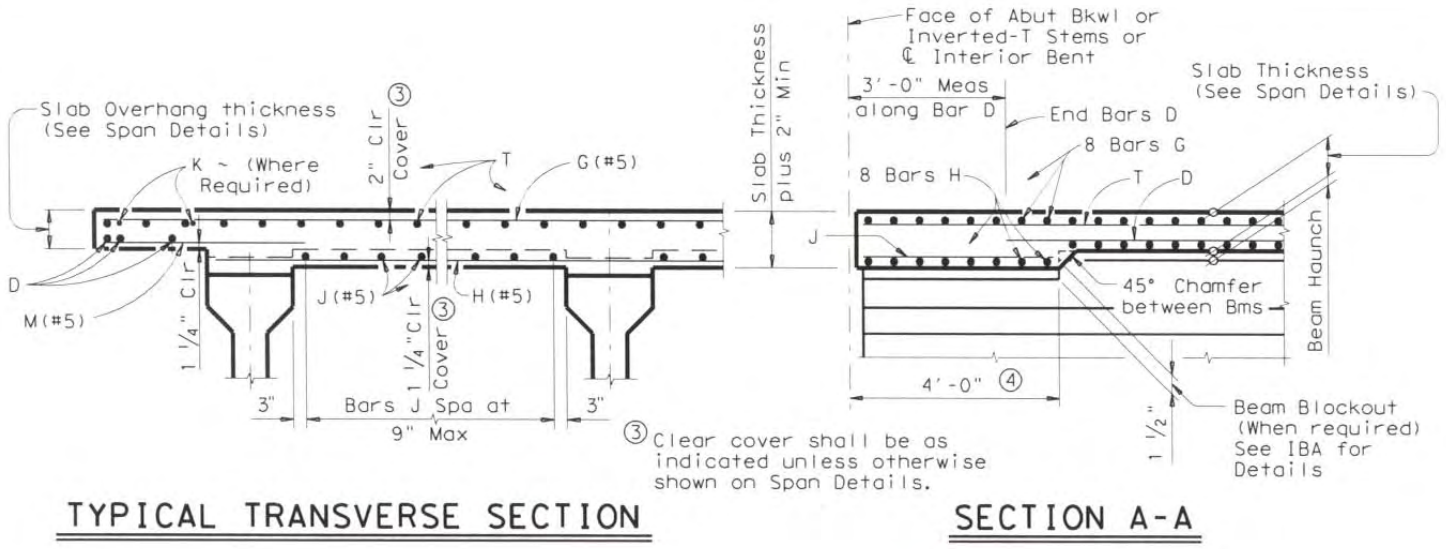

Figure 1.2 IBTS detail: Elevation view

1.2 PREVIOUS BRIDGE DECK RESEARCH

As discussed in the previous section, previous bridge deck research focused on the slab behavior when the loads were applied at interior locations. Research studies that contribute to understanding the behavior of a cast-in-place (CIP) bridge decks and bridge decks with stay-in-place PC panels (PCP) are summarized in the following sections.

1.2.1 Buth, Furr and Jones (1972)

To experimentally and theoretically investigate the ability of the composite bridge deck of PCP and CIP concrete topping to distribute wheel loads and behave as a composite unit, Buth, Furr and Jones (1972) conducted a series of fatigue static tests on a full-scale specimen and a segment of a full-scale bridge deck. Various locations on the full-scale bridge slab were tested; the emphasis was on the deck performance at the butt joint between two adjacent panels. In addition to investigating the performance of PCP, various techniques for transferring forces across the PCP/CIP slab interface were investigated. The three techniques for improving bond were: Z-bars used for shear and tensile bonding (Figure 1.3), portland cement grout used as a bonding agent, and no treatment of the panel or interface (as-delivered) for the remaining sections of the slab. Dowel bars were placed on the surface of the panels over select transverse butt joints to investigate load transfer over those joints. During testing, transverse cracks were observed in the CIP concrete topping, which was attributed to shrinkage effects. These cracks did not have any detrimental effect on the performance of the bridge deck. The details used for ensuring shear, bond and load transfer did not provide any measurable improvement in performance. After the series of fatigue and static failure load tests, which all failed in punching shear at loads higher than those predicted by the ACI punching shear theory, Buth, Furr and Jones (1972) concluded the bond at the interface between the PCP and CIP concrete topping showed no distress under the fatigue and static loading.

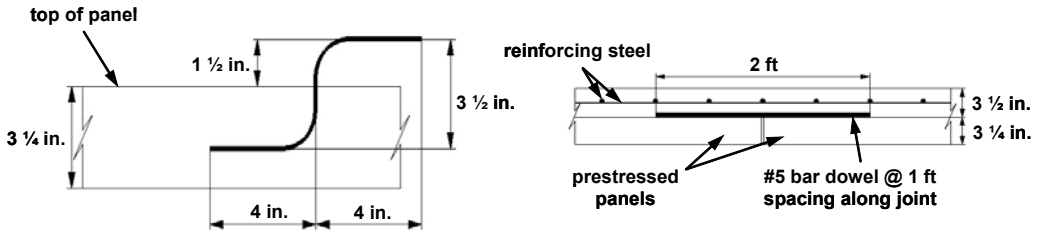

(a) Z bars (b) dowel bars

Figure 1.3 Techniques for transfer of forces across PCP and CIP interface (Buth, Furr and Jones 1972)

1.2.2 Bieschke and Klingner (1982)

After PCP had been in use for some time, construction techniques were developed to provide better quality control of PCP. This included producing more consistent shapes of PCP by having a continuous casting bed. In order to incorporate the continuous casting bed, the strand extensions needed to be eliminated from the PCP's transverse end. Bieschke and Klingner (1982) investigated bridge performance using PCP with and without strand extension under static and fatigue loading. It was concluded that overall bridge deck behavior and local behavior were not different when PCP with and without strand extension were used. Yield line and punching-shear theories provided conservative estimates of actual failure loads for concentrated loadings.

1.2.3 Fang, Tsui, Burns and Klingner (1990)

As previous research on arching action in cast-in-place concrete bridge decks have been conducted on scaled specimens, Fang, et al. (1990) investigated the fatigue behavior of panel decks, differences between PCP deck and CIP concrete decks under fatigue loading and the effects of intermediate diaphragms in a full-scale specimen. A full-scale 20 ft by 50 ft. bridge decks was constructed using TxDOT standard details for Ontario-type decks. One half of the deck consisted of a CIP section and the other half was the composite section of PCP and CIP topping. The specimen was subjected to fatigue and static loading based on AASHTO truck loadings and impact factor. Fang, et al. (1990) concluded that panel decks under positive and negative moment loading performed similarly and satisfactorily compared to CIP decks at current AASHTO design loads. Fatigue loading did not significantly change the behavior of the deck under AASHTO service and overload conditions. Intermediate diaphragms had not significant effect on local stiffness, stresses and moment distribution under loading. PCP decks were concluded to be superior to CIP decks in terms of cracking and stiffness of the deck.

1.2.4 Dolan and Frank (1994)

Dolan and Frank (1994) investigated the reason for failures of armored bridge deck joint joints installed in TxDOT bridge decks. Several failed expansion joints were tested after their removal from the bridge decks. Inspection of the joints where stud failures occurred showed evidence of lack of concrete consolidation in that area. One cause for lack of complete concrete consolidation is incorrect placement of reinforcing steel (i.e. too close the joint). Failures of these types of joints were concluded to be caused by lack of concrete consolidation, which can be avoided by having higher quality control during placement of slab concrete.

1.2.5 Graddy, Kim, Whitt, Burns and Klingner (2002)

Graddy, et al. (2002) studies the punching-shear behavior of bridge decks under fatigue loading by testing full scale CIP and PCP deck specimens. CIP test specimens were 6 ft by 7ft and 7 ½ in. thick, and PCP specimens were 6 ½ ft x 8 ft and 7 ¼ in. thick. Flexural capacities were calculated using yield-line analysis, and compressive membrane forces, estimated by previous research and finite-element analysis, were used in calculations of flexural capacity. AASHTO LRFD and ACI 318-95 punching-shear provisions were used to estimate the punching-shear capacity of the specimens. Graddy, et al. (2002) found that the AASHTO and ACI punching-shear provisions were conservative and could be improved based on the shape of the experimental punching shear failure surface. The beneficial effect of arching action were insignificant in terms of shear capacity when compared to the flexural capacities predicted by yield-line theory.

1.3 SITE VISITS

To observe the IBTS detail as constructed in the field, two site visits were made prior to building the first specimen. The first bridge visited, located on IH-35 in San Marcos, TX, crossed the San Marcos River. The second bridge was an overpass on US 290, at US 183. Witnessing the construction of slab ends allowed for observations of differences between the IBTS detail and other slab ends during construction.

As mentioned previously, most TxDOT bridge construction includes PCP as stay-in-place formwork in the interior of the deck, up to the IBTS detail. Prestressed concrete girders were used in both bridges; Figure 1.4 shows the top of a girder with stirrups extending into the deck.

Sealed expansion joints were cast into the top end of the decks at the expansion joints (Figure 1.5). Although this is the standard detail in TxDOT designs, it was not included in the first and second test specimens. The armor and sealed expansion joints are assumed not to contribute to the strength of the slab at the joint in design calculations. However, the reserve capacity provided by the armor joint (AJ) and the sealed expansion joint (SEJ) was of interest to TxDOT engineers.

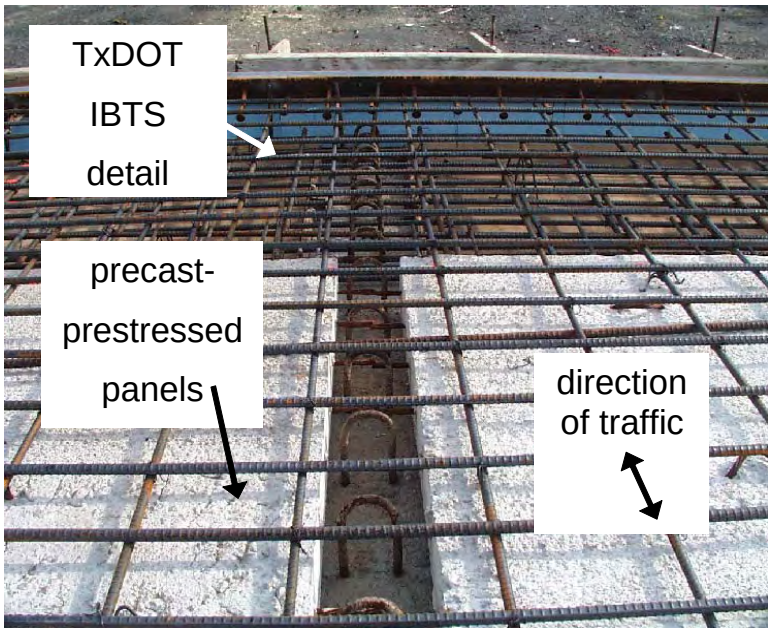

Figure 1.4 Prestressed panels and shear stirrups

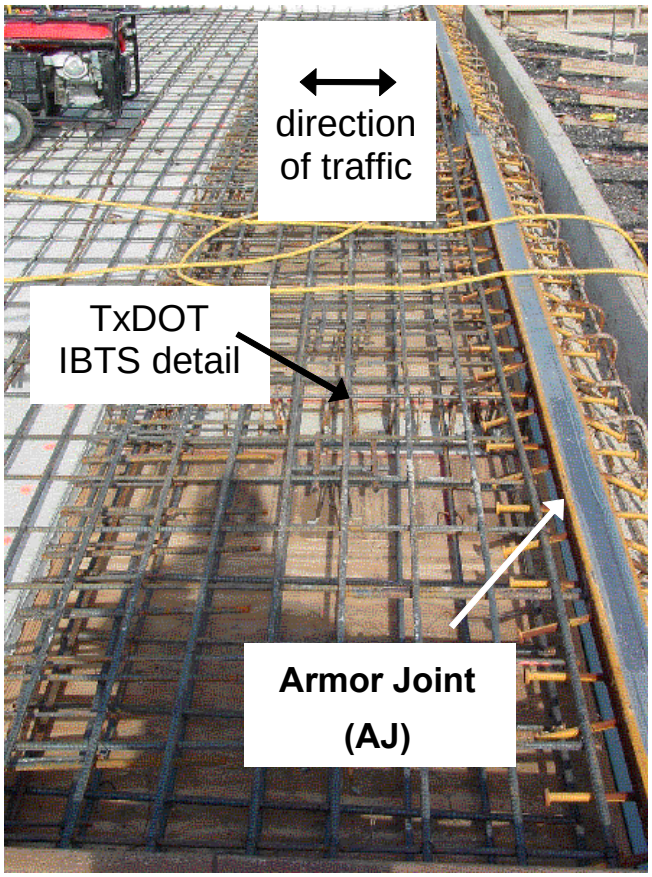

Figure 1.5 IBTS detail prior to concrete placement

In the field, deck concrete was placed using a concrete pump, and was consolidated using mechanical vibrators. The surface was leveled using a vibrating, movable screed on temporary rails, and finished with bull floats. Concrete placement was a continuous process, allowing for long lengths of decks to be placed efficiently.

1.4 OBJECTIVES AND SCOPE

The objectives of the TxDOT research study were as follows:

- To understand and explain the behavior of slab ends at expansion joints, with special emphasis on skewed ends.
- To determine the performance of the IBTS detail when loaded with design loads (DT and 1.25DT) and typical overloads.
- To determine the ultimate capacity and failure mechanism of the IBTS detail.
- To test an alternate end details (UTSE and PCP) and compare the behavior with the IBTS detail.
- To evaluate the reserve capacity provided by armor and sealed expansion joints.
- To test and determine the behavior of overhang slabs.
- To develop guidelines for TxDOT engineers to follow in designing bridge-deck end details, if current practice is shown to be inadequate.

Three test specimens have been constructed. The first specimen, built with 0^o skew, had both the IBTS and alternate Uniform Thickness Slab End (UTSE) details and was tested to compare the performance of those details. Results for the tests on the first specimen are given in Ryan (2003). The second specimen, built with 45^o skew, had both the IBTS and UTSE end details and was tested to understand the effects of skew on the slab end behavior. Results for the tests on the second specimen are given in Griffith (2003). The third specimen, built with 0^o skew, with stay-in-place prestressed concrete deck (PC) panels and cast-in-place concrete topping. Test results from the PCP specimen are given in Coselli (2003). The following the report summarizes the behavior of the end details at design and overload load levels, as well as the influence of the expansion rails on the behavior of slab ends. The punching shear provisions using the AASHTO LRFD Bridge Design provisions and ACI 318-02 are also compared with the experimental results.

CHAPTER 2:
SPECIMEN AND TEST SETUP

2.1 INTRODUCTION

The goal of the experimental program was to investigate the behavior of slabs at expansion joints, with emphasis on skewed slabs, as well as to develop design guidelines for slab end details at expansion joints. Three full-scale specimens were constructed and tested. The test specimens were designed to behave as full-scale bridge slabs while allowing investigation of the effect of different design parameters on the behavior of the slab at the expansion joints. This chapter summarizes the specimen designs and test setup, including the design parameters and specimen layouts.

2.2 TERMINOLOGY

Throughout this report, different areas of the slab specimens and PC panels (PCP) are referenced. To avoid confusion, different areas have been defined as either the end or the edge of the slab or panel, as shown in Figure 2.1.

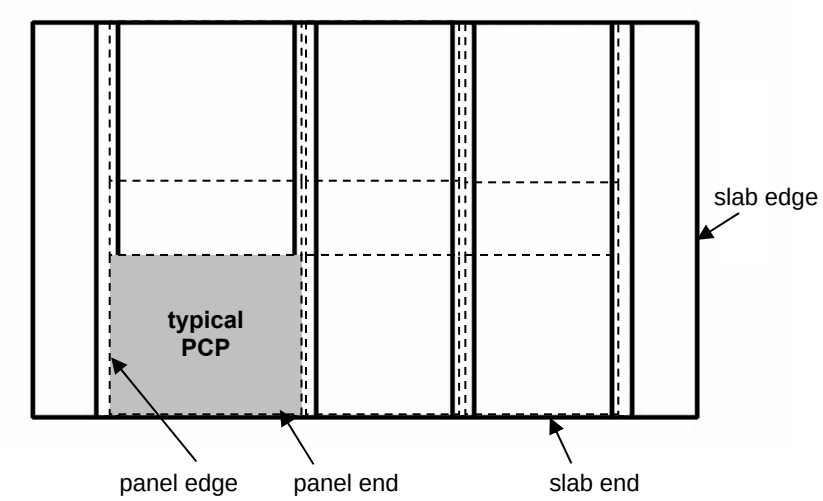

Figure 2.1 Slab and panel terminology

2.3 DESIGN PARAMETERS

The following design parameters were established and were used consistently throughout the construction and testing of the three specimens:

- End detail – IBTS, UTSE, and PCPE
- Girder spacing
- AASHTO loading configuration
- Skew angle
- Moment maximized in each test area.

2.3.1 End Details

Three details were constructed and tested to observe their behavior at design, overload and failure load levels. For the CIP 0^o and 45^o skewed specimens, two end reinforcing details were used, the standard 10 in.

thick TxDOT end detail and a proposed 8 in. thick alternate end detail. The IBTS detail has a total of 16 No. 5 reinforcing bars, 8 bars on the top and 8 bars on the bottom, placed parallel to the slab end spaced 6 in. on center. The detail, shown in Figure 2.2, is 4 ft wide, measured perpendicular to the slab end. As the skew angle increases, the longitudinal length of the end section increases. To accommodate the skewed end, PCPs are stair stepped and stopped a given distance away from the expansion joint detail, shown in Figure 2.3. The use of PCP at the end of a skewed bridge slab includes numerous modifications to the PCP and construction techniques, which indicated that the use of PCP at the end is most advantageous for a 0^o skewed bridge slab.

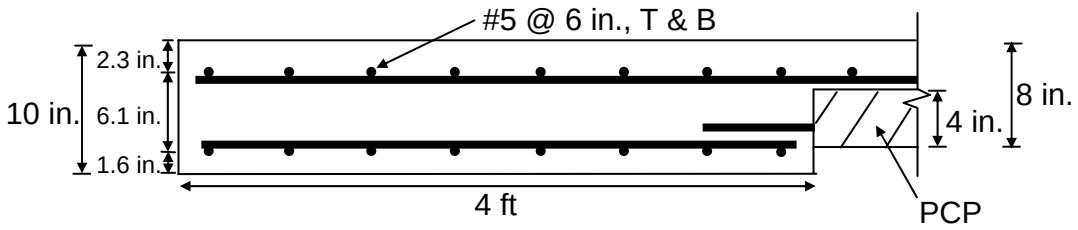

Figure 2.2 Cross-sectional view of IBTS detail

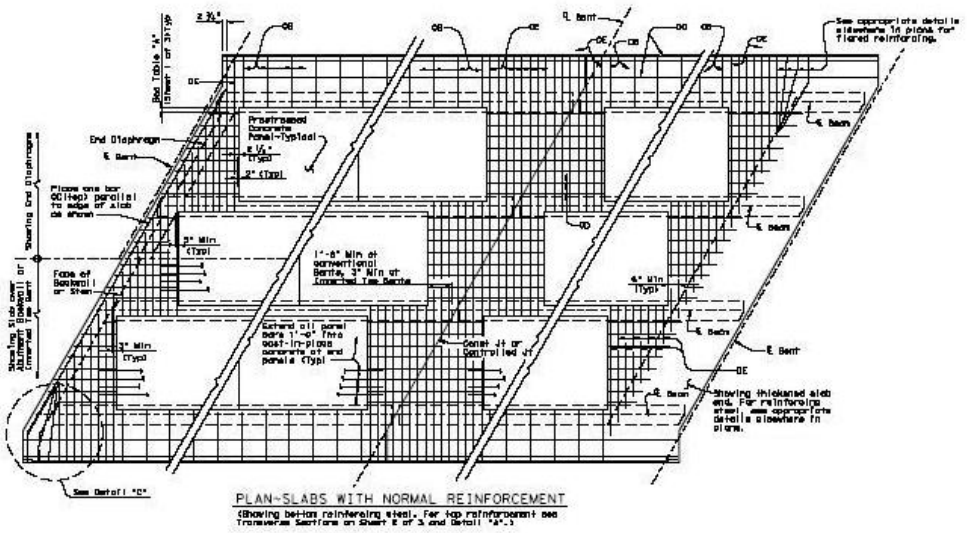

Figure 2.3 Stair-stepped PCPs in bridge slab

In the CIP 0^o and 45^o skewed specimens, an alternate detail was designed for testing the end opposite the IBTS end detail. Typically, 4-in. thick prestressed concrete (PC) panels are topped with 4 in. of CIP concrete to form the bridge decks. The PCPs eliminate the need for formwork at the interior, but at slab ends, formwork is constructed in the field for the thickened end. Therefore, an 8 in. thick end detail would be expected to improve construction efficiency and economy by creating a uniform thickness over the entire length of the bridge deck.

The alternate 8 in. thick slab end detail, the Uniform Thickness Slab End (UTSE) detail, was developed, and for consistency with standard IBTS detail, the same size of reinforcement (No. 5) was used. However to achieve the same moment capacity as the IBTS detail, the transverse reinforcement spacing was reduced to 3-7/8 in. from 6 in., increasing the number of reinforcing bars from 16 to 24 (Figure 2.4).

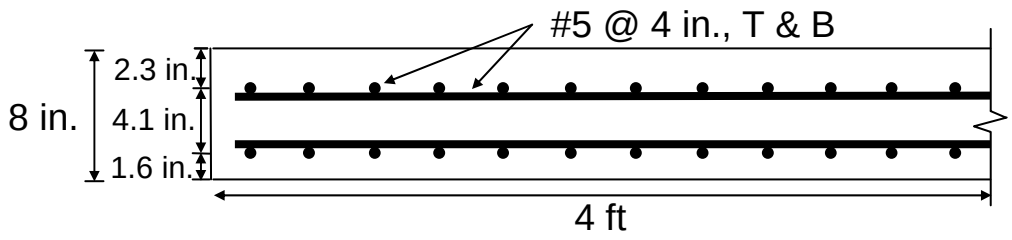

Figure 2.4 Cross-sectional view of UTSE detail

After testing the IBTS and UTSE details, the possibility of eliminating all formwork by using the PCPs in the end detail was explored. The effects of varying the top reinforcement spacing was studied. The influence of armor and sealed expansion joints on the performance of the slab end details was examined. Similar to the development of the UTSE detail, a 4 ft. wide section of the end detail containing PCP was analyzed. A panel with eight 3/8 in. diameter, 7-wire low relaxation prestressing strands, spaced 6 in. on center was needed to develop a moment capacity comparable to the IBTS and UTSE end details (Figure 2.5). In developing the pre-cast panel end (PCPE) detail, the top reinforcement spacing was assumed to be identical to the UTSE detail (approximately 3-7/8 in.) due to their same concrete depth. Since the improvement of design procedures was another primary objective of the research study, the top reinforcement spacing of 6 in. was also tested by continuing this spacing from the interior of the bridge deck to the slab ends for simplicity of construction.

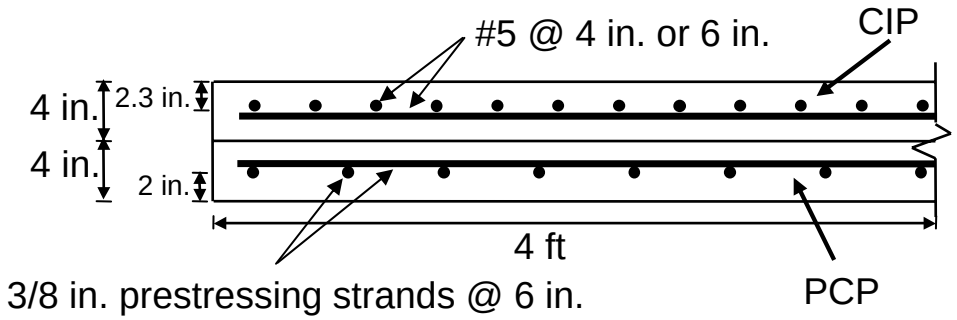

Figure 2.5 Cross-sectional view of PCPE detail

For each detail, sectional analyses were conducted for a 4 ft. wide section and the obtained moment-curvature response of the three details is shown in Figure 2.6. The reinforcing bars in the UTSE detail yielded at about 11% higher moment than the IBTS detail in positive bending. The flexural capacity of the UTSE detail is 5% higher than IBTS detail in positive bending, due to the increased reinforcement ratio. Due to its reduced depth, the UTSE detail has a lower stiffness before and after cracking. In reality, the continuity of the rest of the slab will cause cracking to initiate at the slab end and penetrate into the slab. The flexural capacity of the PCPE detail is 35% and 26% lower than the UTSE and IBTS details in positive bending, respectively. Due to the use of the prestressed concrete panels, the PCPE detail has a higher stiffness before and after cracking. The sectional analysis was intended only to provide a comparison between the three end details. The actual cracking moments and stiffnesses for both sections were higher than the analytical values, because the actual slab is restrained along the interior boundary of the end slab section.

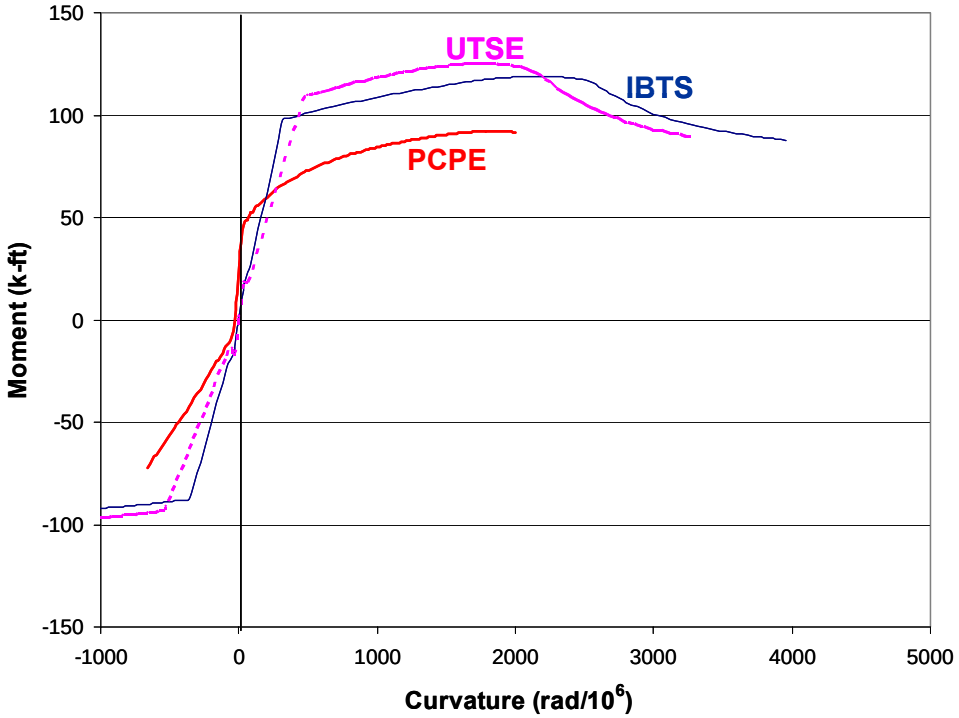

Figure 2.6 Moment-curvature response of slab end details

2.3.1.1 Armor and Sealed Expansion Joints

Armor and sealed expansion joints are commonly used in construction of bridge decks at expansion joints. Current TxDOT design procedures do not account for any increase in capacity by using these expansion joints. In order to determine the influence of these expansion joints on the behavior of the bridge slab, the armor and sealed expansion joints were installed in the PCP specimen.

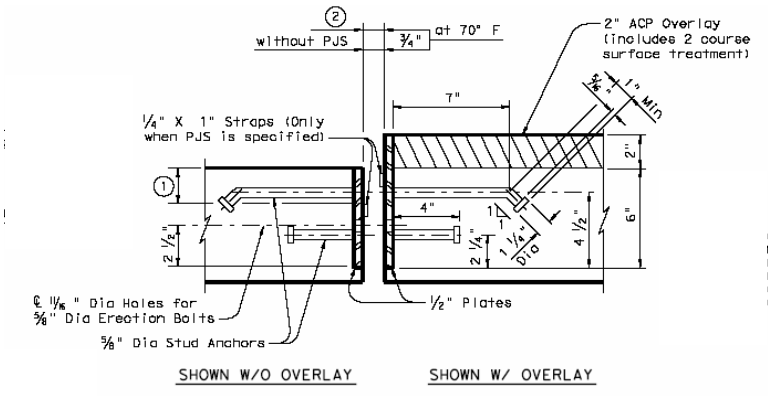

(a) Armor joint (AJ)

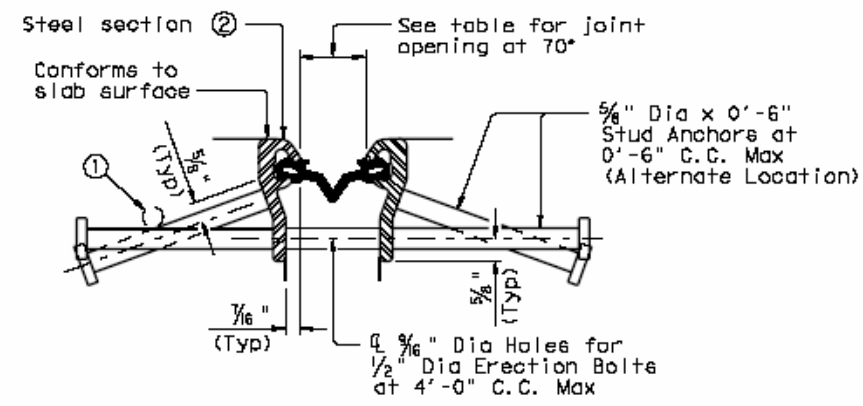

(b) Sealed expansion joint (SEJ)

Figure 2.7 TxDOT armor and sealed expansion joint details

An issue arose in the use of armor and sealed expansion joints concerning the constructability of the two joints when the end details include the 4 in. PCPs. In current TxDOT practice, the armor and sealed expansion joints are installed on the bridge deck in the CIP IBTS detail. However, the panel would interfere with the location of the bottom stud anchor in the AJ. In order to accommodate the panel depth, the bottom anchors were raised a ¼ in. and the plate was installed in the deck by notching the form, so the ½ in. armor plate can be placed (Figure 2.8) relative to PCP and CIP concrete topping. For the sealed expansion joint, the angled anchor bolts (shown in Figure 2.7b) were heated and then bent so the anchors fit above the top surface of the PCPs (Figure 2.9).

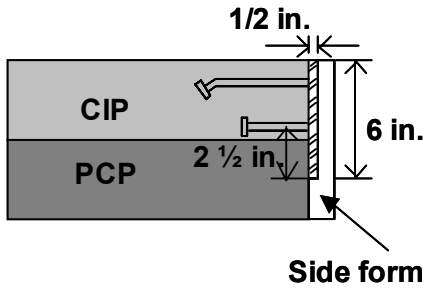

Figure 2.8 Construction modification for AJ

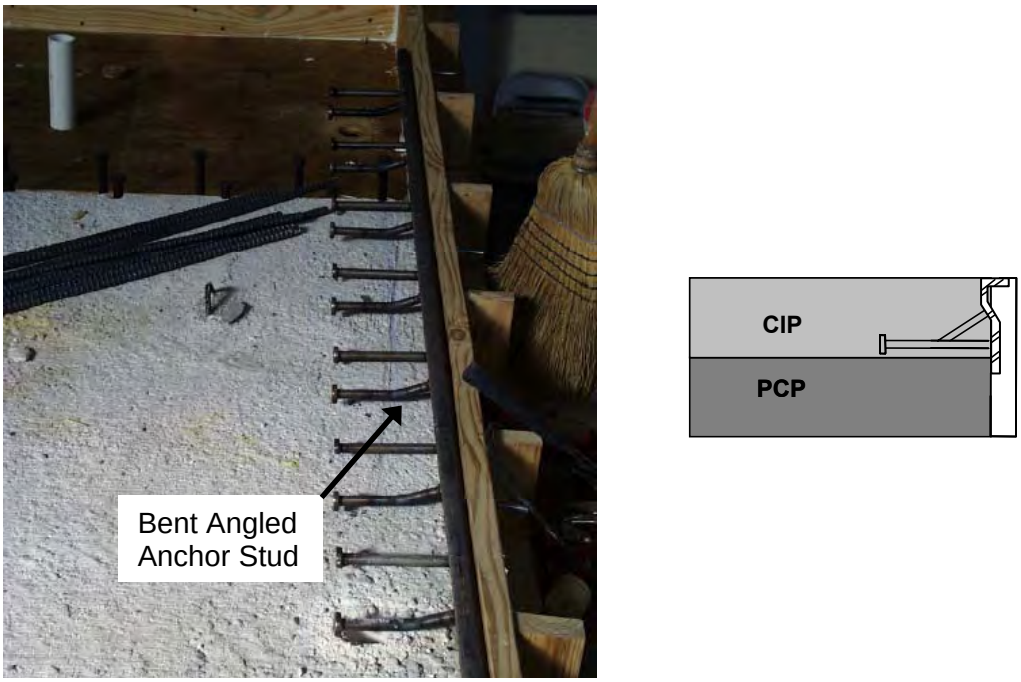

Figure 2.9 Bent angled anchors on SEJ

2.3.1.2 Slab Reinforcement

All slab reinforcement and panel sizes for the three specimens were detailed using the TxDOT PCP, IBTS detail, and interior span standards. The TxDOT PCP standards were used to size panels and position strands in the panels. TxDOT standards were used as a guide for reinforcing the remainder of the slab.

2.3.2 Girder Spacing

Although TxDOT bridge standards include bridges with up to six girders, the three specimens had only four girders, since six girders would result in a bridge width that could not be tested in the laboratory. Linear-elastic parametric studies done by Ryan (2003) indicated that a four-girder bridge would adequately represent five- or six-girder bridge behavior at slab ends. A detailed discussion of this analysis is given in Ryan (2003).

The girder spacing of the west-exterior bay was 10 ft (Figure 2.1). The girder spacing of the east-exterior bay and the interior bay was 8 ft. The 8 ft. girder spacing was chosen since 8 ft. girder spacing is commonly used in TxDOT highway bridges. The 10 ft. girder spacing was used to represent the largest girder spacing typically used by TxDOT in highway bridges.

In order to simplify specimen fabrication, reduce cost and increase productivity, without compromising from the accuracy of the test results, structural steel beams were used to support the bridge deck specimens. The flexural stiffness of the beams was considered to be inconsequential as the bridge deck specimens were loaded at or very close to the slab ends. Similarly, the torsional stiffness of the beams was considered to be of secondary importance, considering the relative stiffness of the slab end details. More specifically, analyses conducted to estimate the girder rotation under the service and overload levels indicated that very small (< 0.03 deg.) girder rotations were to be expected. Test results confirmed this expectation. Girders were instrumented to measure their twist under the applied loads and the twist angles measured during the tests were always in the “noise” range of the linear potentiometers used to estimate the twist.

2.3.3 AASHTO Loading Configuration

One of the main objectives of this research study was to determine the behavior of the three details when subjected to AASHTO LRFD design loading. Two primary types of vehicles were considered for design loading, similar to the TxDOT Bridge Design Manual (Figure 2.10). In order to determine the critical loading configuration, preliminary tests under service load levels were conducted. The rebar strains were measured within the 4-ft-long slab end region under AASHTO LRFD Design Truck (32 kips / axle placed at the slab end) and AASHTO LRFD Design Tandem (25 kip / axle, 2 axles placed at the slab end) loads. Strain measurements indicated that AASHTO LRFD Design Tandem Loading configuration (50 kips acting over the 4-ft wide strip) was more critical than the AASHTO LRFD Deign Truck (32 kips acting over the 4-ft wide strip). Hence, the AASHTO LRFD Design Tandem (DT) was used as a basis for all the load tests conducted in this study.

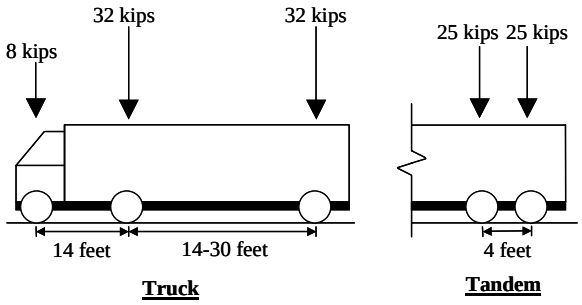

Figure 2.10 AASHTO LRFD design vehicles

2.3.4 Skew angle

The first specimen was chosen to be 0° skew in order to study the effect of the design parameters other than skew on the behavior at the expansion joints. A 45° skew was chosen for the second specimen due to the fact that a 45° skew is close to the largest skew used in practice by TxDOT (Figure 2.11). Only 3 load plates were used in this skewed specimen to simulate the AASHTO design tandem loading configuration, where the fourth tire would be assumed to be off the slab deck.

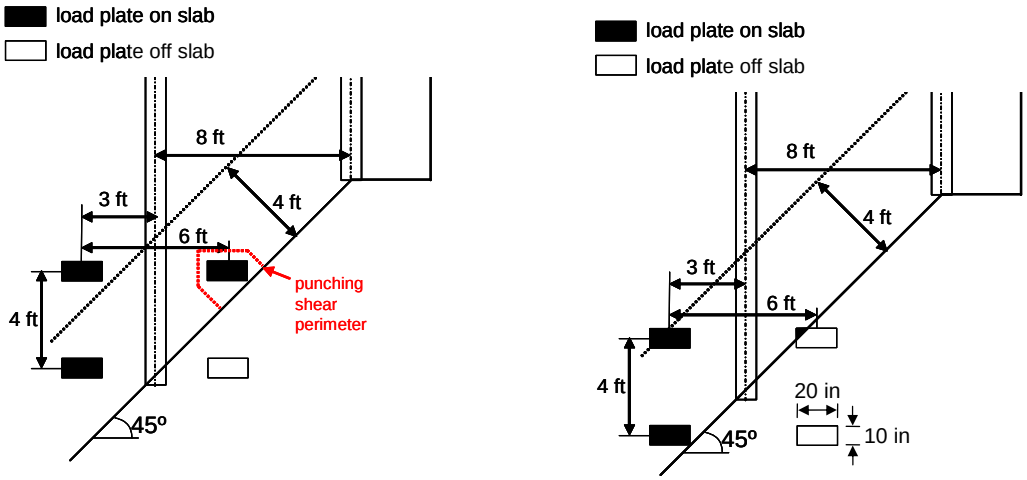

(a) 45° skew, 3 load plates (b) 45° skew, 4 load plates

Figure 2.11 Placement of tandem loading plates

2.3.5 Moment Maximized in Each Test Area

In order to evaluate the behavior of the slab at expansion joints, two types of load placements were used in testing the three end details. Those two types of test areas were: maximizing negative moment over the girder and maximizing positive moment at midspan of one of the bays. The negative-moment test areas were done in the 8 ft bays and the positive-moment test areas were performed in the 10 ft bays.

2.4 CONSTRUCTION

For all three test specimens, the slab and steel girder assembly was elevated on eight columns, 4 ft tall and 2 ft in diameter. Elevating the slab was necessary to install the loading frame and instrumentation, and to provide access to view cracking. The columns were positioned on the laboratory floor, and the steel girders were placed on top of them. The girders were placed on 2 in. thick neoprene pads and a load cell that was sandwiched between two steel plates. Load cells were installed under the girders on the side of the slab being tested, and steel plates were used to maintain a constant beam elevation of the opposite side. Formwork for the concrete slab was then constructed. For the PCPE specimen, 1-in. wide by 1-in. thick 60 psi foam bedding strips were attached to the top flange along the length of the girders for placing the PCPs. The bedding strips were placed to provide space for at least 1- ½ in. of mortar to flow under the PCPs as the topping slab is placed. After the bedding strips were attached, the PCPs were placed using the laboratory crane.

After formwork was completed, the reinforcement was installed. For the PCP specimen, the armor (AJ) and sealed expansion joint (SEJ) rails were installed before the reinforcement was placed. The rails were temporarily supported by 5/8 in. anchor bolts through the joint and side forms. Block-outs of PVC pipe were placed in either the formwork or panels where loading rods would pass through the slab.

Concrete was transported and placed with a bottom-drop bucket hoisted by a crane. The concrete was consolidated using electric vibrators. An aluminum screed was used to level the top surface of the bridge slab. Bull floats and hand trowels were used to create a smooth, flat surface. The entire surface of the three specimens was then covered in burlap and plastic sheeting to reduce evaporation and then cured for seven days. After seven days, the side forms were stripped and block-outs removed.

2.5 TEST SETUP

2.5.1 Load Application

All three specimens were built and tested on the strong floor of the Ferguson Structural Engineering Laboratory. Since the test specimen was full scale and large simulated truck loads had to be applied at a number of different locations, a compact, reconfigurable load frame was designed and built to fit underneath the bridge slab and be moved using a small forklift (Figure 2.12). This arrangement was much simpler and less costly than a reaction fame constructed over the deck.

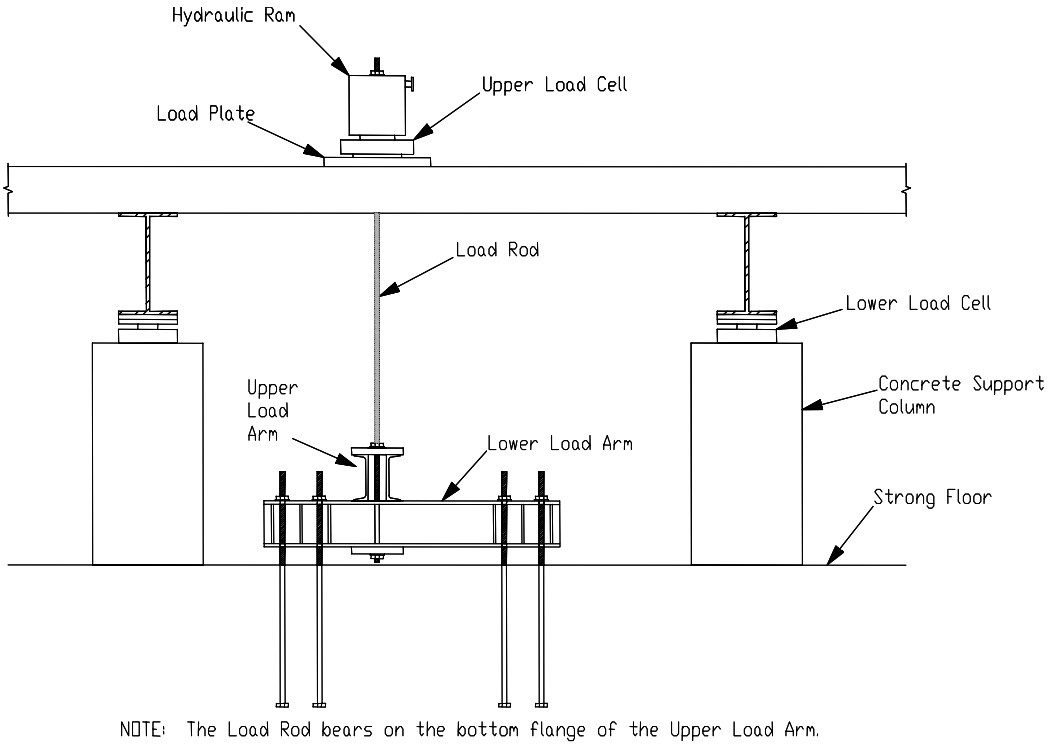

Figure 2.12 Drawing of loading frame

2.5.1.1 Contact Area

Section 3.6.1.2.5 of the AASHTO LRFD Bridge Design Specification, 1999 Supplement specifies that design be carried out using an assumed tire contact of 20-in. wide (transverse direction) and 10-in. long (longitudinal direction). Steel plates measuring 20-in. long, 10-in. wide and 2 ½ in. thick were used to simulate tire contact areas. In two of the tests conducted by Ryan (2003) the plate size was increased based on the 1998 edition of the AASHTO LRFD Bridge Design Specifications. In section 3.6.1.2.5 of this code, a constant tire contact area of 10-in x 20-in. is given as well as a formula to determine the tire contact area based on the load factor, dynamic load allowance and load magnitude. The use of this formula results in a length of 15-in. for the tandem vehicle. Therefore, to investigate the beneficial effects of an increased tire contact area, 15-in. by 20-in. by 2½-in. steel load plates were used for the positive bending tests conducted on UTSE and IBTS end details. Grout was placed under the steel plates for uniform distribution of loads to the slab. Since the additional benefit of using a larger load plates proved to be considerably less than the estimations based on the pure punching shear strength (punching shear formula included in the AASHTO LRFD Specifications) for all other tests, 10-in.x20-in. loading plates were used.

2.5.2 Instrumentation

To document the behavior of the test specimens during loading, strains gauges, linear potentiometers, and load cell readings were monitored and recorded during testing. Strain gauges could not be installed on the PCPs during their prefabrication for the PCP specimen. Instrumentation for the PCP was adjusted from the CIP 0^o and 45^o skewed specimens to include a deflection transducer for measuring elongation of the bottom surface of the PCPs.

2.5.2.1 Strain Measurements

Strain gauges were used to measure strains in individual reinforcing bars as a function of the applied load. In the CIP specimens, strain gauges were placed on the top and bottom mats of reinforcement. For the 0^o skewed specimen, strain gauges were placed on every reinforcing bar in the end detail. Strain gauges were placed on the top mat reinforcement (Figure 2.13) in the negative moment regions, and where positive moment would be maximized the gauges were placed on the bottom mat reinforcement. For the For the 45^o skewed specimen, strain gauges were placed on every second reinforcing bar starting at the reinforcing bar closest to the slab end in the end region. Strain gauges were placed on either face of the girder in the negative-moment regions, and at midspan of each bay for the positive-moment regions. For the PCP specimen, strain gauges were only placed on the top reinforcing mat, since strain gauges were not placed on the prestressing strands before their prefabrication. Strain gauges were placed over the edge of the panel on either face of the girder. A second strain gauge was attached at the face of the girder on the first flexural reinforcing bar nearest the slab end to compare the stresses with the CIP specimen tests. Strain gage locations over the girders are shown in Figure 2.13. Strain gauges were placed on every second reinforcing bar in the end region. Strain gauges were also attached at locations along the AJ and SEJ rails. In order to estimate the strain at the bottom face of the panel, a deflection transducer was used.

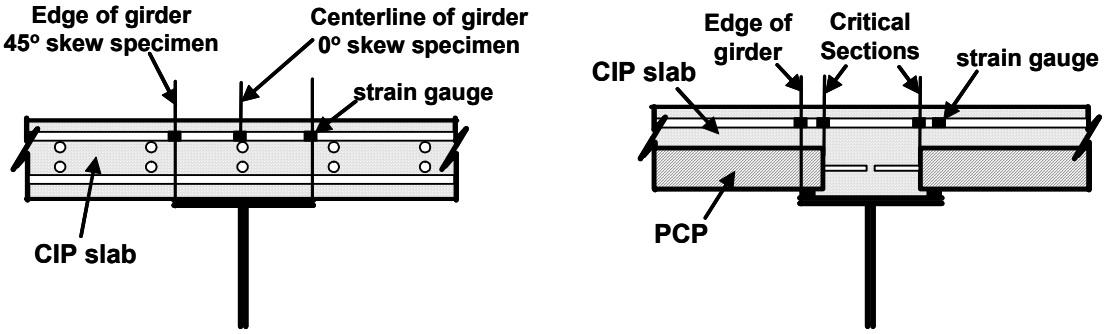

(a) CIP specimens (0^o and 45^o skew) (b) PCP specimen (0^o skew)

Figure 2.13 Strain gauge locations over girders

2.5.2.2 Load Measurements

Load cells, located underneath the girders (lower load cells) and at the hydraulic rams (upper load cells) were used to provide a means to check the load distribution in the slab. The lower load cells were only used under the girders at the end of the bridge slab being tested. The load cells on the loading plates were the primary transducers for measuring the applied load. In addition, a pressure transducer was attached to the hydraulic line at the hydraulic pump to verify load cell readings.

2.5.2.3 Deflection Measurements

Deflection measurements were made under the girders and midspan, using linear and string potentiometers. Under girders and at midspan, deflections were measurements were taken at the end of the slab, and 4 ft from the end in the longitudinal direction of the slab. String potentiometers were used in congested locations. In addition to these deflection locations, linear potentiometers were placed at the corners of the panels in the PCP specimen to measure deflections due to compression of the bearing pads on the girders.

2.5.3 Data Acquisition

Voltage reading (analog signal) from the various sensors was scanned and converted to digital format readable by the data acquisition software installed on a personal computer. Real-time test data could also be plotted to allow for the monitoring of the behavior during loading.

2.5.4 Material Properties

To better interpret the acquired test data, tests were performed to measure material properties of the reinforcing steel and concrete in the three specimens. Results of material tests were also used to check the strengths reported by the manufacturers.

2.5.4.1 Reinforcing Steel

The reinforcing steel used in the three specimens was Grade 60 ksi reinforcement. Two lengths of the reinforcing bar for each heat used in each of the three specimens were tested in tension. An extensometer and strain gauge were used to determine strains, and load cells in the test machine were used to measure applied loads. The average yield stress for the three specimens ranged from 63 to 65 ksi. The average yield strain for the reinforcement in all three specimens was approximately 2200 με.

2.5.4.2 Concrete

The TxDOT Bridge Design Manual currently requires a minimum 28-day compressive strength of 4000 psi for concrete used in bridge slabs. A mix design was ordered with a target compressive strength between 3500 psi and 5000 psi.

Table 2.1 Concrete mixture design for bridge slab (one yard batch)

Mix #	Description	f_c' (psi)	Cement	Fly Ash	Course agg.	Fine agg.	Water	Admixture
225	UT4000A ¾ in.	3500 to 5000	470	0	1625	1655	250	20.0

* All quantities are in units of pounds (lbs).

Compressive and Splitting Tensile Strength

The 28-day compressive strengths of the CIP 0^o and 45^o skewed specimens were approximately 6000 psi and 4000 psi, respectively. The 28-day compressive strength of the concrete topping slab on the PCP specimen was approximately 4100 psi.

Split cylinder tests were performed on each of the concrete batches for the three specimens. The splitting tensile strength, f_{ct}, was determined using Equation 2.1, with P equal to the failure load.

$$f_{ct} = \frac{2P}{\pi l d} \qquad \textit{Equation 2.1}$$

The average splitting tensile strengths of the CIP 0^o and 45^o skewed specimens were approximately $7.3\sqrt{f_c'}$ and $6.7\sqrt{f_c'}$. For the PCP specimen, the approximate splitting tensile strength was $5.5\sqrt{f_c'}$, which is slightly lower than $6\sqrt{f_c'}$ often used in design.

Prestressed Precast Concrete (PC) Panels

The PCPs were manufactured in accordance with the TxDOT standards that specify a minimum 28-day design concrete compressive strength of 5000 psi and a minimum release strength of 4000 psi. PCPs were reinforced with 3/8 in. diameter, 7-wire low-relaxation prestressing strands stressed to 16.1 kips per strand.

2.5.5 Test Specimens and Test Locations

The CIP test specimens were constructed with four expansion joint test areas, shown in Figure 2.14 (a) and (b). Each of the CIP test specimens had a negative-moment and positive-moment test area for the IBTS and UTSE details. The PCP specimen was constructed with six expansion joint test areas, shown in Figure 2.14 (c). There were four failure test areas similar to the CIP 0^o skewed specimen, and two additional serviceability test areas where negative moment was maximized to test the two top reinforcement spacings (3-7/8 in. vs. 6 in.) and the two types of expansion joints (AJ vs. SEJ). For all test specimens, negative moment was maximized over girder in the 8-ft girder spacings, and positive moment was maximized at midspan of the 10-ft girder spacing.

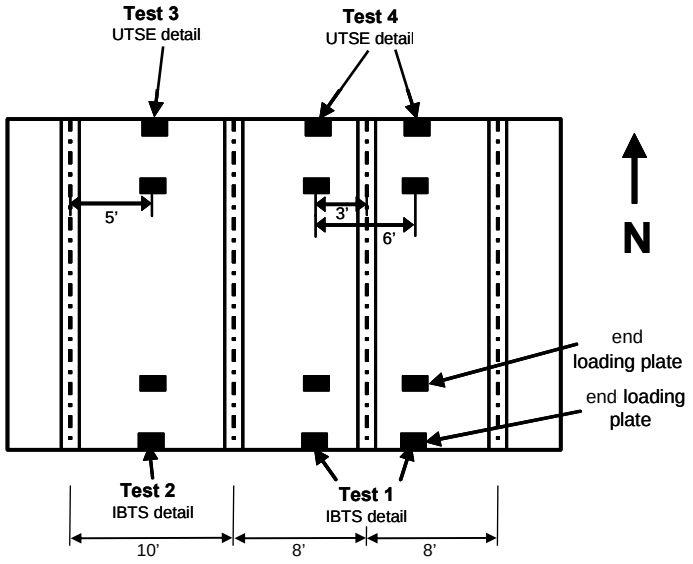

(a) CIP 0^o skewed specimen

Figure 2.14 Test specimens and test areas

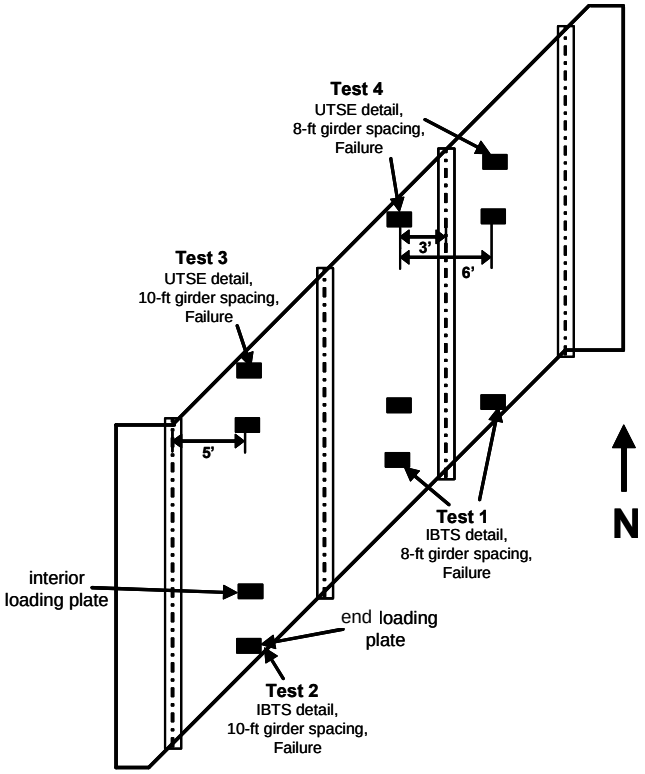

(b) CIP 45° skewed specimen

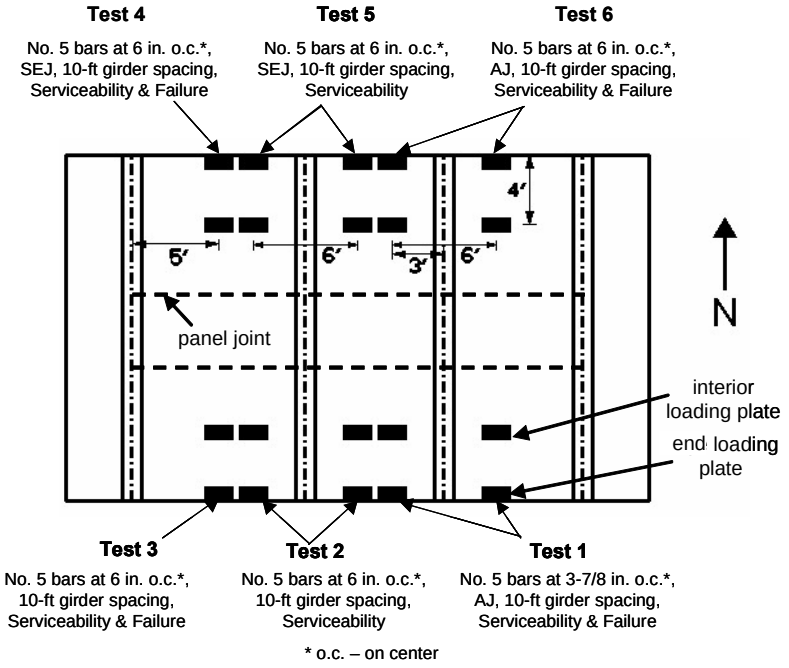

(c) PCP, 0° skewed specimen

Figure 2.14 cont'd Test specimens and test areas

In the CIP 0^o skewed specimen, each test area was loaded to failure before moving to the next test area. For the CIP 45^o skewed specimen and the PCP specimen, all test areas were tested to service level loads before loading the test areas to failure. Service-level tests were first performed on each area to view cracking behavior in each test section before severe damage occurred anywhere else in the slab. For each area, loads were applied until cracking began to extend into neighboring test regions. The area was then unloaded, and the loading frame was moved to the next test area.

Load was applied in increments to the test specimen with 60-ton hydraulic rams connected to a pneumatic hydraulic pump with all rams connected to the same manifold. The data-acquisition system required 10 seconds to record readings from 110 channels, so load was increased in small increments to permit generation of continuous force deformation plots. During testing, a load-strain plot of the most critical strain gauge was generated to monitor the response of the slab to applied loads. Intermittently, loading was paused so that cracks could be traced, measured, photographed and recorded.

Each expansion joint test area was loaded to design-level loads, overloads as multiples of that design-level, and to failure. The load levels where deflections, strains, and cracking were measured were: DT, 1.25DT, 1.5DT, 2.2DT, 3.75DT and failure. Factors of 1.25 and 1.5DT loading may be considered as typical overload factors to account for overloaded trucks. Overload levels of 2.2 and 3.75DT were also tested while the specimens were being loaded to failure.

CHAPTER 3:
IBTS END DETAIL "I – BEAM THICKENED SLAB"

3.1 INTRODUCTION

As discussed in Chapter 2, the IBTS detail is the standard TxDOT detail used at expansion joints. The detail was constructed and tested on both 0^o and 45^o skewed slabs. The test data gathered from the 0^o and 45^o skewed specimens enabled comparison of the response of the IBTS detail at the slab end with varying skews. In this chapter, a summary of failure modes, capacities and service-load level behavior of the IBTS detail are compared for the two specimens. Detailed test results are reported in Ryan (2003) and Griffith (2003).

3.2 NEGATIVE-MOMENT TESTS

In the 0^o and 45^o skewed specimens, negative moment was maximized over the girder between two 8-ft bays. In the 0^o skewed specimen, four point loads were applied in the end region in the negative moment tests. However in the 45^o skewed specimen, only three loads could be applied simultaneously in the AASHTO negative moment. Figure 3.1 shows the deflection envelopes for the two negative moment tests performed on the IBTS detail on the 0^o and 45^o skewed specimens. For the negative moment loading tests, the IBTS end detail on both skews had nearly identical initial slab end stiffness. Deflections at design load levels, overload levels, and at failure for both the 0^o and 45^o skews were similar. Relative end deflections were extremely small compared to the girder spacing (less than 1/3800).

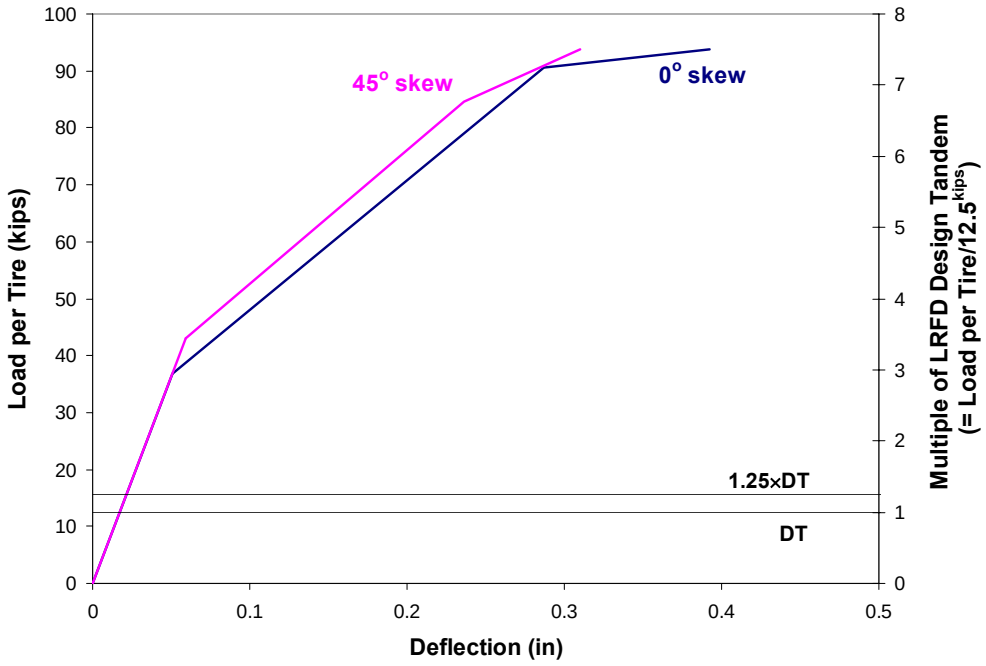

Figure 3.1 Deflection envelopes: Negative moment tests, IBTS detail

Tensile strains at DT and 1.25DT were negligible, all under 5% of yield strain. The maximum strains measured at design and overload load levels are reported in Tables 3.1 and 3.2. Strains reported from the 0^o skewed specimen may not be the maximum strains occurring in the flexural reinforcement in the end region. Strain gauges were attached at locations above the centerline of the girder (Section 2.5.2.1), but larger strains probably occurred at locations along either face of the girder. These strains are included, but are only intended as a relative guide to maximum measured strain in 0^o skewed test areas.

For all test areas, flexural cracking was first observed above design load levels. The first significant change in stiffness occurred at loads higher than 3.0DT. The first significant change in stiffness was accompanied by increased crack widths (typically > 0.010 in.) and development of an extensive crack pattern. Crack widths at design and overload levels are given in Tables 3.1 and 3.2. These widths were measured from the tests performed, and are intended to serve only as a comparative index of crack severity.

Table 3.1 Summary of IBTS detail: Negative-moment region, 0^o skew

	Deflections			Maximum strains (% of steel yield strain)	Maximum crack width, negative moment region (in.)
	Maximum deflection (in.)	Flexural Cracking (Yes/No)	Clear span to deflection ratio		
DT	0.016	No	6000	4	N/A
1.25DT	0.02	No	4800	4	N/A
1.5DT	0.03	No	3200	6	N/A
2.2DT	0.04	No	2400	18	N/A
3.75DT	0.09	Yes	1070	44	0.002
Failure, 7.5DT	0.39	Yes	250	$> \varepsilon_y$	0.018

*Strain measurement made at centerline of girder and may not be the maximum strain

Table 3.2 Summary of IBTS detail: Negative-moment region, 45^o skew

	Deflections			Maximum strains (% of steel yield strain)	Maximum crack width, negative moment region (in.)
	Maximum deflection (in.)	Flexural Cracking (Yes/No)	Clear span to deflection ratio		
DT	0.025	No	3840	1	N/A
1.25DT	0.026	No	3690	1	N/A
1.5DT	0.03	No	3200	2	N/A
2.2DT	0.04	No	2400	2	N/A
3.75DT	0.10	Yes	960	24	0.005
Failure, 7.5DT	0.83	Yes	120	$> \varepsilon_y$	0.045

Figure 3.2 shows the locations of major cracks at failure in both maximum negative moment tests. In the 0° skewed specimen, a punching shear failure occurred at the end load plate of the interior bay. In the 45° skewed specimen, a punching-shear failure initiated at the interior load plate of the interior bay, where the slab depth was 8 in. The failure surface formed at this interior plate, and then propagated toward the end plate.

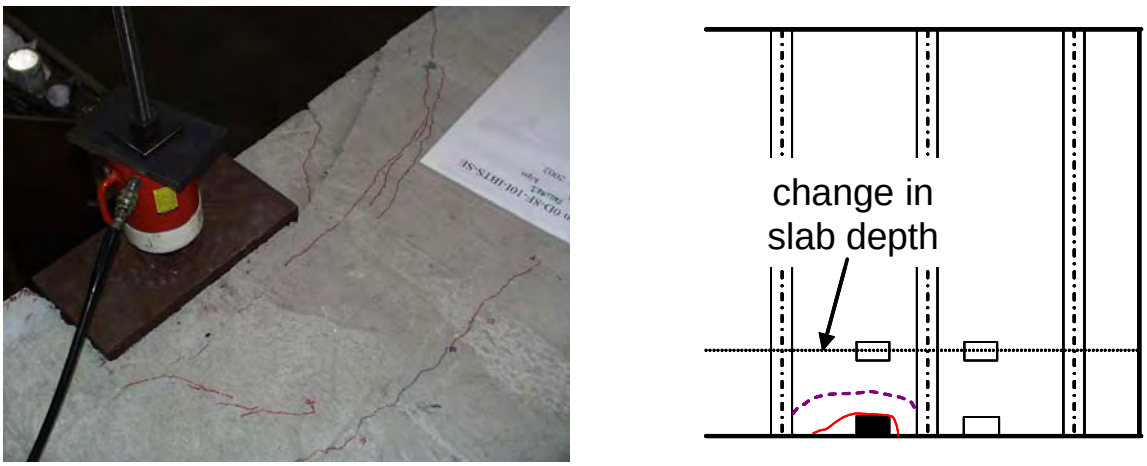

(a) 0° skewed specimen

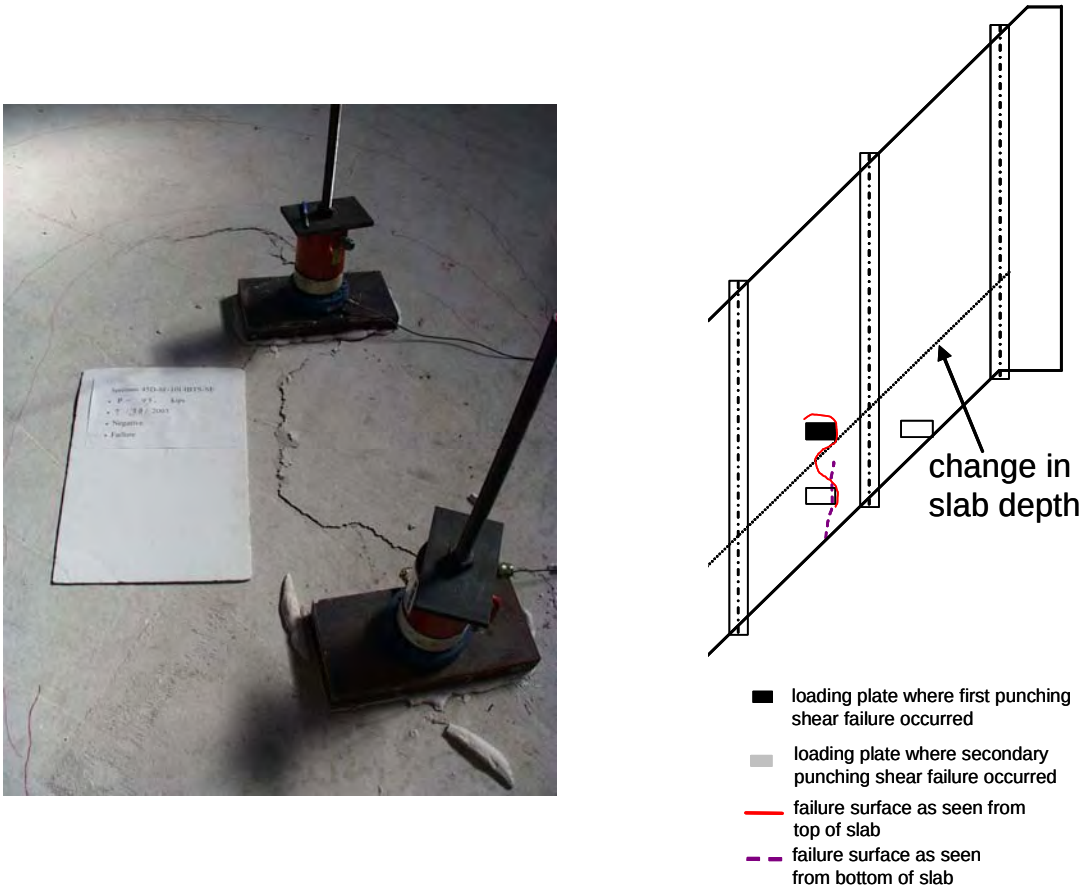

(b) 45° skewed specimen

Figure 3.2 Locations of punching shear failures: IBTS negative-moment tests

In the areas where negative moment was maximized, failure mechanisms were similar. Punching shear failure occurred on the side of the load points closest to the girder. Skew had no effect on the failure loads (7.5DT, 94 kips) of the negative-moment test areas. Design provisions for punching shear capacity and calculated capacities for all tests are discussed in Chapter 6.

3.3 POSITIVE MOMENT-TESTS

In the 0^o and 45^o skewed specimens, positive moment was maximized at midspan of the 10-ft bay. In both specimens, two point loads were applied in the end region at midspan in the AASHTO tandem configuration. Figure 3.3 shows the deflection envelopes for the two positive moment tests performed on the IBTS detail on the 0^o and 45^o skewed specimens. For the positive moment loading tests, the IBTS end detail of both specimens exhibited nearly identical behavior at DT and 1.25DT load levels. Relative end deflections were larger for the 45^o skewed test areas, but were extremely small compared to the girder spacing (less than 1/1700) at design load levels.

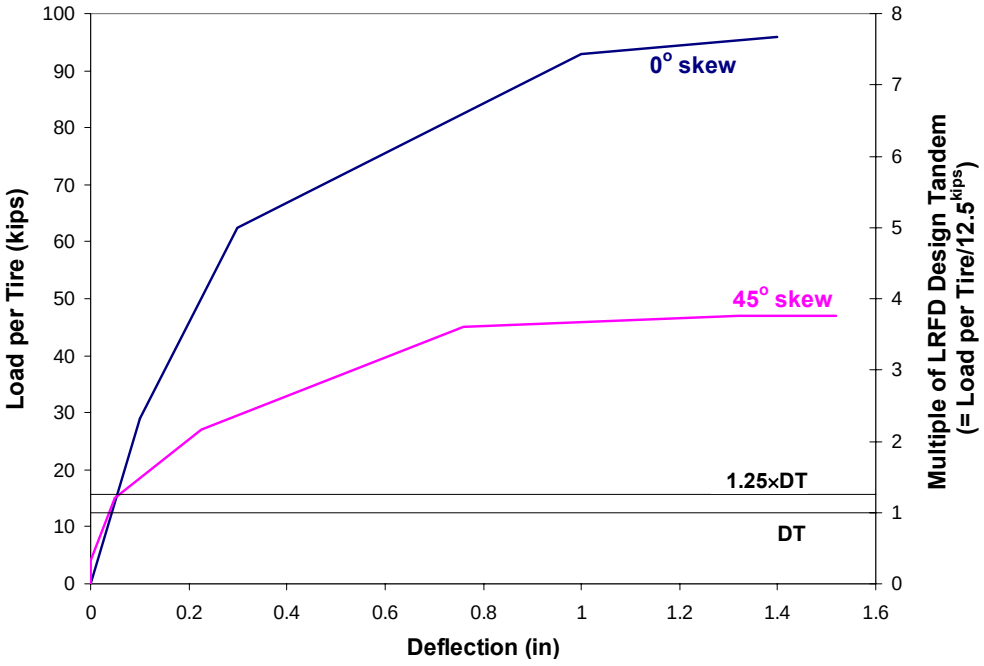

Figure 3.3 Deflection envelopes: Positive moment tests, IBTS detail

Tensile strains at DT were 6% of the yield strain, and at 1.25DT, strains were less than 10% of yield strain. Due to the larger reinforcement spacing, tensile strains exceeded yield strain in at least one location in every test region.

For all test areas, flexural cracking was first observed at or above design load levels. The first significant change in stiffness occurred at loads higher than 1.2DT. Crack widths at design and overload levels are given in Table 3.3 and Table 3.4.

Table 3.3 Summary of IBTS detail: Positive-moment region, 0° skewed specimen

	Deflections			Maximum strains (% of steel yield strain)	Maximum crack width, negative moment region (in.)
	Maximum deflection (in.)	Flexural Cracking (Yes/No)	Clear span to deflection ratio		
DT	0.03	No	3750	6	N/A
1.25DT	0.05	No	2400	8	HL
1.5DT	0.06	Yes	2000	10	0.002
2.2DT	0.08	Yes	1500	14	0.003
3.75DT	0.16	Yes	750	31	0.008
Failure, 7.7DT	1.40	Yes	90	$> \varepsilon_y$	0.033

*Strain measurement made at centerline of girder and may not be the maximum strain

Table 3.4 Summary of IBTS detail: Positive-moment region, 45° skewed specimen

	Deflections			Maximum strains (% of steel yield strain)	Maximum crack width, negative moment region (in.)
	Maximum deflection (in.)	Flexural Cracking (Yes/No)	Clear span to deflection ratio		
DT	0.003	No	32000	4	N/A
1.25DT	0.006	Yes	16000	6	HL
1.5DT	0.10	Yes	960	15	HL
2.2DT	0.23	Yes	420	41	0.009
Failure, 3.8DT	1.52	Yes	400	$> \varepsilon_y$	0.025

Figure 3.4 shows the locations of major cracks at failure in both positive moment tests. In the 0° skewed specimen, a punching shear failure occurred at 7.7DT (96 kips) the end load plate of the interior bay. In the 45° skewed specimen, a one-way shear failure occurred at 3.8DT (48 kips). Only one test area failed in one-way shear, and test data from the one test area is too limited to provide a precise explanation for the different failure mode and capacity. However, two possible factors for influencing the failure loads of the test section are the geometry of the test specimen, the location of the critical section for shear and the predicted shear stress at that critical section, which is discussed further in the Section 3.3.1.

3.3.1 Shear and Skewed Slab Geometry

The critical section for beam shear is different on either side of the load points. Due to slab end geometry and the load configuration, one potential beam shear failure plane is shorter than the other, leading to a lower calculated shear resistance. As illustrated in Figure 3.5, the critical plane is on the east side of the load points. The difference in critical locations for shear is important when combined with a simple

linear-elastic analysis of shear stresses on either side of the load points. Figure 3.5, shows two elastic analyses idealizing the end detail as a wide beam. In one analysis, the interior girder acts like a fixed support; in another, like a simple support. The actual support conditions and flexural restraint of the interior girder are expected to be somewhere between these two conditions, possibly closer to the fixed support condition. Because of the differences in edge fixity, the shear stresses on the east side of the load points could be up to 38% greater than the shear stresses on the west side of the load point. This simple model may not be an exact representation of the actions occurring in these sections. However, combining the two effects, the IBTS detail would be expected to experience higher shear forces at a location where the length of the critical section for beam shear is shorter.

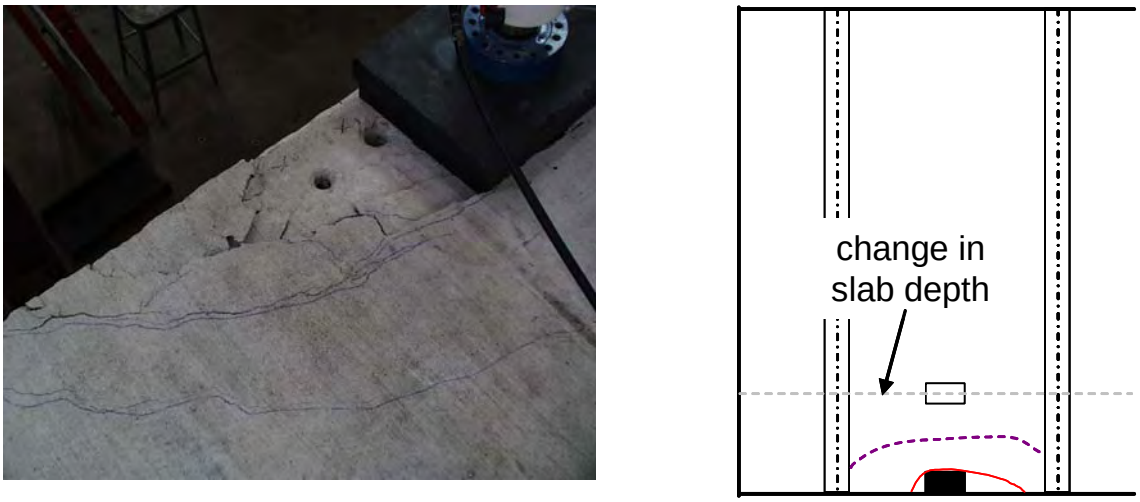

(a) 0° skewed specimen

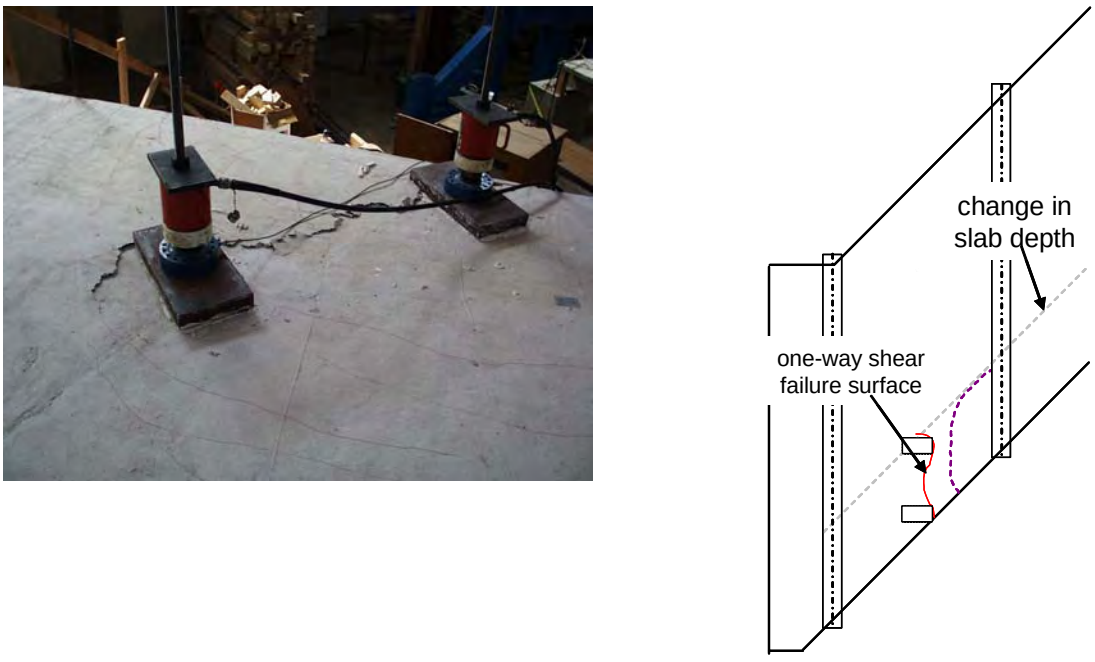

(b) 45° skewed specimen

Figure 3.4 Locations of failure surfaces: IBTS positive-moment region

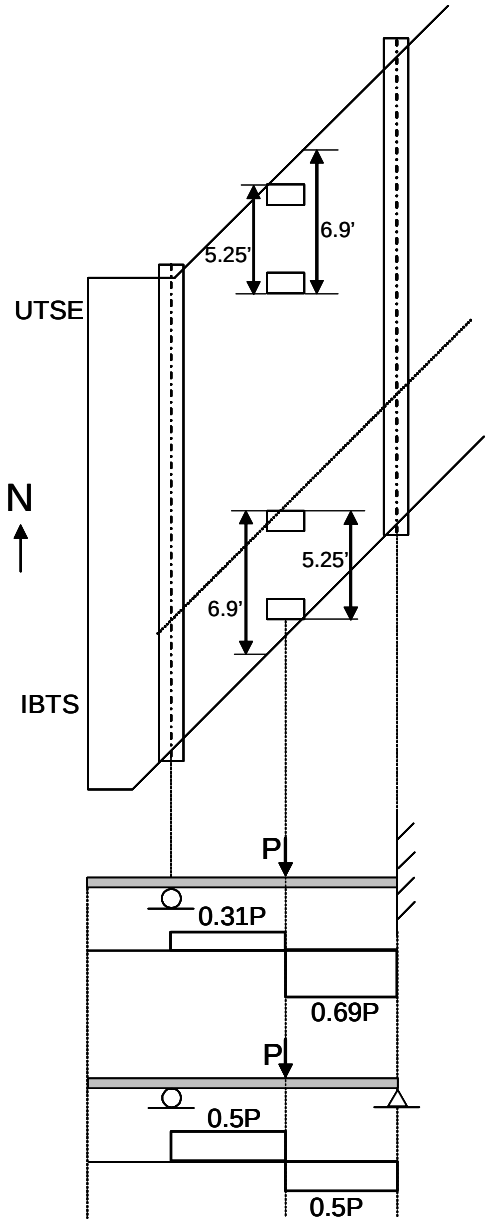

Figure 3.5 Elastic shear distribution: Positive-moment tests

3.3.2 Torsion

Torsion also contributed to the difference in failure mode and capacities of the 10-ft bays on the 45° skewed specimen. Although somewhat more limited in the 8-ft bays, torsional cracking was observed in every test area on the 45° skewed specimen. These cracks appeared on the receding corners of each bay (Figure 3.6), the load points and the girder. These cracks indicate that torsion could have affected the capacities and distribution of stresses in the receding corners of the test areas with 10-ft girder spacing.

Torsional moments may have also affected the capacity of the positive-moment test areas, because the failure surface formed on an existing torsional crack in the IBTS, positive-moment test area in the 45^{o} skewed specimen. To fully understand the effects of torsion on beam shear and punching shear, investigations beyond the scope of the current investigation study are needed.

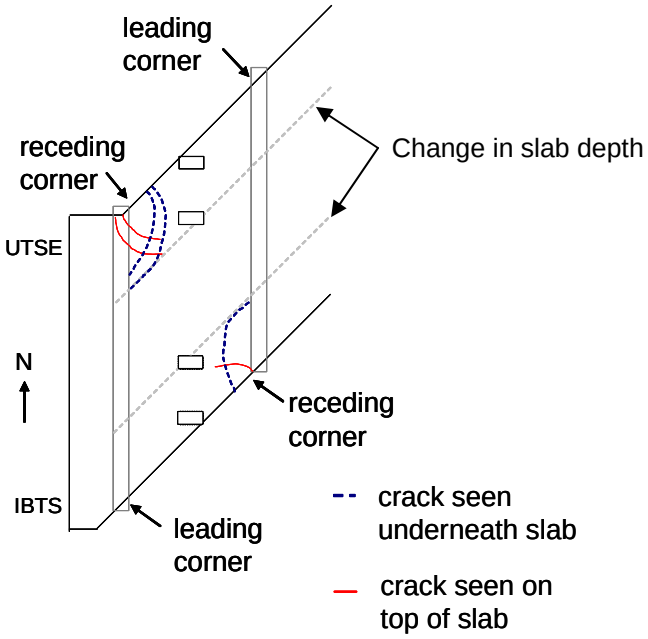

Figure 3.6 Torsional cracks in 10-ft bays

3.4 EFFECT OF SKEW

The end details usually had lower first cracking loads when skew was increased from 0^o to 45^o, but were still at or above design load levels. Skew angle did not have a noticeable effect on the measured strain on the instrumented reinforcing bars. Skew angle did not have a noticeable effect on maximum slab end deflections in the 8-ft girder spacings, but did result in increased slab end deflections in the 10-ft girder spacings. However, midspan end deflections at DT and 1.25DT load levels were small compared to the girder spacing.

Slab end skew angle had an insignificant effect on the failure load and mechanism in the negative-moment test regions. The slab end skew angle had a significant effect on the failure load and mechanism in the positive-moment test areas. All test areas failed in punching shear, except for the positive-moment test area in the 45^o skewed specimen, which failed in one-way shear. As discussed in Section 3.3, the change in failure mechanism is most likely attributed to the geometry of the slab specimen and consequent torsional moments.

3.5 SUMMARY

The IBTS detail performed well at DT and 1.25DT design loads. Measured end deflections were small compared to the girder spacing (1/3800), and strain levels were less than 8% of yield strain at design load levels. Even though some instrumented reinforcement reached yield strain, the load level at which yield strain was reached was above 3.75DT. The detail failed at loads well above design load levels. Overall, skew angles of 45^o or less had no significant effect on the performance of the detail at design load levels. Slab end skew angle did have a noticeable effect on the failure load and mechanism in the positive moment test area of 10-ft girder spacing.

CHAPTER 4:
UTSE DETAIL "UNIFORM THICKNESS SLAB END"

4.1 INTRODUCTION

As discussed in Chapter 2, an alternate detail to the standard TxDOT IBTS detail was developed and tested. The Uniform Thickness Slab End (UTSE) detail is 8 in. thick detail and uniform with the thickness of the interior portion of most bridge decks. The detail has a similar moment capacity as the IBTS detail, as discussed in Section 2.3.1. The detail was constructed and tested on both 0^o and 45^o skewed slabs. The test data gathered from the 0^o and 45^o skewed specimens enabled comparison of the response of the UTSE detail at the slab end with varying skews. In this chapter, failure modes, capacities and service-load level behavior of the UTSE detail are compared for the two specimens, as well as a comparison of responses with the IBTS detail. Detailed test results are reported in Ryan (2003) and Griffith (2003).

4.2 NEGATIVE-MOMENT TESTS

In the 0^o and 45^o skewed specimens, negative moment was maximized over the girder between two 8-ft bays. In the 0^o skewed specimen, four point loads were applied in the end region in the negative moment tests. However in the 45^o skewed specimen, only three loads could be applied simultaneously due to the geometry of the skew and the design tandem loading. Figure 4.1 shows the deflection envelopes for the two negative moment tests performed on the UTSE detail on the 0^o and 45^o skewed specimens. For the negative moment tests, the UTSE end detail on both skews was nearly identical to loads about double the DT and 1.25DT load levels. Relative end deflections at design load levels were extremely small compared to the girder spacing (less than 1/12000).

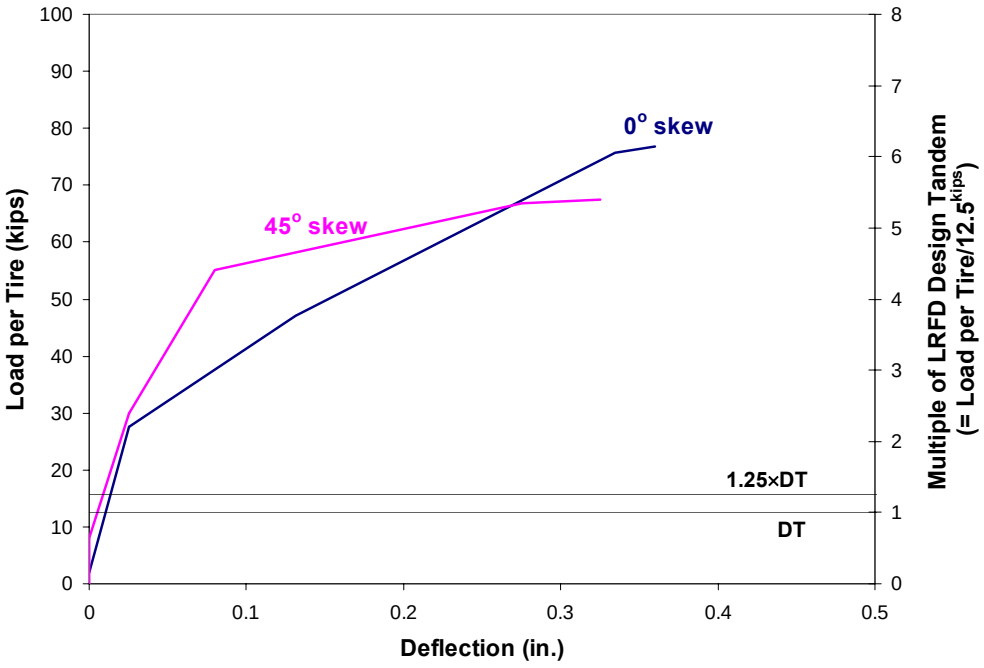

Figure 4.1 Deflection envelopes: Negative moment tests, UTSE detail

Tensile strains at DT and 1.25DT were negligible, all under 5% of yield strain. Due to the smaller reinforcement spacing, none of the instrumented flexural reinforcement measured steel strains exceeding yield strain. The maximum measured strain at various design and overload load levels are summarized in Tables 3.1 and 3.2.

For all test areas, flexural cracking was first observed above design load levels. Significant changes in stiffness occurred at loads higher than 2.0DT. Crack widths at design and overload load levels are given in Tables 4.1 and 4.2. These widths were measured from the tests performed, and are intended to serve only as a comparative index of crack severity.

Table 4.1 Summary of UTSE detail: Negative-moment region, 0° skew

	Deflections			Maximum strains (% of steel yield strain)	Maximum crack width, negative moment region (in.)
	Maximum deflection (in.)	Flexural Cracking (Yes/No)	Clear span to deflection ratio		
DT	0.006	No	16000	3	N/A
1.25DT	0.008	No	12000	4	N/A
1.5DT	0.02	No	4800	8	N/A
2.2DT	0.05	No	1920	15	HL
3.85DT	0.13	Yes	740	37	0.003
Failure, 6.1DT	0.36	Yes	270	71	0.009

*Strain measurement made at centerline of girder and may not be the maximum strain

Table 4.2 Summary of UTSE detail: Negative-moment region, 45° skew

	Deflections			Maximum strains (% of steel yield strain)	Maximum crack width, negative moment region (in.)
	Maximum deflection (in.)	Flexural Cracking (Yes/No)	Clear span to deflection ratio		
DT	0.006	No	16000	1	N/A
1.25DT	0.007	No	13710	1	N/A
1.5DT	0.008	No	12000	2	N/A
2.2DT	0.03	Yes	3000	5	0.002
3.85DT	0.16	Yes	600	42	0.015
Failure, 5.4DT	0.32	Yes	300	89	0.04

Figure 4.2 shows the locations of major cracks at failure in both negative moment tests. In the 0° skewed specimen, a punching shear failure occurred at the end load plate of the interior bay. In the 45° skewed specimen, a punching-shear failure occurred around the loaded point in the interior bay. Of all of the locations where load was applied in this test area, this load plate was closest to the end and had the smallest shear perimeter calculated in accordance with AASHTO LRFD Bridge Design Specifications and ACI 318-02 provisions.

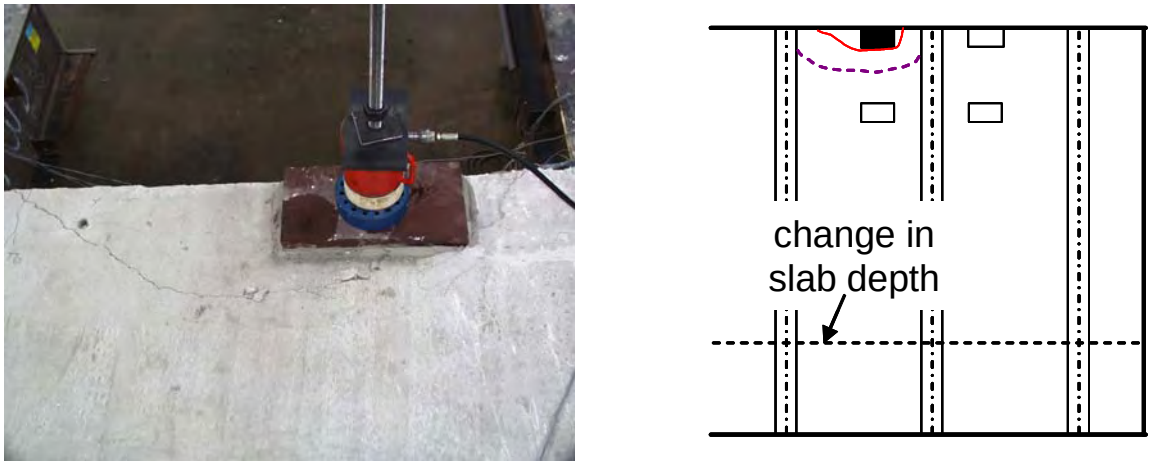

(a) 0° skewed specimen

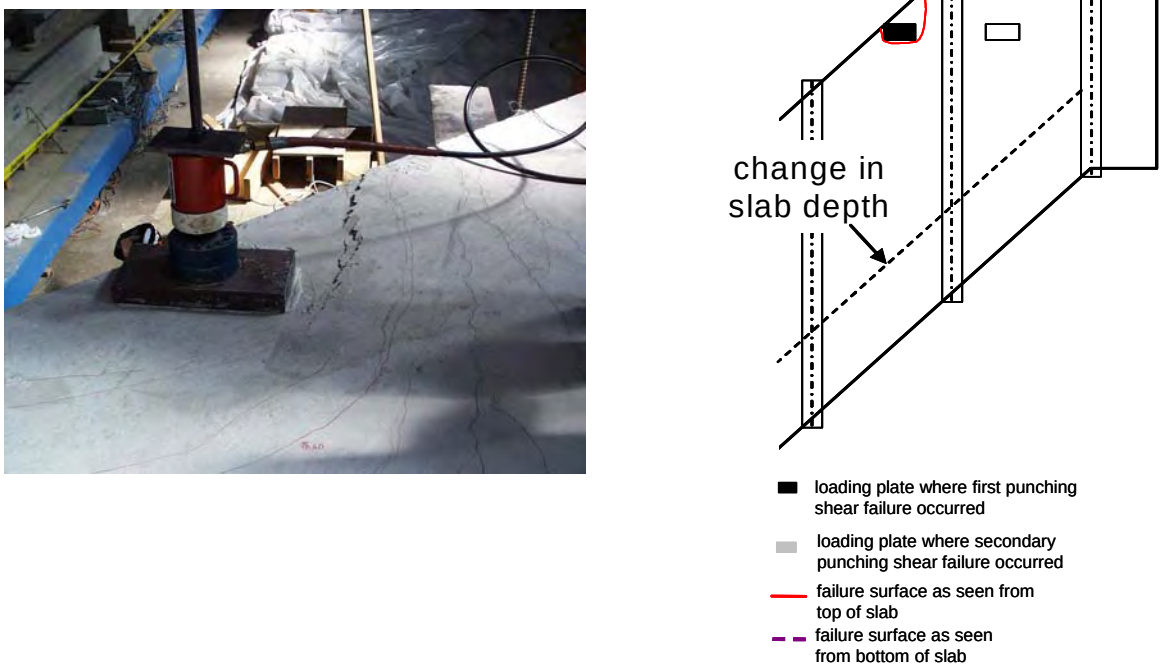

(b) 45° skewed specimen

Figure 4.2 Locations of punching shear failure: UTSE negative-moment tests

In the areas where negative moment was maximized, failure mechanisms were similar. Skew had little effect on the failure loads with a 20% difference between the failure loads (6.1DT, 0° skew and 5.4DT, 45° skew) of the negative-moment test areas. Punching shear design provisions and calculated capacities for all tests are discussed in Chapter 6.

4.3 POSITIVE-MOMENT TESTS

In the 0° and 45° skewed specimens, positive moment was maximized at midspan of the 10-ft bay. In the both specimens, two point loads were applied in the end region at midspan in the AASHTO tandem configuration. Figure 4.3 shows the deflection envelopes for the two positive moment tests performed on the UTSE detail on the 0° and 45° skewed specimens. For the positive moment loading tests, the UTSE end detail on both skews had nearly identical performance at DT and 1.25DT load levels. Relative end deflections at design load levels were larger for the 45° skewed test areas, but were still small compared to the girder spacing (less than 1/1200).

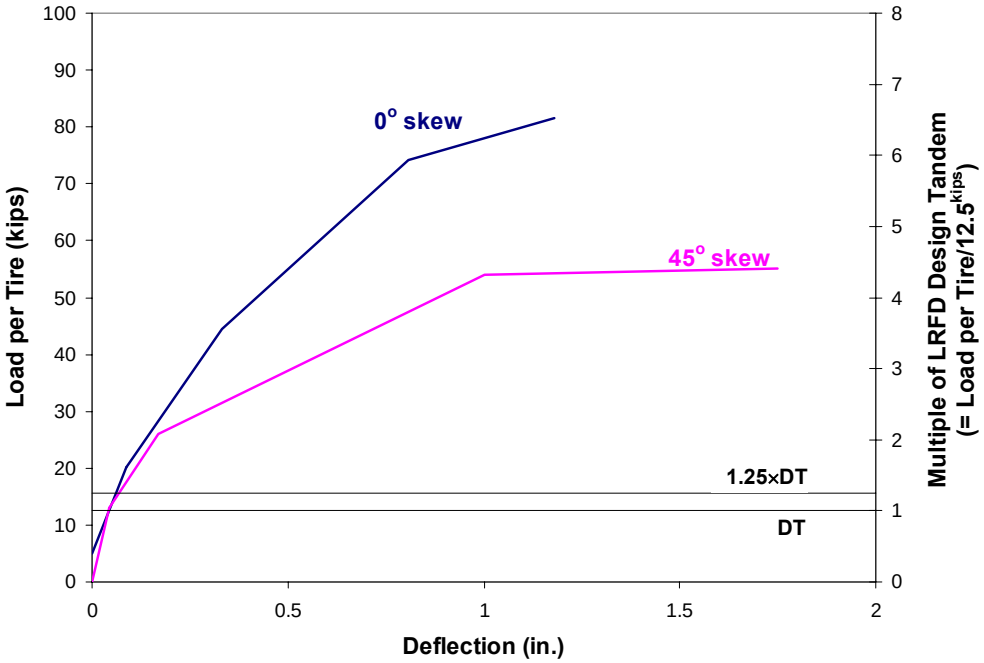

Figure 4.3 Deflection envelopes: Positive moment tests, UTSE detail

Tensile strains at DT were 7% of the yield strain, and at 1.25DT, strains were less than 10% of yield strain. None of the instrumented flexural reinforcement reached yield strain before failure in any of the test areas. The maximum measured strains are summarized in Tables 4.3 and 4.4.

For all test areas, flexural cracking was first observed at or above design load levels. The significant change in stiffness for the test areas occurred at loads higher than DT. Crack widths at design and overload levels are given in Table 4.3 and Table 4.4.

Table 4.3 Summary of UTSE detail: Positive-moment region, 0° skew

	Deflections			Maximum strains (% of steel yield strain)	Maximum crack width, negative moment region (in.)
	Maximum deflection (in.)	Flexural Cracking (Yes/No)	Clear span to deflection ratio		
DT	0.03	No	37500	7	N/A
1.25DT	0.07	No	1710	10	HL
1.5DT	0.07	No	1710	12	0.002
2.2DT	0.14	Yes	860	20	0.003
3.75DT	0.34	Yes	350	40	0.007
Failure, 6.6DT	1.18	Yes	100	74	0.04

*Strain measurement made at centerline of girder and may not be the maximum strain

Table 4.4 Summary of UTSE detail: Positive-moment region, 45° skew

	Deflections			Maximum strains (% of steel yield strain)	Maximum crack width, negative moment region (in.)
	Maximum deflection (in.)	Flexural Cracking (Yes/No)	Clear span to deflection ratio		
DT	0.05	Yes	1920	5	N/A
1.25DT	0.08	Yes	1200	10	HL
1.5DT	0.10	Yes	960	14	0.002
3.75DT	0.22	Yes	440	25	0.009
3.75DT	0.82	Yes	120	73	0.015
Failure, 4.4DT	1.74	Yes	60	99	0.022

Figure 4.4 shows the locations of major cracks at failure in both specimens for the UTSE positive moment test areas. In the areas where negative moment was maximized, failure mechanisms were similar. Slab end skew angle had an effect on the failure loads with an approximately 35% lower load at the skewed end. Punching shear failures occurred at 6.6DT (83 kips) in the 0° skewed specimen and 4.4DT (55 kips) in the 45° skewed specimen.

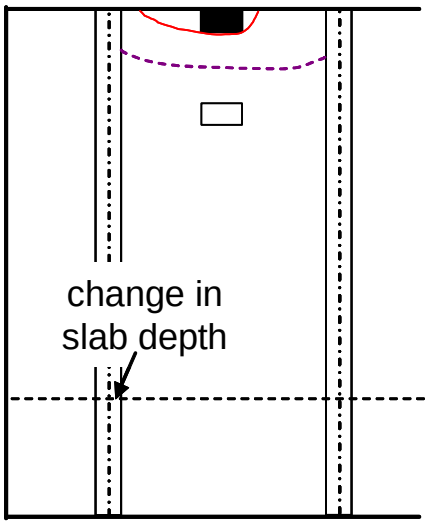

(a) 0^o skewed specimen

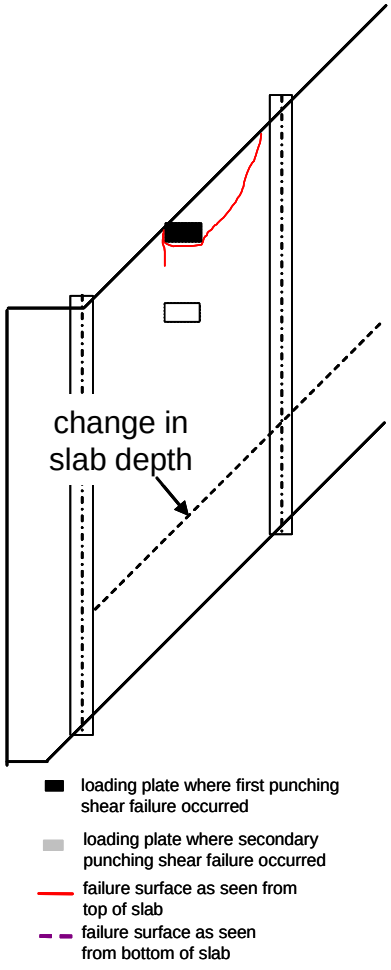

(b) 45^o skewed specimen

Figure 4.4 Locations of punching shear failure: UTSE positive-moment tests

4.4 COMPARISON OF RESPONSES OF IBTS AND UTSE DETAILS

The primary objective of the study was to understand the behavior of slab ends at expansion joints constructed with the IBTS end detail. In addition to understanding the behavior of the IBTS detail, an alternate, simpler detail, UTSE, was also investigated. In this section, the effects on varying end skew angle and girder spacing on cracking loads, deflections, reinforcing bar stress levels and failure loads for the two details are discussed.

4.4.1 Load-Deflection Behavior

Load-deflection envelopes for all test areas are shown in Figure 4.5. As seen in Figure 4.5, all negative moment test areas and all positive moment test areas showed nearly identical performance through at DT and 1.25DT load levels. Relative end deflections measured at midspan at design and overload levels for both details are summarized in Table 4.5.

Increasing design loads from DT to 1.25DT resulted in nearly proportional increases in slab end deflections measured in all test areas. For the negative moment test areas, the deflections were small compared to the girder spacing (1/3800), and were smaller in the test areas with the UTSE detail than the IBTS detail. However, the opposite was true for the positive moment test areas, where the IBTS detail deflected less than the UTSE detail. Again, the deflections measured at design load levels in the positive moment test areas were small relative to the girder spacing. Test areas reached the maximum service-deflection allowed by AASHTO LRFD provisions (1/800) at loads ranging from 1.5DT to 3.75DT. While increased end skew angle had an insignificant effect on maximum slab end deflection in the negative moment test areas, it resulted in increased end deflections in the positive moment test areas.

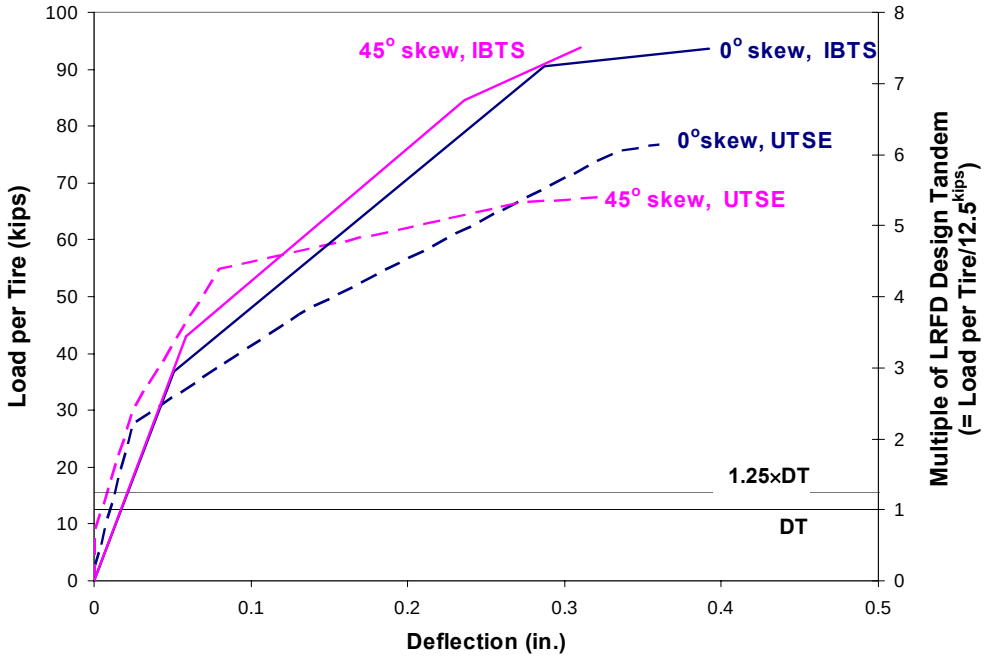

(a) negative moment tests

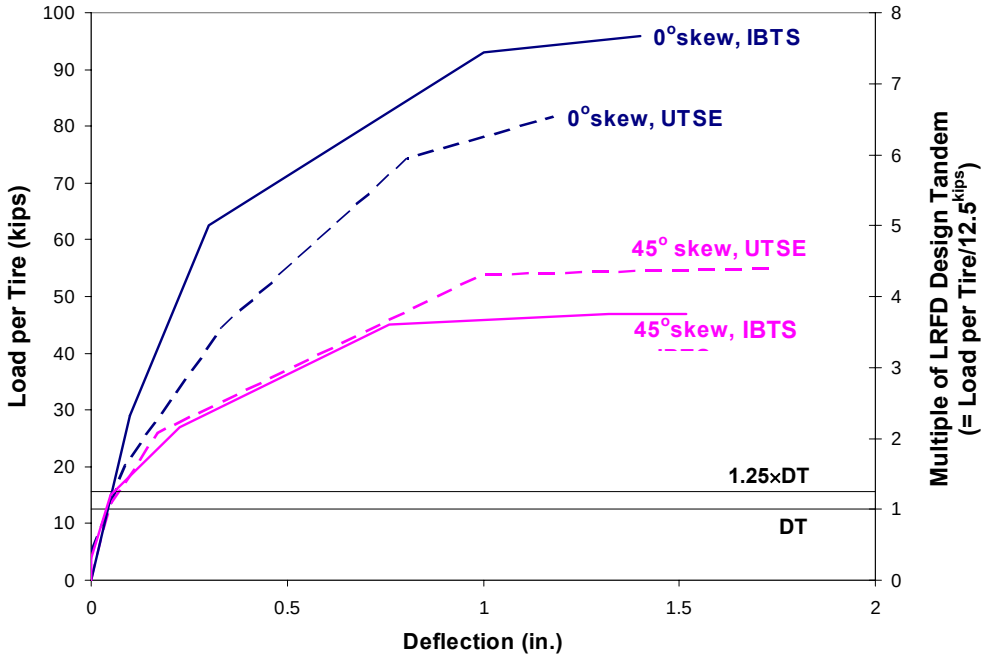

(b) positive moment tests

Figure 4.5 Load deflection envelopes

Table 4.5 Measured end deflections (in.)

Moment Maximized	Negative				Positive			
End Detail	IBTS		UTSE		IBTS		UTSE	
Skew Angle	0^o	45^o	0^o	45^o	0^o	45^o	0^o	45^o
HS-20	0.016	0.025	0.006	0.0	0.03	0.003	0.03	0.05
HS-25	0.02	0.026	0.008	0.007	0.05	0.006	0.07	0.08
1.2 HS-25	0.03	0.03	0.02	0.008	0.06	0.10	0.07	0.10
1.75 HS-25	0.04	0.04	0.05	0.03	0.08	0.23	0.14	0.22
3 HS-25	0.09	0.10	0.13	0.16	0.16	-	0.34	0.82
Failure	0.39	0.83	0.36	0.32	1.40	1.52	1.18	1.74

4.4.2 Reinforcement Strains

The maximum tensile strains measured at DT, 1.25DT and overload levels for both details are summarized in Table 4.6. For all tests performed on both details, tensile strains were less than 10% (220 με) of the yield strain at 1.25DT load level. At 3.75DT load levels, the maximum strains were less than 50% of yield strain except for the positive moment sections of the 45^o skew in the UTSE detail where strains reached about 70% of yield. As noted in Section 3.2, strains reported for the 0^o skewed specimen were at locations over the centerline of the girder, but slightly larger strains probably occurred at locations along either face of the girder.

Table 4.6 Maximum measured tensile strains (% of steel yield strain)

Moment Maximized	Negative				Positive			
End Detail	IBTS		UTSE		IBTS		UTSE	
Skew Angle	0^o	45^o	0^o	45^o	0^o	45^o	0^o	45^o
DT	4	1	3	1	6	4	7	5
1.25DT	4	1	4	1	8	6	10	10
1.5DT	6	2	8	2	10	15	12	14
2.2DT	18	2	15	5	14	41	20	25
3.75DT	44	24	37	42	31	-	40	73
Failure	$> \varepsilon_y$	$> \varepsilon_y$	71	89	$> \varepsilon_y$	$> \varepsilon_y$	74	99

*Strain measurement made at centerline of girder and may not be the maximum strain

4.4.3 Crack Formation

Test data gathered indicate that an increase in design loads from DT to 1.25DT would have little effect on the formation of cracks in decks with girder spacings of 10-ft or less and skews of 45^o or less. First cracking loads are summarized in **Table 4.7**. Based on test results, slab ends with either detail can be expected to remain uncracked under DT and 1.25DT design loads for 0^o skewed slabs and slabs constructed with 8-ft girder spacings. For specimens tested with 10-ft girder spacings, first cracking loads were reduced, but still remained at or above DT. The combination of 10-ft girder spacing and 45^o skew resulted in the lowest load at first cracking.

Table 4.7 First cracking loads (× DT)

Moment Maximized	Negative		Positive	
Skew Angle	0°	45°	0°	45°
IBTS	2.6	2.7	1.3	1.2
UTSE	2.2	1.8	1.5	1.0

For all test regions, cracks were first observed at loads between DT and 3.75DT. However, first observed cracking did not cause a noticeable difference in stiffness in the negative moment test areas and only a minor reduction in stiffness in the positive moment test areas. A significant change in stiffness was associated with more extensive cracking – wider cracks, increase in length, and the number of cracks. Such changes in stiffness occurred at loads around or above 1.5DT.

In the IBTS test regions, there were usually fewer and wider cracking occurring than in the UTSE test regions. Crack widths at design, overload and failure load levels are shown in Table 4.8, and are to provide only a comparison of crack severity.

Table 4.8 Measured crack widths (in.)

Moment Maximized	Negative				Positive			
End Detail	IBTS		UTSE		IBTS		UTSE	
Skew Angle	0°	45°	0°	45°	0°	45°	0°	45°
DT	N/A	N/A	N/A	N/A	N/A	N/A	N/A	N/A
1.25DT	N/A	N/A	N/A	N/A	HL	HL	HL	HL
1.5DT	N/A	N/A	N/A	N/A	0.002	HL	0.002	0.002
2.2DT	N/A	N/A	HL	0.002	0.003	0.009	0.003	0.009
3.75DT	0.002	0.005	0.003	0.015	0.008	-	0.007	0.015
Failure	0.018	0.045	0.009	0.04	0.033	0.025	0.04	0.022

4.4.4 Failure

All end regions failed in punching shear with the exception of the IBTS positive moment test area on the 45° skewed specimen, which failed in one-way shear. The UTSE detail failed at loads 20 to 30% lower than failure loads recorded for the IBTS detail (Figure 4.6). According to the punching shear provisions of the AASHTO LRFD and ACI 318-02, shear capacity is proportional to the distance from the extreme compressive fiber to the centroid of the tensile reinforcement. This distance in the IBTS detail is 2 in. greater than the corresponding distance in the UTSE detail. Based on this punching-shear model, for two identical punching shear failure surfaces, the capacity of an IBTS section should be higher than that of a UTSE section. The test results support this hypothesis, as the punching shear capacity of the UTSE detail slab ends were less than those of the IBTS detail slab ends for similarly configured test sections. All test results, regardless of end detail, showed reserve strength that was much greater (4 to 7.5 × DT) than AASHTO design load levels.

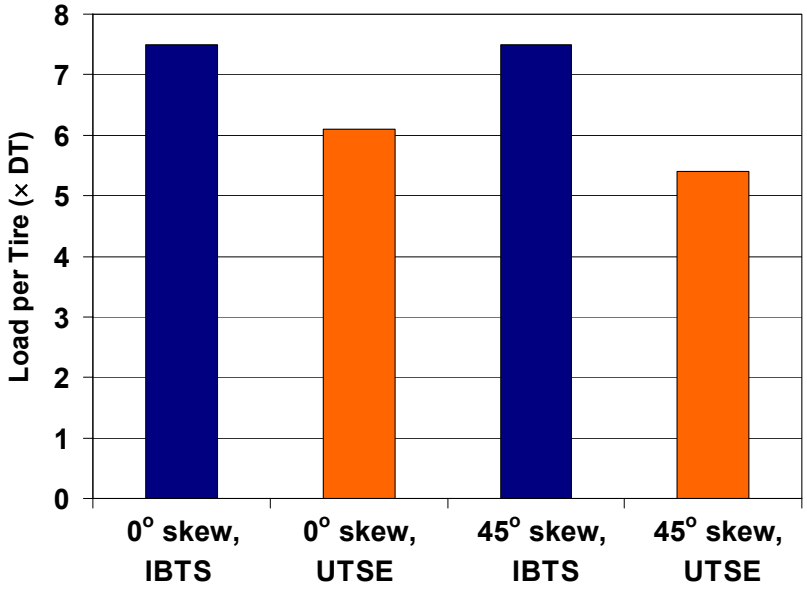

(a) negative moment tests

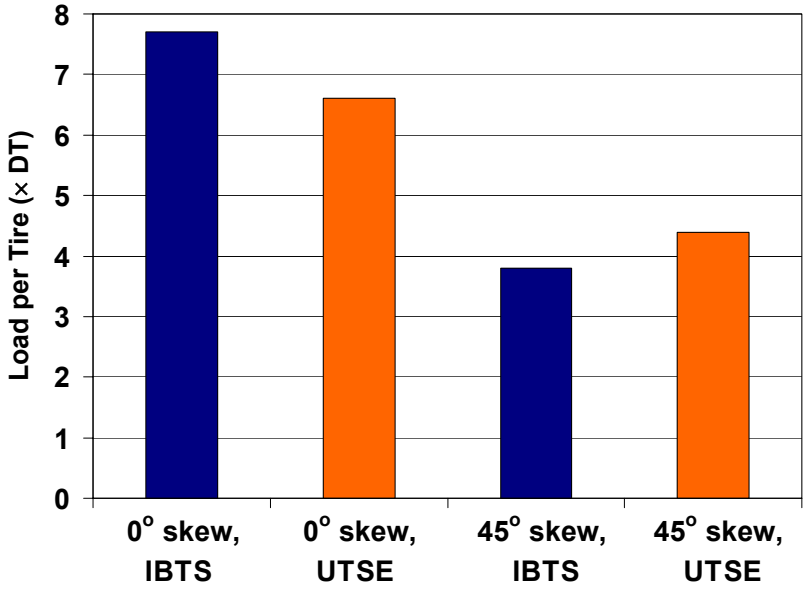

(b) positive moment tests

Figure 4.6 Failure loads

Skew angle had an effect on the failure load level and mechanism for the positive moment test areas, especially the IBTS detail. Failure load levels were lower in the 45° skewed specimen when compared to the 0° skewed specimen in those test areas. In addition to the lower failure load levels, the IBTS detail positive moment test area in the 45° skewed specimen failed in one-way shear, and as discussed in Section 3.3.1, this behavior can possibly be attributed to the geometry of the specimen and torsional moments, that were evident from the crack pattern.

4.5 SUMMARY

Overall, the alternate UTSE detail performed well under service loads compared to the standard IBTS detail. First cracking in the positive moment area occurred at slightly lower loads in the UTSE end than the IBTS end. Skew angles of 45^{o} or less had no significant effect on the performance of the details at design load levels. Slab end deflections under positive moment loading in the 10-ft bay and 45^{o} skew was larger than in ends with no skew. The UTSE detail failed at loads approximately 20 to 30% lower than those for the IBTS detail, which is expected due to the 2 in. section depth difference. Even though failure loads were lower than the IBTS detail, the loads were still well above design load levels.

CHAPTER 5:
PCPE DETAIL

5.1 INTRODUCTION

After test results showed that the UTSE detail performed as well as the IBTS detail at design loads and reached ultimate capacities at load levels well above design load levels, a simpler alternate detail was developed using the stay-in-place precast prestressed concrete panels (PCP) in the end detail. This detail is referred to as the PCPE detail. The detail has a similar moment capacity as the IBTS and UTSE details. The detail was constructed and tested on a 0^o skew slab, with expansion joints included on one end. In addition to the influence of expansion joints, two different top reinforcement spacings were investigated. The test data gathered from the PCPE specimen will be compared with the response of the 0^o skew IBTS and UTSE details in this chapter. The performances of PCPE detail with and without expansion joints will also be compared. Detailed test results are reported in Coselli (2004).

5.2 NEGATIVE-MOMENT TESTS

Similar to the 0^o skew specimen, negative moment was maximized over the girder between two 8-ft bays and four point loads were applied in the end region in the negative moment loading tests. Figure 5.1 shows the deflection envelopes for the negative moment tests performed on the PCPE specimen. Some of the tests were stopped at lower loads to avoid producing damage that might have affected the performance of the positive moment sections. Overall, the negative moment test areas behaved similarly under AASHTO design loads. Deflections at the DT load level were larger in the test areas without the armor joint (AJ) and the sealed expansion joint (SEJ), and were extremely small (less than 1/4000 for all tests) compared to the girder spacing. As expected the deflections were larger at negative sections that had larger spacing of the top slab reinforcement over the girder.

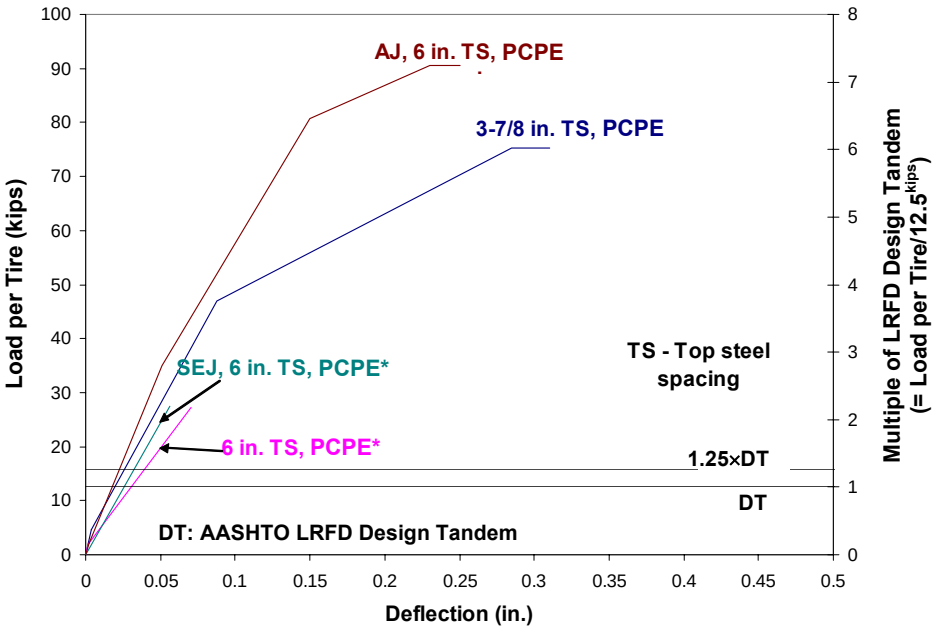

*Test areas were loaded only to service load levels

Figure 5.1 Deflection envelopes of PCPE specimens: Negative moment tests

Tensile strains at DT were negligible, under 10% of yield strain, and tensile strains at 1.25 DT did not exceed 15% in any test areas. The maximum measured strains at various design and overload load levels are summarized in Tables 5.1 through 5.4.

Table 5.1 Summary of 3-7/8 in. top reinforcement spacing PCPE: Negative-moment test

	Deflections			Maximum strains (% of steel yield strain)	Maximum crack width, negative moment region (in.)
	Maximum deflection (in.)	Flexural Cracking (Yes/No)	Clear span to deflection ratio		
DT	0.021	No	4570	6	0.007
1.25DT	0.026	No	3700	7	0.007
1.5DT	0.03	No	3200	7	0.007
2.2DT	0.04	Yes	2400	9	0.009
3.75DT	0.09	Yes	1070	30	0.013
Failure, 6.0DT	0.37	Yes	160	$> \varepsilon_y$	0.02

Table 5.2 Summary of 6-in. top reinforcement spacing PCPE: Negative-moment test

	Deflections			Maximum strains (% of steel yield strain)	Maximum crack width, negative moment region (in.)
	Maximum deflection (in.)	Flexural Cracking (Yes/No)	Clear span to deflection ratio		
DT	0.03	No	4290	15	0.005
1.25DT	0.04	No	3080	20	0.007
1.5DT	0.05	No	2550	20	0.009
2.2DT	0.07	Yes	1690	40	0.013

Table 5.3 Summary of 6-in. top reinforcement spacing PCPE with SEJ: Negative-moment test

	Deflections			Maximum strains (% of steel yield strain)	Maximum crack width, negative moment region (in.)
	Maximum deflection (in.)	Flexural Cracking (Yes/No)	Clear span to deflection ratio		
DT	0.026	No	4620	7	0.007
1.25DT	0.03	No	3640	10	0.007
1.5DT	0.04	No	3080	11	0.007
2.2DT	0.06	Yes	2150	17	0.009

Table 5.4 Summary of 6-in. top reinforcement spacing PCPE with AJ: Negative-moment test

	Deflections			Maximum strains (% of steel yield strain)	Maximum crack width, negative moment region (in.)
	Maximum deflection (in.)	Flexural Cracking (Yes/No)	Clear span to deflection ratio		
DT	0.017	No	5650	4	0.004
1.25DT	0.021	No	4570	8	0.005
1.5DT	0.024	No	4000	9	0.005
2.2DT	0.04	No	2530	21	0.009
3.75DT	0.08	Yes	1280	30	0.01
Failure, 7.2DT	0.24	Yes	400	63	0.013

At a very low load (7.5 kips per load point or 0.6DT) when conducting the first test to serviceability loads, the slab was checked for cracking. At this load, very narrow cracks (maximum 0.002 in. width) were found along the girder and the joints between adjacent PCPs. Calculations were carried out to determine if a load of 0.6DT was sufficient to cause such cracking in the CIP concrete topping. Assuming that typical concrete strains due to shrinkage effects are about 300 με, and adding the effects of the applied loads, it was found that such low applied loads would produce cracking at locations where shrinkage stresses developed. Therefore since testing was done before shrinkage cracking had developed, it is likely that small additional stresses from the first loading and the tensile stresses due to restrained shrinkage effects caused the CIP concrete topping to crack at such a low load.

For all test areas, flexural cracking was first observed at loads above design levels. As shown in the Tables 5.1-5.4, the crack widths were larger at service load levels for the test area with 6-in. top reinforcement spacing. The test area with smaller top reinforcement spacing, 3-7/8 in., provided better control of crack widths at service load levels.

Figure 5.2 shows the locations of major cracks in the two negative moment regions that were taken to failure. For the 8-ft girder spacing, 3-7/8 in. top reinforcement spacing, a punching shear failure initiated at the end load plate of the interior bay at 6.0DT (75 kips). The failure surface formed at the end load and then propagated toward the interior plate.

At the 8-ft girder spacing with the armor joint (AJ) and 6-in. top reinforcement spacing, punching shear failure initiated at the interior load plate of the exterior bay at 7.2DT (90 kips). The failure surface formed around the interior load plate, 4 ft from the armor joint, and propagated toward the end load plate. This failure surface indicates that the presence of the armor joint had an effect on the punching shear capacity.

Failure mechanisms were similar for the negative moment loadings. Punching shear failure occurred in the region between the load points and the closest girder. With an armor joint test area, punching shear failure began at the load point away from the end. There was a 20% difference between the failure loads for the two test areas.

Punching shear capacities can be calculated using design provisions detailed in the ACI-318 code. Design provisions and predictions of capacity for all tests on this specimen are discussed in Chapter 6.

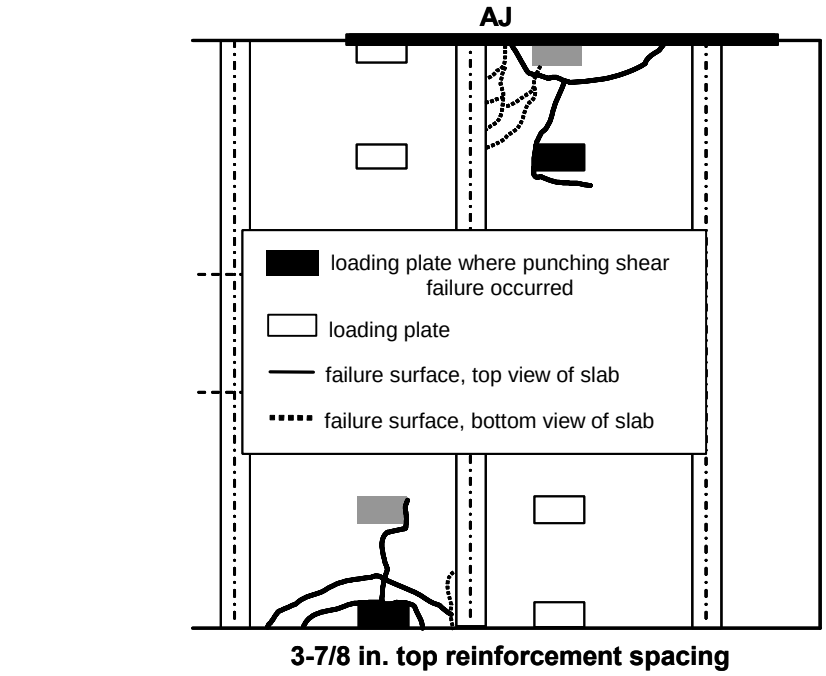

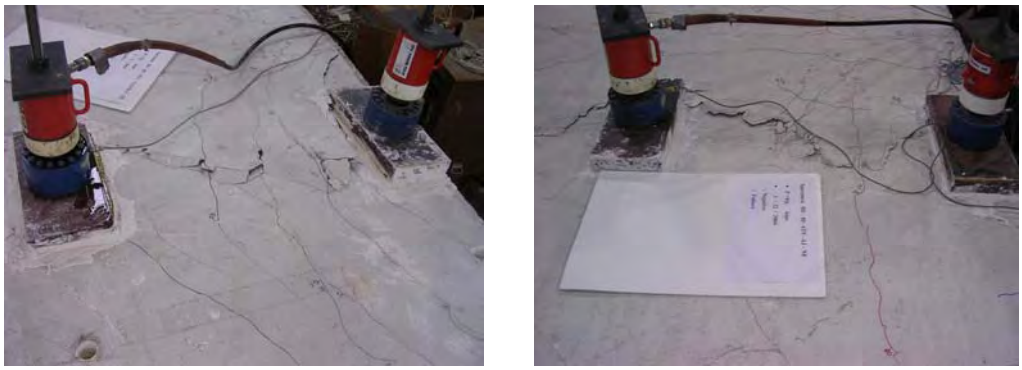

(a) 3-7/8 in. top reinforcement spacing (b) Armor Joint

Figure 5.2 Locations of punching shear failures of PCPE specimens: Negative-moment tests

5.3 POSITIVE-MOMENT TESTS

Similar to the 0^o skew specimen, positive moment was maximized at midspan in the 10-ft bay by applying two point loads in the end region. Figure 5.3 shows the deflection envelopes for the two positive moment tests. The sealed expansion joint (SEJ) end detail was somewhat stiffer than the end detail (6-in. top reinforcement spacing) without the sealed expansion joint. Deflections at the DT load levels were almost 1.5 times larger in the area without an expansion joint than test areas with the SEJ. However, both deflections were relatively small compared to the girder spacing (1/2000 for the test area without SEJ and 1/3000 for the test area with SEJ).

Tensile strains at DT and 1.25DT were small, less than 10% of the yield strain for both test areas. Strains were approximately 2.5 times higher in the test area without SEJ compared to the test area with SEJ at design load levels, where the SEJ contributed to the capacity of the end region. No yielding of the reinforcing steel was observed. As mentioned in Section 2.5.2.1, strains measured during the testing were measured only on the top flexural reinforcing bars over the girder. Strands in the PCPs were not

instrumented. Strains summarized in Tables 5.5 and 5.6 are not likely to be the maximum strain levels in the test area, but are only intended to provide a relative guide to the maximum strain levels in the test areas.

For both test areas, flexural cracking was first observed around 2.2DT. In both tests, first flexural cracking caused a very small change in slab stiffness. The major change in stiffness coincided with multiple cracks forming and widening, and did not occur until approximately 3.75DT. The cracks were fewer and wider in the test area without SEJ than those where the SEJ was used.

Figure 5.4 shows the locations of major cracks at failure in both of the test areas where positive moment was maximized. Both test areas failed in punching shear, at 5.4DT (68 kips) for the test area without SEJ and 6.8DT (85 kips) for the test area with SEJ.

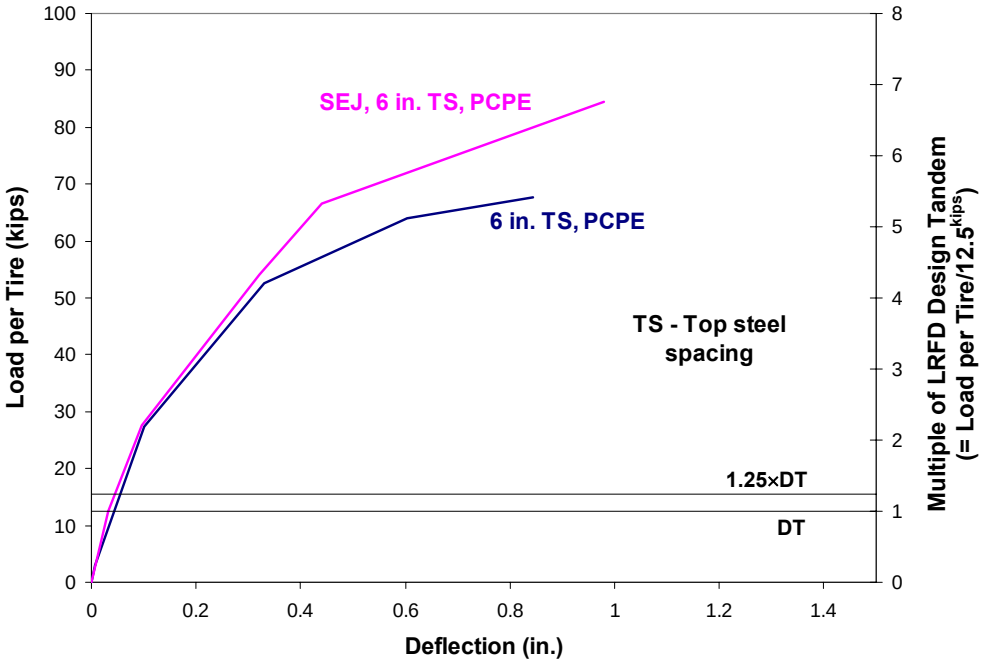

Figure 5.3 Deflection envelopes of PCPE specimens: Positive moment tests

Table 5.5 Summary of positive-moment region with 6-in. top reinforcement spacing PCPE

	Deflections			Maximum strains (% of top steel yield strain)	Maximum crack width, negative moment region (in.)
	Maximum deflection (in.)	Flexural Cracking (Yes/No)	Clear span to deflection ratio		
DT	0.06	No	2070	8	N/A
1.25DT	0.07	No	1770	15	N/A
1.5DT	0.09	No	1330	16	N/A
2.2DT	0.10	Yes	1200	16	0.003
3.75DT	0.28	Yes	430	37	0.01
Failure, 5.4DT	0.84	Yes	150	67	0.025

Table 5.6 Summary of positive-moment region with SEJ and 6-in. top reinforcement spacing PCPE

	Deflections			Maximum strains (% of top steel yield strain)	Maximum crack width, negative moment region (in.)
	Maximum deflection (in.)	Flexural Cracking (Yes/No)	Clear span to deflection ratio		
DT	0.04	No	3080	3	N/A
1.25DT	0.05	No	2450	6	N/A
1.5DT	0.06	No	2000	7	N/A
2.2DT	0.10	Yes	1200	12	0.002
3.75DT	0.25	Yes	480	22	0.007
Failure, 6.8DT	1.01	Yes	120	67	0.03

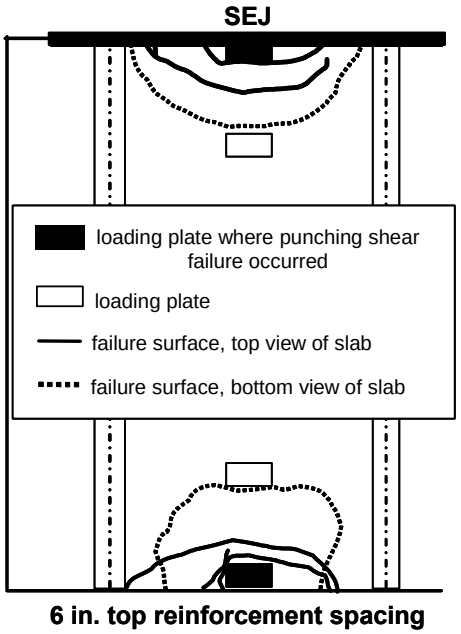

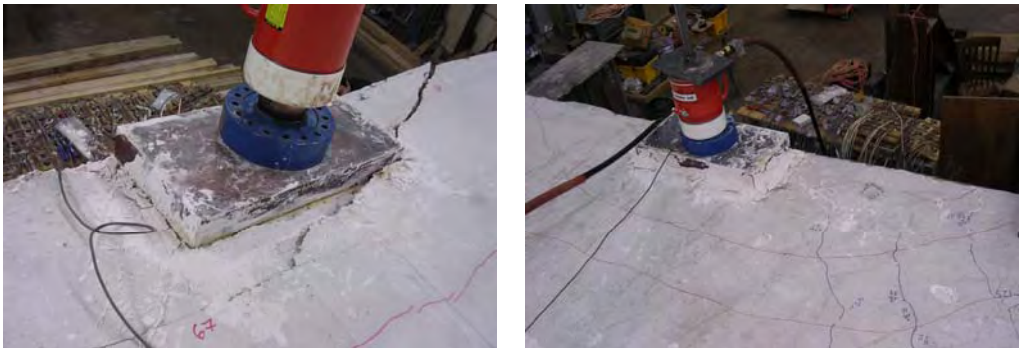

(a) 6-in. top reinforcement spacing (b) Sealed expansion joint

Figure 5.4 Locations of punching shear failures of PCPE specimens: Positive-moment tests

The SEJ end region had a higher capacity than the end region without the SEJ. The 25% difference in capacities is mostly likely due to the contribution of the SEJ. Each end region had a similar failure surface around the end load plate. Both test areas showed some signs of delamination, although the delamination was greater in the test area without the expansion joint than the test area with the SEJ. A section of the panel spalled off in both test areas near the interior girder at failure in both test areas.

5.4 COMPARISON OF RESPONSES OF IBTS, UTSE AND PCPE DETAILS

The primary objective of the study was to understand the behavior of the IBTS end detail at expansion joints, as well as investigate the alternate end details including the UTSE detail and details using stay-in-place PCPs –PCPE detail. In this section, the change in overall performance of the IBTS, UTSE, and PCPE details on a 0^o skew slab under an increase in design load levels and the inclusion of PCPs in the end detail are discussed. In addition, the effects on the AJ and SEJ expansion joints on cracking loads, deflections, reinforcing bar stress levels, and failure loads are addressed.

5.4.1 Load-Deflection Behavior

Load-deflection envelopes for all test areas are shown in Figure 5.5. As seen in Figure 5.5, the PCPE details have a slightly lower stiffness than the IBTS and UTSE details in the negative moment test areas. For the positive moment test areas, all details showed nearly identical initial slab end stiffnesses. Relative end deflections for all test areas measured at DT and 1.25DT load levels were extremely small compared to the girder spacing (less than 1/1700). Relative end deflections measured at midspan at design and overload levels for both details are summarized in Tables 5.7 and 5.8.

Increasing design loads from DT to 1.25 DT had an insignificant effect on the relative slab end deflection measured in all test areas. For the negative moment test areas (8-ft girder spacings), the deflections were small compared to the girder spacing (1/3000). The UTSE end detail had smaller deflections in the 8-ft girder spacing than the IBTS and PCPE details. For positive bending test, 10-ft girder spacing, the IBTS detail and the PCPE detail with the SEJ had smaller deflections than the UTSE detail and the other PCPE details. The maximum service-deflection allowed by AASHTO LRFD provisions (AASHTO 2.5.2.6.2) is 1/800. For negative bending tests performed in the 8-ft girder spacings, slab end deflections reached this level at loads ranging between 3.75DT (55 kips) to 5.6DT (70 kips). For the 10-ft girder spacings, positive moment region, slab end deflections reached this deflection at loads about 2.5DT (31 kips) to 3.6DT (45 kips).

The inclusion of the expansion joints resulted in lower end deflections at failure compared to the PCPE details without the expansion joints. The larger top reinforcement spacing (6 in.) resulted in a larger maximum end deflection than was observed for the end detail with 3-7/8 in. top reinforcement spacing.

5.4.2 Reinforcement Strains

The maximum tensile strains measured at DT, 1.25DT and overload levels for both details are summarized in Tables 5.9 and 5.10. For all tests performed on both details, tensile strains were less than 15% (330 με) of the yield strain at 1.25 DT load level. For all tests, the strain levels at both DT and 1.25DT load levels were insignificant, and the increase in strains between DT and 1.25DT load levels was slight. Instrumented reinforcement reached yield strains in the IBTS end regions, both negative and positive moment regions, and the PCPE regions with 3-7/8 in. top reinforcement spacing, negative moment-region. In the other PCPE regions and the UTSE end regions, the instrumented reinforcing bars did not reach yield strain. Strains measured on the expansion joints indicated the joints contributed to the distribution of stresses throughout the end regions. Strains measured on the reinforcing bars in the end regions with SEJ or AJ were smaller compared to reinforcing bar strains in regions without SEJ or AJ.

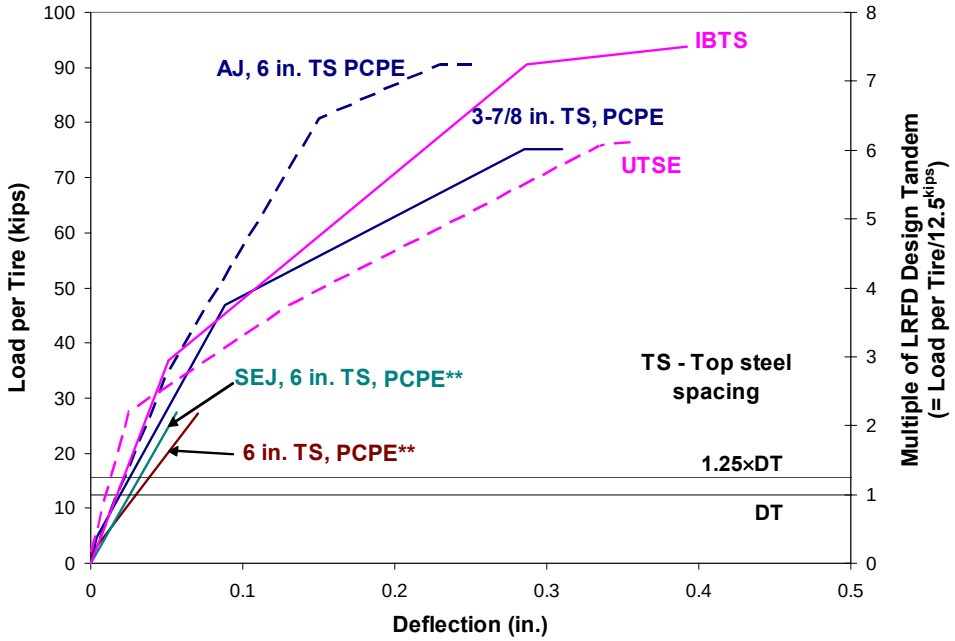

(a) negative moment test areas

** test area was only loaded to service load levels

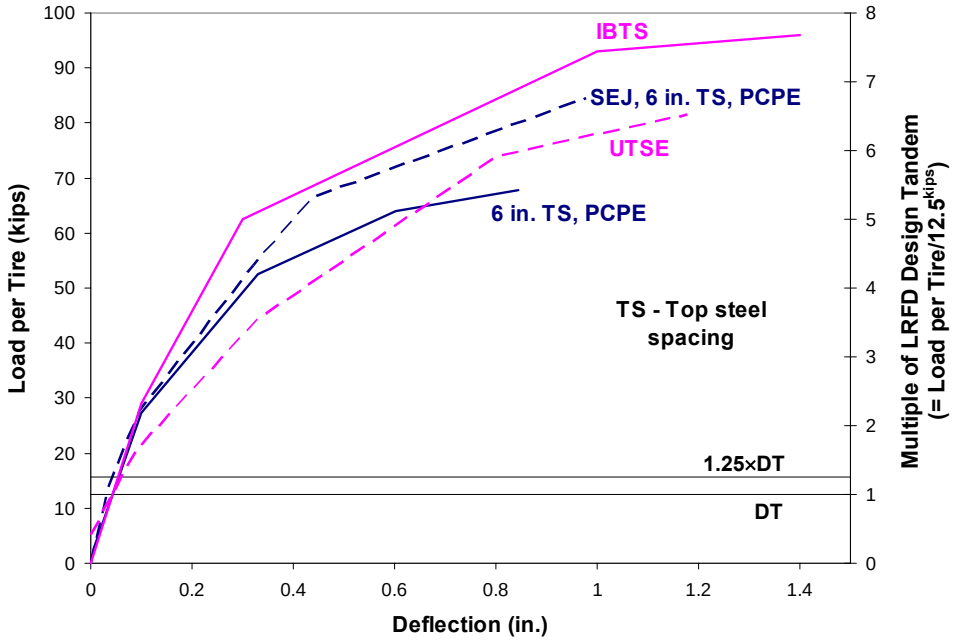

(b) positive moment test areas

IBTS detail – 10 in. thick, all other details – 8 in. thick

Figure 5.5 Deflection envelopes for 0° skewed specimens

Table 5.7 Measured end deflections for 0° skewed specimens: Negative moment tests (in.)

	IBTS	UTSE	3-7/8 in. TS, PCP	6 in. TS, PCPE*	SEJ, PCPE*	AJ, PCPE
DT	0.016	0.006	0.021	0.028	0.026	0.017
1.25DT	0.02	0.008	0.026	0.04	0.03	0.021
1.5DT	0.03	0.02	0.04	0.05	0.04	0.024
2.2DT	0.04	0.05	0.04	0.07	0.06	0.04
3.75DT	0.09	0.13	0.09	N/A	N/A	0.08
Failure	0.39	0.36	0.37	N/A	N/A	0.24

* test areas were only loaded to service load levels

Table 5.8 Measured end deflections for 0° skewed specimens: Positive moment tests (in.)

	IBTS	UTSE	6 in. TS, PCPE	SEJ, PCPE
DT	0.03	0.03	0.06	0.04
1.25DT	0.05	0.07	0.07	0.05
1.5DT	0.06	0.07	0.09	0.06
2.2DT	0.08	0.14	0.10	0.20
3.75DT	0.16	0.34	0.28	0.25
Failure	1.40	1.18	0.84	1.01

Table 5.9 Maximum measured tensile strains over the girder for 0° skewed specimens: Negative moment tests (% of top steel yield strain)

	IBTS[+]	UTSE[+]	3-7/8 in. TS, PCP	6 in. TS, PCPE*	SEJ, PCPE*	AJ, PCPE
DT	4	3	6	15	7	4
1.25DT	4	4	7	20	10	8
1.5DT	6	8	7	20	11	9
2.2DT	18	15	9	40	17	21
3.75DT	44	37	37	N/A	N/A	30
Failure	$>\varepsilon_y$	71	$>\varepsilon_y$	N/A	N/A	63

[+]Strain measurement made at centerline of girder and may not be the maximum strain

- Test areas were loaded only to service load levels

Table 5.10 Maximum measured tensile strains over girder for 0° skewed specimens: Positive moment tests (% of top steel yield strain)

	IBTS+	UTSE+	6 in. TS, PCPE*	SEJ, PCPE*
DT	6	7	8	3
1.25DT	8	10	15	6
1.5DT	10	12	16	7
2.2DT	14	20	21	12
3.75DT	31	40	37	22
Failure	$>\varepsilon_y$	74	67	67

+Strain measurement made at centerline of girder and may not be the maximum strain

* strain measurement made at edge of PCPs

5.4.3 Crack Formation

First cracking loads are summarized in Table 5.11. Based on test results, slab ends with any detail can be expected to remain uncracked under DT and 1.25DT design loads for slab with and without panels and slabs constructed with 8-ft girder spacings. For specimens tested with 10-ft girder spacings, first cracking loads were reduced, except for the PCPE details with the different top reinforcement spacings, the 6-in. top reinforcement spacing end detail had a higher cracking load than the 3-7/8 in. top reinforcement spacing end detail. Even though most of the first cracking loads were lower in the 10-ft girder spacings than the 8-ft girder spacings, the loads still remained above DT. The lower first cracking loads in the 8-ft girder spacings may be attributed to significant positive moments imposed due to applied loads in order to maximize negative moment in the 8-ft girder spacings.

Table 5.11 First cracking loads for 0° skewed specimens: IBTS, UTSE and PCPE details

End Detail	Section (Negative or Positive)	First Cracking Load (x DT)
IBTS	Negative	2.6
IBTS	Positive	1.3
UTSE	Negative	2.2
UTSE	Positive	1.5
3-7/8 in. TS, PCP	Negative	1.8
6 in. TS, PCPE	Positive	2.8
AJ, PCPE	Negative	2.8
SEJ, PCPE	Positive	2.2

For all test regions, cracks were first observed at loads between 1.3DT and 2.8DT. In the positive moment test areas, first cracking caused a minor reduction in stiffness of the slab end. However, first cracking did not cause a noticeable difference in stiffness in the negative moment test areas. Significant changes in stiffness did not occur until loads greater than 1.6DT.

A distinct crack pattern began to emerge as applied loads were increased after a significant change in stiffness occurred. Cracks in the IBTS test regions were usually fewer and wider than the cracks

occurring in the UTSE test regions. The crack patterns in the PCPE details were similar, but wider compared to the cracks developed in the UTSE detail test regions. Crack widths at design, overload and failure load levels are shown in Tables 5.12 and 5.13. These widths were measured from the tests performed, and are intended to serve only as a comparative index of crack severity.

Table 5.12 Measured crack widths for 0° skewed specimens: Negative moment tests (in.)

	IBTS	UTSE	3-7/8 in. TS, PCP	6 in. TS, PCPE*	SEJ, PCPE*	AJ, PCPE
DT	N/A	N/A	0.007	0.005	0.007	0.004
1.25DT	N/A	N/A	0.007	0.007	0.007	0.005
1.5DT	N/A	N/A	0.007	0.009	0.007	0.005
2.2DT	N/A	HL	0.009	0.013	0.009	0.009
3.75DT	0.002	0.003	0.013	N/A	N/A	0.01
Failure	0.018	0.009	0.02	N/A	N/A	0.013

*Test areas were loaded only to service load levels

Table 5.13 Measured crack widths for 0° skewed specimens: Positive moment tests (in.)

	IBTS	UTSE	6 in. TS, PCPE	SEJ, PCPE
DT	N/A	N/A	N/A	N/A
1.25DT	HL	HL	N/A	N/A
1.5DT	0.002	0.002	N/A	N/A
2.2DT	0.003	0.003	0.003	0.002
3.75DT	0.008	0.007	0.01	0.007
Failure	0.033	0.04	0.25	0.03

5.4.4 Failure

All end regions failed in punching shear. The UTSE and PCPE details failed at loads 20 to 30% lower than failure loads recorded for the IBTS detail (Figure 5.6). According to the punching shear provisions of the AASHTO LRFD and ACI 318-02, shear capacity is proportional to the distance from the extreme compressive fiber to the centroid of the tensile reinforcement. This distance in the IBTS detail is 2 in. greater than the corresponding distances in the UTSE and PCPE details. Based on this punching-shear model, for identical punching shear failure surfaces, the capacity of an IBTS section should be higher than that of a UTSE and PCPE sections. The test results support this hypothesis, as the punching shear capacity of the UTSE and PCPE details were less than those of the IBTS detail slab ends for similarly configured test sections. However, end details in the PCP specimen with the expansion joints had higher punching shear capacities than the UTSE details for similarly configured test areas.

In addition to the section depth, the flexural reinforcement ratio of a section may influence the punching shear capacity (CEB-FIP 6.4-18). The flexural reinforcement ratio of the UTSE detail was higher than the IBTS detail. The flexural reinforcement ratio of the PCPE detail with the expansion joints are difficult to quantify, but were significant enough that the punching shear capacity of the end regions were higher than those of the UTSE detail (Figures 5.1, 5.3, 5.5 and 5.6). The expansion joints act as shear

reinforcement as well, which increase the punching shear capacity of the end region. Also, the prestressing strands of the PCPE regions increased the punching-shear capacity when compared to the typical 8 in. CIP section (UTSE). Although test results reflect the influence of flexural reinforcement ratio, the tests were too limited to allow for study of the relationship between the ratio and punching-shear capacity. All test results, regardless of end detail, showed the reserve strength of the slab end greatly exceeds AASHTO design load levels.

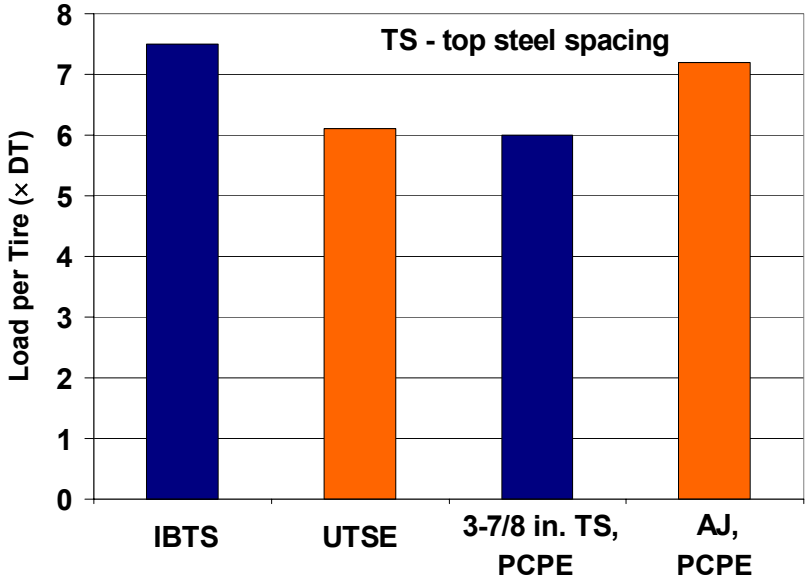

(a) negative moment tests

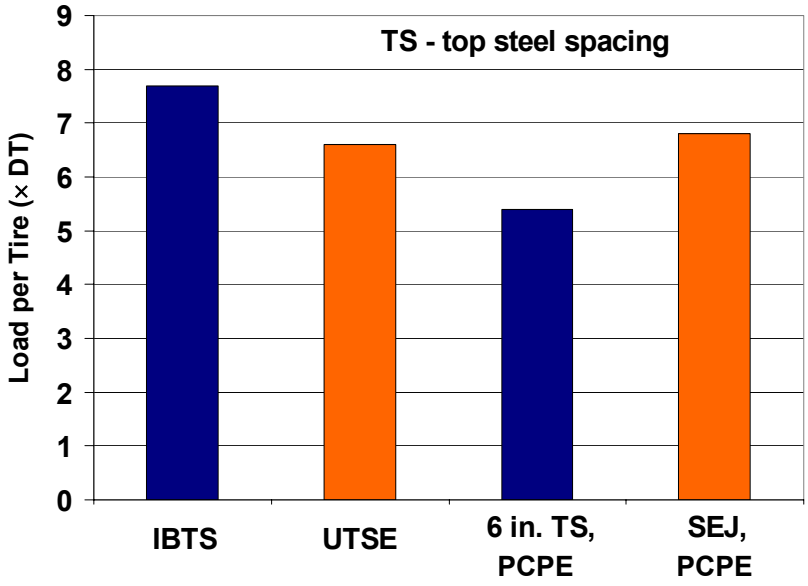

(b) positive moment tests

Figure 5.6 Failure loads

5.5 SUMMARY

Comparisons have been made between the cast-in-place details, IBTS and UTSE, and the PCPE details. At design loads, the PCPE details performed as well or better than the standard IBTS and alternate UTSE details. At design loads, the deflections were small compared to the girder spacing for all the details (less than 1/1700). Overall, the load-deflection responses of the PCPE details were similar to the cast-in-place details. Almost all PCPE details had higher first flexural cracking loads than the IBTS and UTSE details. The cracking patterns in the PCPE detail test areas were similar to the UTSE detail, but crack widths were larger. Overall, the strains measured in the PCPE details were similar to strains measured in the UTSE detail. The PCPE details all failed in punching shear around load levels similar to the UTSE detail, since both details had the same slab thickness (8 in.). All details reached failure at loads well above design load levels. In cases where SEJ and AJ were used, they acted as shear reinforcement, which increased the punching shear capacity of the end region. In addition, the precast prestressed panels used in the PCPE detail increased the punching-shear capacity when compared to the UTSE detail.

CHAPTER 6:
PUNCHING SHEAR STRENGTH OF BRIDGE DECKS AT SLAB ENDS

6.1 INTRODUCTION

All tests terminated with failure in punching shear, with the exception of the IBTS detail in the positive-moment region of the 45° skewed specimen, which failed in one-way (beam) shear. The punching-shear capacities were predicted using Section 5.13.3.6 and 5.8.3.3 of the AASHTO LRFD Bridge Design Code (and Sections 11.8.6 and 11.12 of the ACI 318-02 code). Punching shear is generally not intended to be the controlling failure mechanism in design. In this chapter, the related punching shear provisions are introduced and predicted punching shear capacities for slab end regions by the use of concentric and eccentric shear models are discussed.

6.2 CONCENTRIC SHEAR MODEL: AASHTO AND ACI PROVISIONS

As discussed in Section 3.3.1, the IBTS detail in the positive-moment region (10-ft girder spacing) on the 45° skewed specimen failed in one-way shear. The difference in failure mechanism could be attributed to the geometry of the test specimen and the consequent torsional moments. However, test data is too limited to quantify these effects on their influence of behavior.

The beam-shear strength of bridge slabs is addressed in Section 5.8.3.3 of the AASHTO LRFD Bridge Design Code and reviewed here. That section requires that Equation 6.1a be used for calculating the nominal beam-shear capacity of a nonprestressed section without shear reinforcement. In that equation, b is the length of the critical perimeter, a minimum distance of d/2 from the load plate; d is the distance between the extreme compression fiber and longitudinal reinforcement in tension; f_c' is the specified compressive strength of concrete in ksi at 28 days; and β is 2 for a nonprestressed section. These provisions are similar to those of ACI 318-02 Section 11.8.6 (Equation 6.1b).

$$V_c = 0.0316\beta\sqrt{f_c'}\cdot b_v d_v \; ; \qquad (f_c' \text{ in ksi}) \qquad \textit{Equation 6.1a}$$

$$V_c = \beta\sqrt{f_c'}\cdot b_v d_v \; ; \qquad (f_c' \text{ in psi}) \qquad \textit{Equation 6.1b}$$

Using Equation 6.1, one-way nominal shear capacities for the positive moment test on the 45° skewed specimen was calculated for a section 68 in. wide for the IBTS detail. The predicted nominal capacity of the IBTS section was 72 kips. Using the bounding cases illustrated in Figure 3.5, an elastic analysis indicates shear at the location of failure to be between 47 kips for simple supports and 69 kips for a fixed support. The beam-shear capacity predicted using AASHTO LRFD and ACI 318-02 provisions is between 0.65 and 0.95 times the measured capacity. Figure 6.1 shows the end that failed in one-way shear during testing.

6.3 OBSERVED BEAM-SHEAR CAPACITY COMPARED TO CALCULATED NOMINAL CAPACITY BY AASHTO AND ACI PROVISIONS

Nominal punching-shear stress is calculated using Section 5.13.3.6 of the AASHTO LRFD Bridge Design Code, shown in Equation 6.2.

$$v_c = \min\left\{0.126\sqrt{f_c'}\,;\left(0.063+\frac{0.126}{\beta_c}\right)\sqrt{f_c'}\right\} \qquad (f_c' \text{ in ksi}) \qquad \textit{Equation 6.2}$$

Figure 6.1 Shear failure: IBTS detail, positive-moment test, 45° skew

The AASHTO LRFD expressions are the practically the same as those prescribed by ACI 318-02 in Section 11.12 for a uniform shear distribution (Equation 6.3). ACI 318-02 has one additional equation, and requires that punching shear stress be computed as the minimum of the terms in Equation 6.3.

$$v_c = \min\left\{4\sqrt{f_c'};\left(2+\frac{4}{\beta_c}\right)\sqrt{f_c'};\left(\frac{\alpha_s d}{b_o}+2\right)\sqrt{f_c'}\right\} \text{ (fc' in psi)} \qquad \textit{Equation 6.3}$$

where f_c' is the specified concrete compressive strength; b_o is the length of the critical perimeter; d is the effective depth of the slab; α_s is 40 for interior loading cases and 30 for end loading cases; and β_c is the ratio of the length of the longest side of the loaded area to the shorter side. Based on these parameters, the nominal punching-shear capacity of the slab is:

$$V_c = v_c b_o d \qquad \textit{Equation 6.4}$$

ACI 318-02 and the AASHTO LRFD Bridge Specification require the critical perimeter to be calculated at a distance d/2 from the end of the loading point. For loading at the end of a slab, the minimum critical perimeter, shown in Figure 6.2, includes three sides of the loading plate (Ryan 2003 and Griffith 2003).

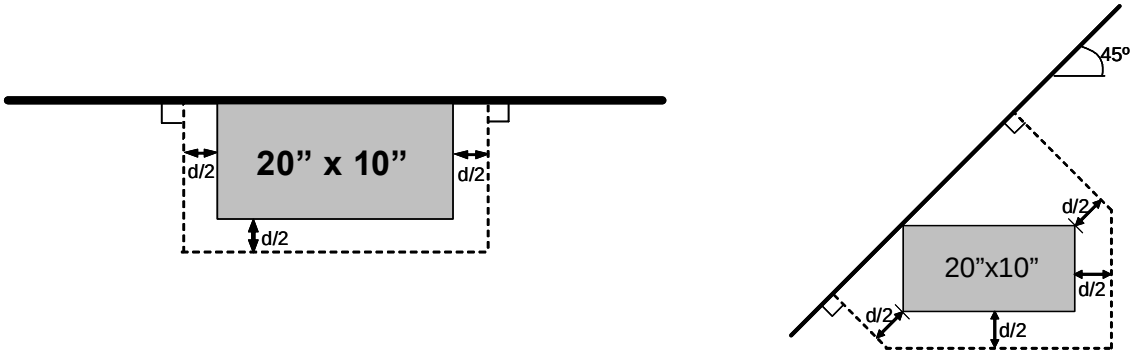

(a) 0° skew (b) 45° skew

Figure 6.2 Critical perimeter used to determine punching-shear capacity with uniform stress distribution on the perimeter of the critical section

The observed punching-shear capacities from the test areas failing in punching shear are compared with the nominal capacity by ACI 318-02 provisions (Equations 6.3 and 6.4), assuming a uniform shear distribution on the perimeter of the critical section are shown in Table 6.1 and Figure 6.3.

Table 6.1 Calculated and experimental punching shear capacities

End Detail	Section depth (in.)	Skew Angle	Plate size (in.)	Moment Maximized	f_c' (psi)	V_{calc}^+ (kips)	V_{exp} (kips)	V_{calc} / V_{exp}
IBTS	10	0^o	10 x 20	Negative	6000	141	94	1.50
IBTS	10	0^o	15 x 20	Positive	6000	166	96	1.73
IBTS	10	45^o	10 x 20	Negative	4000	137	94	1.46
UTSE	8	0^o	10 x 20	Negative	6000	99	77	1.29
UTSE	8	0^o	15 x 20	Positive	6000	118	82	1.44
UTSE	8	45^o	10 x 20	Negative	4000	101	68	1.49
UTSE	8	45^o	10 x 20	Positive	4000	101	55	1.84
3-7/8 in. TS	8	0^o	10 x 20	Negative	4550	84	75	1.12
6 in. TS	8	0^o	10 x 20	Positive	4550	84	68	1.24
AJ	8	0^o	10 x 20	Negative	4550	84	91	0.92
SEJ	8	0^o	10 x 20	Positive	4550	84	85	0.99

*TS – top steel spacing
+ACI or AASHTO

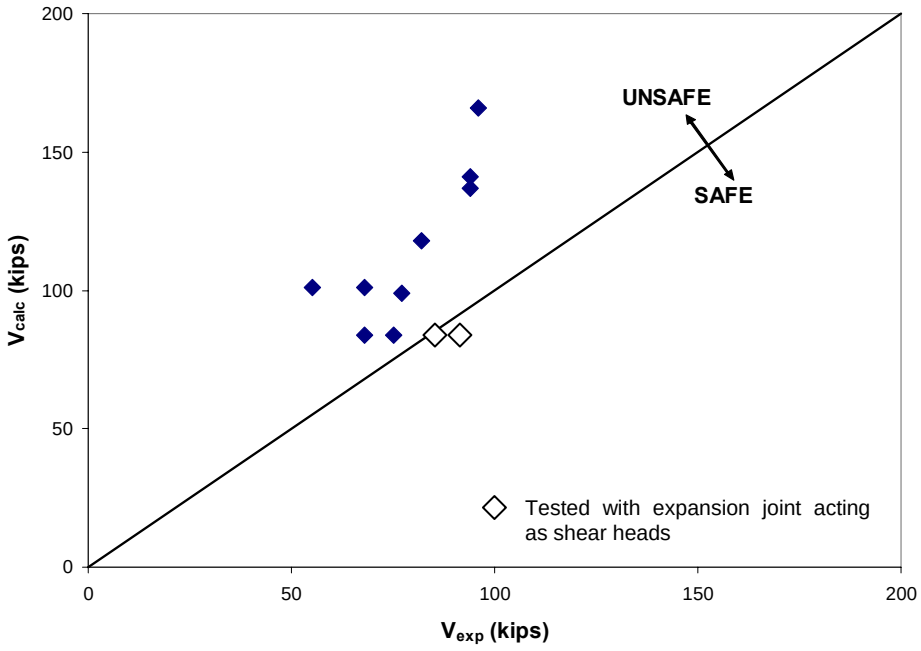

Figure 6.3 Comparisons of ACI 318-02 concentric predictions with experimental results

For the details on the PCPE detail, the contribution of the AJ and SEJ were not included in the nominal capacities computed by ACI 318-02 and AASHTO provisions similar to TxDOT design procedures, since AJ and SEJ were not used as shear reinforcement in design. Although AJ and SEJ were not provided to serve as shear reinforcement, they contributed to the shear strength, as discussed in Section 5.4.4. However, their contribution to the shear strength is not easy to quantify and should not be relied on as part of common design practice. For these reasons and for the sake of simplicity, the contribution of AJ and SEJ to shear strength was ignored.

The concrete compressive strength was adjusted to account for the CIP topping and the PC panels. For most of the test areas, the assumption of uniform stress distribution result in unsafe predictions of punching shear capacity. The punching shear capacity of the bridge slab, loaded with an AASHTO load configuration, ranges from about 45% to 85% of that predicted by ACI 318-02 and AASHTO LRFD provisions assuming a uniform shear stress distribution.

The shape of the critical section assumed in the analysis above for punching shear did not adequately predict the shape of the failure surface for the end loading configuration in the three specimens. Figure 6.4 shows the shape of a typical failure surface, as observed from the top of the slab. Figure 6.5 shows the failure surfaces as observed from the side of the slab. In the observed failure surfaces, the critical perimeter is longer than that used in the previous calculations. ACI 318-02 uses an eccentric shear model to account for this, assuming that a portion of the unbalanced moment is transferred though an eccentricity of shear around the loaded area. A conservative prediction of ultimate strength might be attained by varying the shape of the critical perimeter and applying the eccentric shear model.

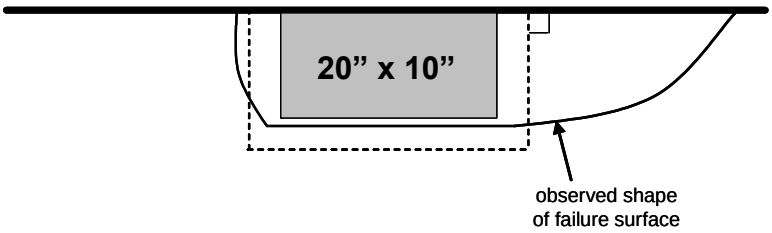

(a) 0° skew

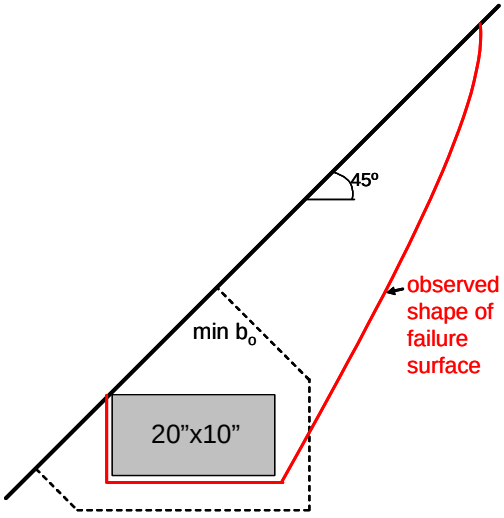

(b) 45° skew

Figure 6.4 Comparison of critical section based on ACI 318-02 and typical experimental failure surface

(a) 0^o skew

(b) 45^o skew

(c) PCP specimen

Figure 6.5 Failure pictures from test specimens: Side view of slab

6.4 ECCENTRIC SHEAR MODEL: ACI 318 PROVISIONS

As discussed in the previous section, the uniform shear stress distribution assumed by the AASHTO and ACI 318-02 codes for punching-shear capacity of bridge slabs yields unconservative values. One reason being that the location of the critical section centroidal axis and the centroidal axis of the loaded area do not coincide for slab end loading cases. Therefore, unbalanced moments resulting from this eccentricity naturally occur at loading areas at ends. In punching-shear strength predictions, the correct use of the code expressions would require the use of the eccentric shear stress model suggested for design of slab-column connections transferring moment. The following two sections discuss the use of the eccentric shear stress model in 0^o skewed slabs and 45^o skewed slabs.

6.4.1 Eccentric Shear Stress Model Applied to 0^o Skewed Slabs

The eccentric shear stress model in ACI 318-02 (Section 11.12.6.2) assumes that a portion of the unbalanced moment is carried by the eccentricity of the shear around the loading area. In the case of combined shear and unbalanced moment, occurring due to the eccentricity of the applied load, the shear stress at the critical perimeter located d/2 away from the loaded area is computed using the following equation:

$$v_u = \frac{V_u}{b_o d} + \frac{\gamma_v (V_u e)}{(J / c_{CD})} \qquad \textit{Equation 6.5}$$

where V_u is the gravity shear, b_o is the length of the critical perimeter, e is the distance between the centroidal axis of the critical section and the centroidal axis of the loaded area as shown in Figure 6.6. The term J is analogous to the polar moment of inertia and is given as follows for end loading areas (Equation (13-27) from MacGregor 1997):

$$J = \frac{d\left(c_1 + d/2\right)^3}{6} + \frac{\left(c_1 + d/2\right)d^3}{6} + 2\left(c_1 + d/2\right)d\left[\frac{\left(c_1 + d/2\right)}{2} - c_{AB}\right]^2 + d\left(c_2 + d\right)c_{AB}^2 \qquad \textit{Equation 6.6}$$

in which c_1 is the side length of the loading area perpendicular to the free end, c_2 is the side length of the loading area parallel to the free end, and d is the effective depth of the slab. According to Figure 6.6, the critical shear stress occurs at the free end of the loading area and this shear stress needs to be checked against the concrete strength.

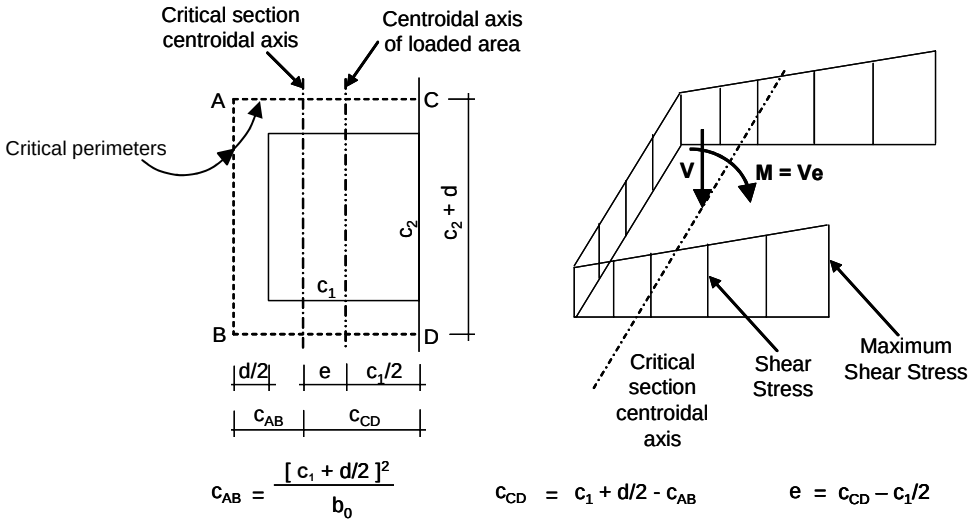

Figure 6.6 Shear stress resistance mechanism at end loading areas

The γ_v factor, to compute the portion of the unbalanced moment transferred by eccentricity of shear, is given by the following equation for end loading cases:

$$\gamma_v = 1 - \frac{1}{1 + \left(\frac{2}{3}\right)\sqrt{\frac{(c_1 + d/2)}{(c_2 + d)}}} \qquad \textit{Equation 6.7}$$

Punching failure is assumed to occur when the critical stress, v_u, computed from Equation 6.5 exceeds the shear strength, v_c, given in Equation 6.3. Rearranging Equation 6.5, the ultimate punching shear strength of an end loading area can be calculated as follows:

$$V_u = \frac{v_c}{\left(\frac{1}{b_0 d} + \frac{\gamma_v e}{J / c_{CD}}\right)} \qquad \textit{Equation 6.8}$$

Punching shear strength predictions based on Equation 6.5 through 6.8 are reported in Table 6.2. Comparisons of code predictions are shown in Figure 6.7 and Table 6.2. Comparisons with the concentric shear stress model are shown in Figure 6.8. According to the predictions of ACI 318-02, when the eccentric shear stress model is used, ultimate strength predictions are in general agreement with the experimental results and are conservative.

6.4.2 Eccentric Shear Stress Model Applied to Skewed Slabs

Similar to the eccentric shear stress model on 0^o skewed slabs, the expressions for skewed slabs consider the effect of unbalanced moments that are produced when the centroid of the loaded area does not coincide with the centroid of the critical perimeter. When the slab end is skewed with respect to the loaded area, unbalanced moments occur in two directions as a result of the asymmetry of the critical perimeter. As seen in Figure 6.9, the geometry of the critical perimeter needs to be considered in developing equations to predict the punching shear capacity using the eccentric shear model on skewed slabs. However, this geometry is complex and is beyond the scope of this project.

Table 6.2 Calculated and experimental punching shear capacities: Eccentric shear stress model, 0^o skewed slabs

End Detail	Section depth (in.)	Plate size (in.)	Moment Maximized	f_c' (psi)	V_{calc} (kips)	V_{exp} (kips)	V_{calc} / V_{exp}
IBTS	10	10 x 20	Negative	6000	78	94	0.83
IBTS	10	15 x 20	Positive	6000	99	96	1.03
UTSE	8	10 x 20	Negative	6000	56	77	0.72
UTSE	8	15 x 20	Positive	6000	71	82	0.87
3-7/8 in. TS PCPE	8	10 x 20	Negative	4550	48	75	0.64
6 in. TS PCPE	8	10 x 20	Positive	4550	48	68	0.71
6 in. TS AJ PCPE	8	10 x 20	Negative	4550	48	91	0.53
6 in. TS SEJ PCPE	8	10 x 20	Positive	4550	48	85	0.56

* TS – top steel spacing

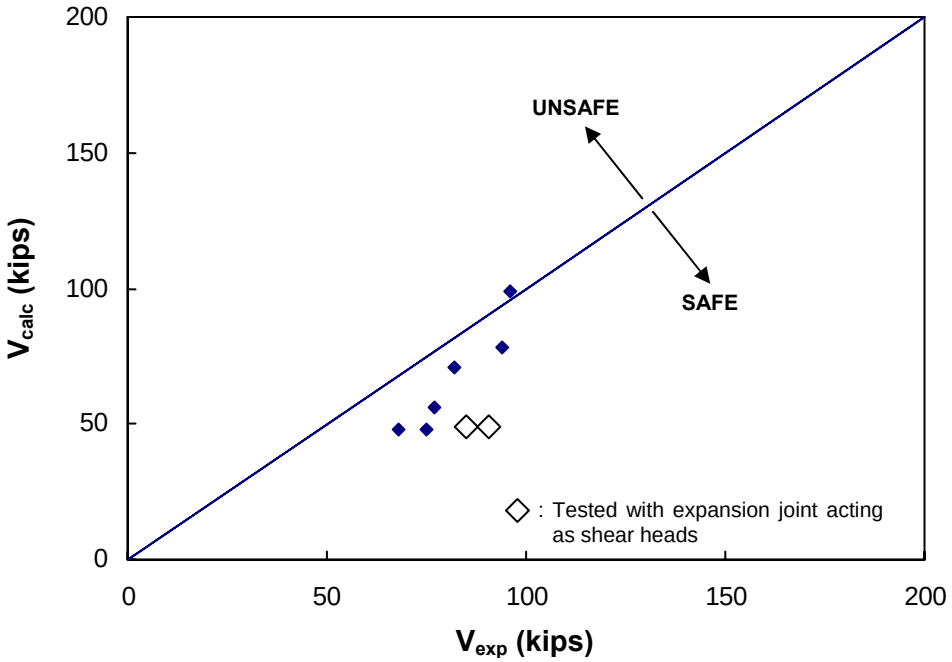

Figure 6.7 Comparisons of ACI 318-02 predictions using the eccentric shear stress model with experimental results, 0^o skewed slabs

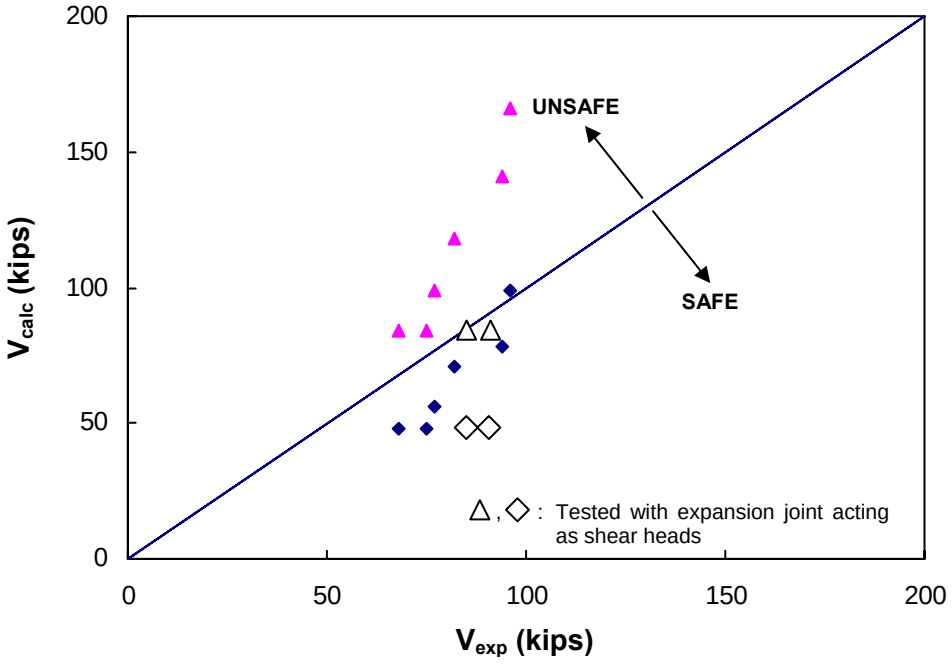

Figure 6.8 Comparison of concentric and eccentric shear stress models with the experimental results, 0^o skewed slabs

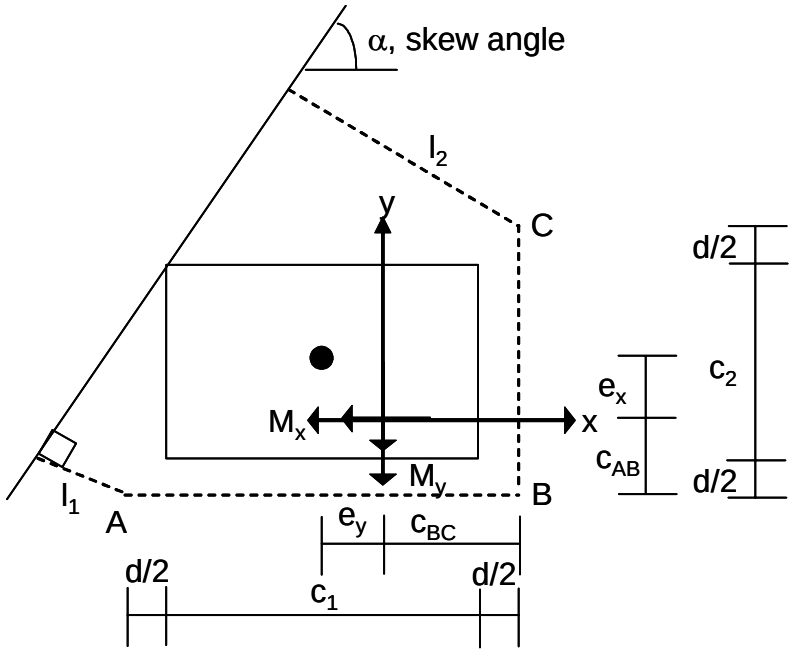

Figure 6.9 Shear stress resistance mechanism at end loading areas on skewed slabs

6.5 SUMMARY

The punching shear provisions in the AASHTO LRFD Bridge Design Code and ACI 318-02 are based on a concentric shear model. However, when calculating the punching-shear capacity of a slab end region, the eccentric shear model provides a better prediction of actual capacity for 0^o skewed slabs than the concentric shear model. When the eccentric shear model is applied to skewed slab ends, the geometry of the critical perimeter should be considered in predicting the punching-shear capacity, but is beyond the scope of this project and should be investigated further. It is also interesting to note that the strain measurements of flexural reinforcing bars indicated that reinforcing bars yielded prior to the punching shear failure. These measurements indicate flexural reinforcing bars contributed to the punching shear capacity of bridge deck specimens. The effect of the amount of flexural reinforcing bars on punching shear capacity was not investigated, since it is beyond the scope of this project. Instead, the structural performances of the existing TxDOT slab end detail (IBTS) and new end details (UTSE and PCPE) were studied.

CHAPTER 7:
OVERHANG TESTS

7.1 INTRODUCTION

In addition of testing the slab ends at expansion joints, full-scale tests were conducted to study the performance of standard TxDOT details for overhangs. A total of eight overhang areas were tested on 45° skewed and PCP specimens. As in TxDOT design standards, breakbacks were constructed in the acute-angle corners of the slab. Because overhangs were not tested in the 0º skewed specimen, two tests were developed to simulate a 0º skewed overhang in the obtuse-angle corners of the 45° skewed slab. Overhang reinforcement was detailed according to TxDOT standards for PC panel bridge decks, with and without armor and sealed expansion joint joints (AJ/SEJ). In this chapter, results from the overhang tests are presented and discussed.

7.2 45° SLAB TEST SPECIMENS

For the 45º skewed specimen, four overhang tests were performed:

(1) 45º skewed breakback overhang: IBTS detail

(2) 45º skewed breakback overhang: UTSE detail

(3) Simulated 0º skewed overhang: IBTS detail

(4) Simulated 0º skewed overhang: UTSE detail

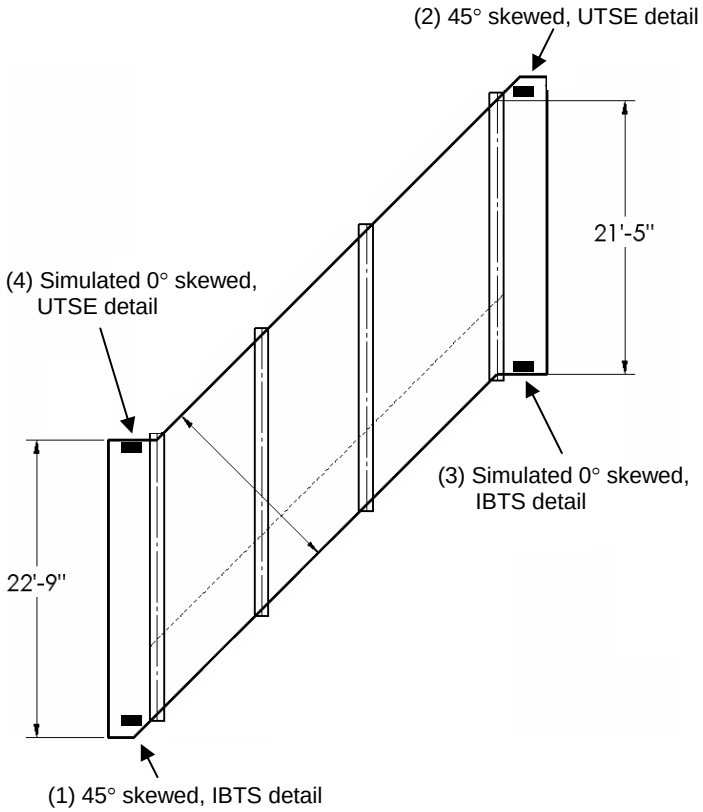

Figure 7.1 Overhang test locations: 45° skewed specimen

Two overhangs incorporated the UTSE detail, and the other two, the TxDOT IBTS detail. In the UTSE overhangs, 12 transverse reinforcing bars were placed 2.3 in. (58 mm) from the top of the slab, and 12 were placed 1.63 in. (41 mm) from the bottom of the slab. All transverse end reinforcement in the UTSE detail was continuous into the overhangs, parallel to the slab end. To illustrate how the transverse reinforcement is bent in the overhangs, a plan view of the top mat of the UTSE transverse reinforcement is shown in Figure 7.2 (a) and (b).

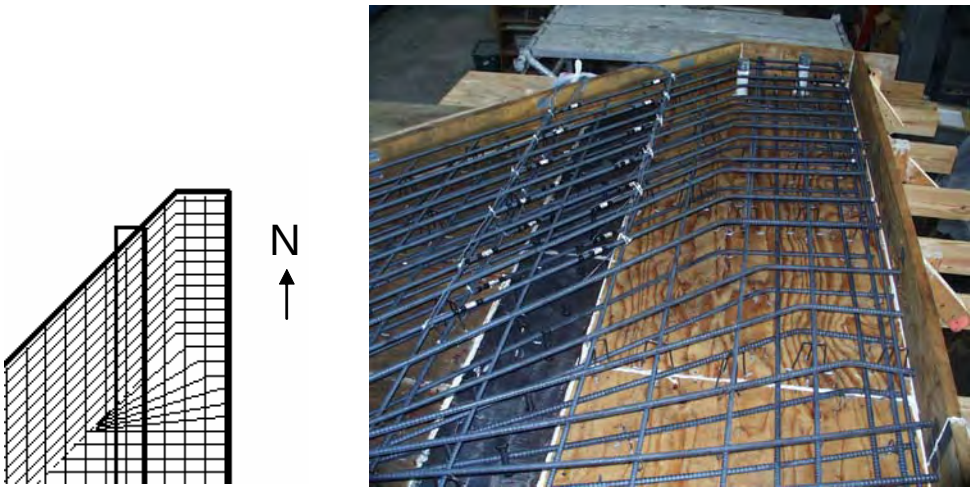

(a) plan view (b) picture

Figure 7.2 UTSE overhang reinforcement: Top and bottom mats

In the TxDOT detail, the depth of the slab was reduced from 10 in. in the IBTS end detail to 8 in. in the overhang. This 2-in. reduction prevented the bottom transverse reinforcement from continuing into the overhang. Instead, four No. 5 bars were placed parallel to the end in the overhang, 1.63 in. from the bottom of the slab. The 8 transverse reinforcing bars in the top mat were 2.3 in. (58 mm) from the top of the slab, and were continuous into the overhang.

7.2.1 Breakback Corners

For slabs constructed with skews greater than 15º, TxDOT design standards require breakbacks at bridge slab corners. "Breakback" is the term used by TxDOT to describe an alternate, simplified method of constructing the acute-angle corners of a skewed slab (Figure 7.3). In this detail, the slab end is perpendicular to the girders for a transverse distance of 2 ft (607 mm), beyond which it is skewed. All transverse reinforcement in the overhang is parallel to the slab end.

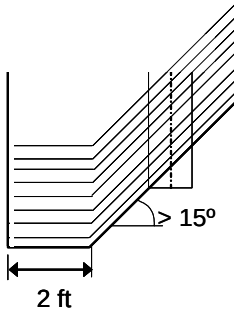

Figure 7.3 Breakback overhang layout

7.2.2 Simulated 0º Skewed Corners

In the 0º skewed specimen, overhangs were constructed but not tested, so the obtuse-angle overhang corners in the 45º skewed specimen were built to simulate corners with zero skew. These corners are similar to the breakback corners, but the reinforcement is bent at the centerline of the girder. A layout of these corners as built in the specimen is shown in Figure 7.4.

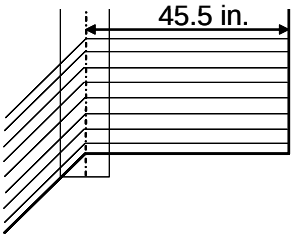

Figure 7.4 Simulated zero skewed overhang

7.3 PCPE TEST SPECIMEN

For the PCPE test specimen, four overhang tests were performed (Figure 7.5):

(5) 3-7/8 in. top reinforcement spacing

(6) 6 in. top reinforcement spacing

(7) Armor expansion joint (AJ)

(8) Sealed expansion joint (SEJ)

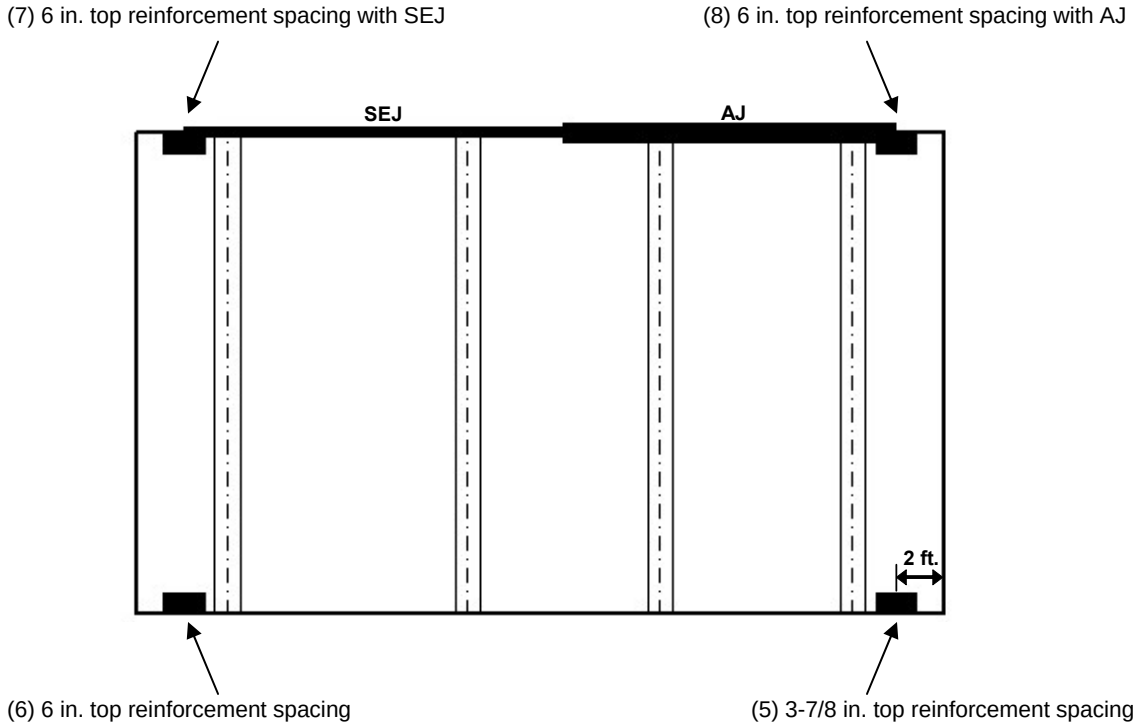

Figure 7.5 Overhang test locations: PCPE specimen

Overhang Test 1 included 12 flexural reinforcing bars placed 2.3 in. from the top of the slab and spaced 3-7/8 in. on center. Overhang Tests 2, 3 and 4 had 8 flexural reinforcing bars spaced 6 in. on center. Overhang Tests 3 and 4 included either the AJ or SEJ, where the joints extended into the overhang, 24 in. from the slab end. All top flexural reinforcement was continuous into the overhangs, parallel to the slab end. Additional 4 ft long No.4 bars were coupled with each top flexural reinforcing bar in the overhang. In TxDOT details for bridge decks with PCP, all overhangs are cast-in-place and have a minimum depth of 8 in. The change to full-depth CIP overhangs from the composite panel section required bottom reinforcement to be placed prior to casting (Figure 7.6).

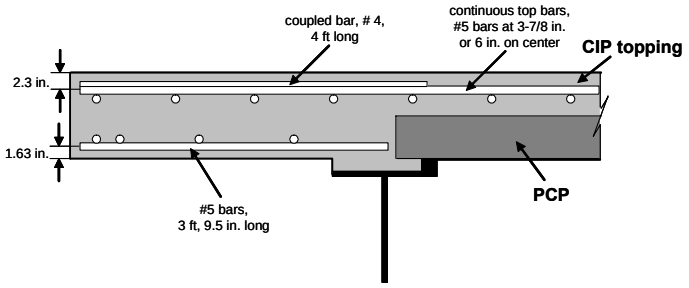

Figure 7.6 Example of overhang reinforcement

7.3.1 Overhang Length

The standard overhang length of a TxDOT highway bridge is 3 ft (914 mm), measured from the centerline of the girder to the slab edge. Designs using AASHTO provisions do not require the center of the loading footprint to be placed in the outer 2 ft of the overhang. The 2-ft distance represents the nominal width of a guardrail (1 ft) and the distance from the edge of a group of tires to the center (1 ft). Therefore, in a standard 3-ft overhang, the center of a load plate could be placed at most 1 ft from the centerline of the beam. For the 20- by 10-in. loading plate footprint required by AASHTO, most of the loading plate would be located directly over the beam, a case not of interest for this research (Figure 7.7(a)).

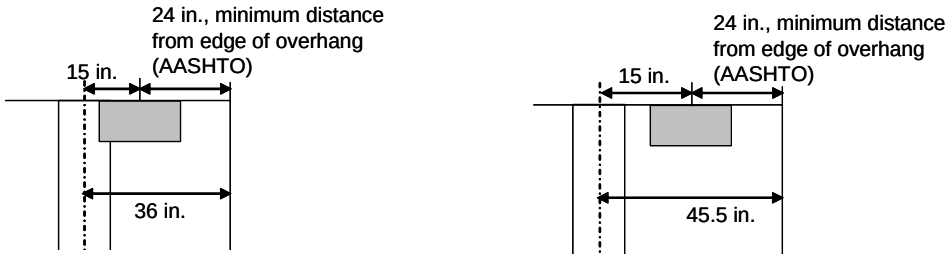

(a) Standard 36-in. overhang (b) 45.5-in. overhang

Figure 7.7 Loading plate locations

In a horizontally curved bridge with 120’ straight beams and a radius of 600 ft, overhangs might be as much as 45.5 in. wide measured from the edge of the girder. Figure 7.7(b) shows the location of the loading footprint for a 45.5-in overhang. This extreme, rare case was the basis for the construction of the 45.5-in overhangs in the 45º skewed specimen, enabling the load plate to be placed further toward the edge of the overhang. The capacity of the extended overhang was tested with the center of the load plate placed 24 in. from the edge of the overhang, as shown in Figure 7.8.

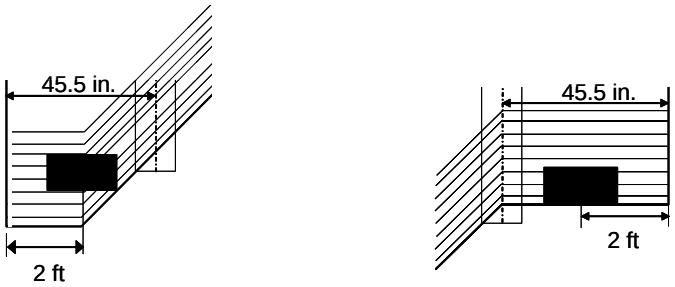

(a) Breakback corner (b) Simulated 0° skewed corner

Figure 7.8 Loading plate location

In a similar way, the overhang length was extended to 45.5 in. for PCP specimen.

7.4 TEST RESULTS

7.4.1 45° Breakback Overhang: IBTS Detail

The breakback IBTS overhang failed in one-way shear at 2.75DT (45 kips). Cracks formed parallel to the skewed slab end. Yielding of reinforcement in tension was first detected at 2.5DT (40 kips) on the west side of the girder (the side closest to the load plate). The tip deflection at DT was 0.21 in. and at 1.25DT was 0.27 in. Crack patterns indicate that torsion played an important role in the inelastic range of the load-deflection response.

7.4.2 45° Breakback Overhang: UTSE Detail

The breakback UTSE overhang had the lowest capacity of all the overhang corners tested, failing in punching shear at 2.3DT (36 kips). Yield of reinforcement first occurred at 2.1DT (34 kips). The maximum measured strain, on the east side of the girder, was 115% of the yield strain. Strains at 1.25DT were as much as 2.3 times strains at DT.

7.4.3 Simulated 0º Skewed Overhang: IBTS Detail

The simulated 0º skewed IBTS overhang failed in punching shear at 3.25DT (51 kips). Tip deflection was 0.12 in. at DT and 0.2 in. at 1.25DT. Extensive cracking occurred over the girder during testing, causing several strain gauges to malfunction at approximately 2.25DT. No strain gauge reached yield strain in reinforcement before malfunctioning or before specimen failure, and the maximum strain in this test area, 73% of yield strain, was measured at 2.25DT. Strains at DT and 1.25DT were small (less than 10% of yield strain).

7.4.4 Simulated 0º Skewed Overhang: UTSE Detail

The simulated 0º skewed UTSE overhang failed in punching shear at 3.4DT (54 kips). Tip deflection was 0.15 in. at DT and 0.21 in. at 1.25DT. Steel reinforcement yield was not detected at a single location on the west side of the girder, but the maximum measured strain on the east side of the girder was 2.2 times the yield strain. While strains at 1.25DT were up to twice the corresponding strains at DT, all were less than 10% of yield strain.

7.4.5 3-7/8 in. Top Reinforcement Spacing: PCPE Detail

The 3-7/8 in. top reinforcement spacing PCPE overhang failed in one-way shear at 4.5DT (72 kips). Cracks on the top surface of the slab formed parallel to the face of the girder and then bent towards the edge of the slab. Cracks on the bottom surface formed perpendicular to the cracks on top of the slab. Reinforcing bars near the slab end reached yield strains around 4DT (64 kips). The tip deflection at DT was 0.08 in. and at 1.25DT was 0.10 in. The maximum tip deflection at failure was 0.97 in. Crack patterns indicate that torsion played an important role in the failure of the overhang.

7.4.6 6 in. Top Reinforcement Spacing: PCPE Detail

The 6 in. top reinforcement spacing PCPE overhang failed in one-way shear at 3.75DT (60 kips). Cracks on the top surface of the slab formed parallel to the face of the girder and then bent towards the edge of the slab. Cracks on the bottom surface formed perpendicular to the cracks on top of the slab. The tip deflection at DT was 0.14 in. and at 1.25DT was 0.16 in. The maximum tip deflection at failure was 1.19 in. Crack patterns indicate that torsion played an important role in the failure mechanism of the overhang.

7.4.7 6 in. Top Reinforcement Spacing: PCPE Detail with SEJ

The 6 in. top reinforcement spacing PCPE overhang with SEJ failed in one-way shear at 5.1DT (82 kips). Cracks on the top surface of the slab formed parallel to the face of the girder and then bent towards the edge of the slab. Cracks on the bottom surface formed perpendicular to the cracks on top of the slab. Reinforcement near the slab end reached yield strain around 4.5DT (72 kips). The tip deflection at DT was 0.09 in. and at 1.25DT was 0.11 in. The maximum tip deflection at failure was 1.34 in. Crack patterns indicate that torsion played an important role in the failure mechanism.

7.4.8 6 in. Top Reinforcement Spacing: PCPE Detail with AJ

The 6 in. top reinforcement spacing PCPE overhang with AJ failed in one-way shear at 5.4DT (85 kips). Cracks on the top surface of the slab formed parallel to the face of the girder and then bent towards the edge of the slab. Cracks on the bottom surface formed perpendicular to the cracks on top of the slab. None of the measured flexural reinforcement reached yield strain before failure. The tip deflection at DT was 0.09 in. and at 1.25DT was 0.10 in. The maximum tip deflection at failure was 1.07 in. Crack patterns indicate that torsion played an important role in the failure mechanism.

7.5 DISCUSSION AND COMPARISON OF OVERHANG TEST RESULTS

Results from overhang tests are summarized in Table 7.1. At failure, both the IBTS and the UTSE breakback overhangs failed in one-way shear at the girder at load levels near 2.5DT. Both the IBTS and UTSE simulated 0° skewed overhangs failed in punching shear at load levels near 3.25DT. All the PCPE overhang test areas failed in one-way shear near the girder between 3.75DT and 5.4DT. Additionally, strain levels and tip deflections were similar for both breakbacks and both simulated 0° skewed overhangs.

The choice of the IBTS versus UTSE detail has only an insignificant effect on overhang capacity and failure mode. Both breakback overhangs behaved similarly, and both simulated 0º skewed overhangs behaved similarly. As in the interior span tests, cracks in the UTSE overhang were more closely spaced and narrower than those in the IBTS overhang. Though the crack patterns were not identical, differences between them were slight. Overall, the similarities in response indicate that the choice of reinforcement details at the overhang (IBTS versus UTSE) have little effect on overhang behavior.

Table 7.1 Summary of results from overhang tests

	Failure load (kips)	Failure mechanism	Strain (% of yield strain)			Tip Deflection (in.)		
			DT	1.25DT	at failure	DT	1.25DT	at failure
Breakback-IBTS	44 (2.75DT)	one-way shear	30	38	132	0.21	0.28	1.3
Breakback-UTSE	37 (2.4DT)	one-way shear	38	53	116	0.30	0.41	-
Simulated 0° Skew-IBTS	51 (3.25DT)	punching shear	3.2	18	-	0.12	0.20	2.2
Simulated 0° Skew-UTSE	54 (3.4DT)	punching shear	6.2	9.7	-	0.15	0.22	2.7
3-7/8 in. top reinforcement spacing (OH Test 1)	72 (4.5DT)	one-way shear	4.6	6.0	130	0.08	0.10	0.97
6 in. top reinforcement spacing (OH Test 2)	61 (3.75DT)	one-way shear	11	13	160	0.14	0.16	1.19
SEJ & 6 in. top reinforcement spacing (OH Test 3)	82 (5.1DT)	one-way shear	5.3	6.2	125	0.09	0.11	1.34
AJ & 6 in. top reinforcement spacing (OH Test 4)	85 (5.4DT)	one-way shear	4.0	5.3	66	0.09	0.10	1.07

In contrast, pronounced differences in behavior were observed between breakback overhangs and simulated 0º skewed overhangs. In overhangs with the same end detail (IBTS or UTSE), cracks at loads near failure in the simulated 0° skewed overhangs were significantly wider than in the breakback overhangs. This may be due to the location of the bend in the reinforcement, as shown in Figure 7.9. In the breakback overhang, this bend occurs beneath the middle of the load plate. In the simulated 0° skewed overhangs, the bend occurs over the girder. As applied loads are increased, the top reinforcement in the simulated 0° skewed overhang begins to straighten out, producing local forces in the concrete perpendicular to the skewed end and cracking along the bars as shown in Figure 7.10. These local forces cause much damage over the girder where wide cracks were observed. The resulting reduction in the flexural capacity of the overhang at the girder significantly influenced the behavior of the overhang at failure load levels and was probably decreased the overhang capacity. In a true 0° skewed deck overhang, the reinforcement would not have been bent at the overhang, and this effect would not have been present.

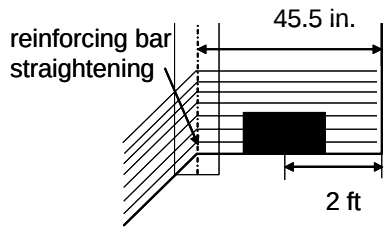

Figure 7.9 Location of reinforcement straightening: Simulated 0° skewed overhang

Figure 7.10 Failure of simulated 0º skewed UTSE overhang: Top view of slab, facing north

At equivalent load levels, reinforcing-bar strains in the breakback details were as much as 10 times the corresponding strains in the simulated 0º skewed overhangs. Although external applied moments are the same for both configurations, the different orientation of the reinforcement in the two sections results in different resistances against the external applied moment. The most efficient orientation of the reinforcement would be perpendicular to the girder, as in the simulated 0° skewed overhang reinforcement orientation, but without the bends in the bars. The orientation of the reinforcement in the breakback overhang results in a reduced efficiency, increased stress, and increased strain (Figure 7.11).

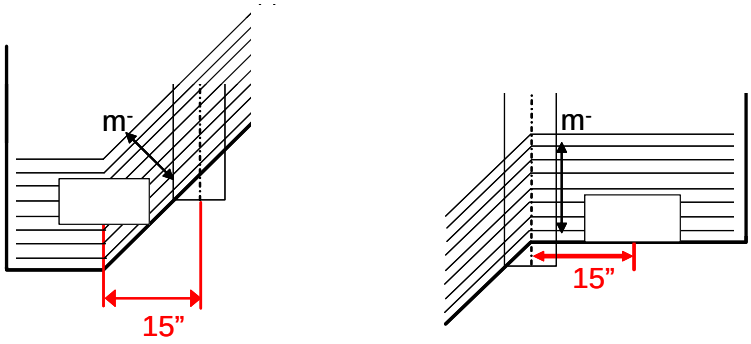

(a) Breakback overhang (b) Simulated 0° skewed overhang

Figure 7.11 Length of reinforcement between load plate and girder

At service load levels, tip deflections were significantly larger in the breakback overhangs than in the simulated 0° skewed overhangs, due to the lower longitudinal stiffness of the breakback overhang. At loads near failure, however, tip deflections in the simulated 0º skewed overhangs were much larger than those of the breakback overhangs. This can be attributed to the extensive cracking experienced in the simulated 0° skewed overhangs, and not in the breakback overhangs.

Crack patterns in the breakback and simulated 0° skewed overhangs indicate that moments were distributed differently in the different overhang corners, but that flexural and torsional cracks formed in every test section. In the breakback overhangs, flexural cracking was observed over the girder. Torsional

cracks, oriented perpendicular to the skewed slab end, were visible primarily on the top of the deck. No cracking was visible on the bottom of the breakback overhangs, with the exception of a single crack in the IBTS breakback overhang.

In the simulated 0° skewed overhangs, flexural cracks formed over the girder, and multiple torsional cracks formed on the top and bottom of the deck. While all overhang crack patterns indicated torsional cracking, more torsional cracks formed in the simulated 0° skewed overhangs. When cracking over the girder became extensive, the flexural capacity of the section was severely reduced, forcing the redistribution of forces in the form of torsion.

All the PCPE overhangs behaved similarly with cracks forming parallel to the girder and then bending towards the edge of the slab. As in the slab end tests, the cracks in the 3-7/8 in. top reinforcement spacing test area were more closely spaced and narrower than the cracks measured in the 6 in. top reinforcement spacing test area. The cracks were narrower and more closely spaced in the two test areas with the AJ and SEJ than the two areas without the joints. Cracks formed at design load levels in the test areas without expansion joints, and for test areas with expansion joints, cracking was first visible at loads beyond the design load levels. Load-deflection responses for all tests were similar at design load levels.

Overall the behavior of the overhang area depended on the top reinforcement spacing and the presence of AJ or SEJ. The test areas with AJ and SEJ behaved similarly and had only a 4% difference in the failure loads. The tip deflections were nearly identical up to failure, where the depth of AJ and SEJ (4 in. vs. 6 in.) made a difference in the tip deflection near and at failure. The two test areas without AJ or SEJ had capacities approximately 28% less than the two test areas with AJ and SEJ. The tip deflection was 1.2 times larger in the 6 in. top reinforcement spacing test area than the 3-7/8 in. top reinforcement test area. There was a 15% difference between the failure loads of the two reinforcement spacing test areas. The 6 in. top reinforcement spacing test area was the only region that measured yielding of any reinforcement.

7.6 SUMMARY

The four overhang corners on the 45º skewed specimen were tested to failure. The two acute slab corners were constructed with breakbacks, a detail used by TxDOT. The two obtuse slab corners were constructed to simulate the overhangs in a 0º skewed slab, as the overhangs were not tested in the 0º skewed specimen. To test the worst-case overhang length, the length of both overhangs was extended from the standard 36 in. to 45.5 in.

Based on the test results, the choice of the IBTS versus UTSE end detail has little effect on the behavior or capacity of the overhang corner. Regardless of the end detail, the capacity of the breakback overhangs was about 2.5DT, and the capacity of the simulated 0º skewed overhangs, about 3.25DT.

In the tests performed in overhangs constructed to simulate 0º skewed overhangs, reinforcement was bent over the girder. During testing, the tensile reinforcement attempted to straighten out at the bend, causing severe cracking over the girder and a torsional redistribution of forces. This probably decreased the capacity of the section, and would not have been observed in a true 0º skewed overhang.

Based on the test results, all the PCPE overhangs performed well at design load levels. The spacing of the top reinforcement and the presence of expansion joints influenced the load-deflection behavior. The test areas with the expansion joints had a higher capacity and had narrower crack widths. The test area with the smaller reinforcement spacing exhibited smaller deflections. The ultimate capacities of all the test areas ranged from 3.75DT (6 in. top reinforcement spacing) to 5.4DT (AJ and 6 in. top reinforcement spacing).

CHAPTER 8:
SUMMARY, CONCLUSIONS, AND RECOMMENDATIONS

8.1 SUMMARY

TxDOT currently uses the "IBTS" standard detail for bridge slab ends at expansion joints, which eliminates the need for expensive diaphragms. The detail provides additional transverse stiffness by increasing the slab thickness by 2 in. Typical bridge deck construction uses stay-in-place precast prestressed panels (PCP) in the interior of the bridge deck topped with a 4 in. concrete slab. The beginning panel location is approximately 6 ft from the expansion joint allowing for a 4 ft wide thickened slab. At the slab ends, formwork is needed for the full-depth cast-in-place (CIP) IBTS detail.

The primary objective of this research study was to evaluate the behavior and capacity of the IBTS and alternate 8-in. (Uniform Thickness Slab End) detail at expansion joints, especially on skewed ends of bridge slabs. The two full-scale CIP specimens with 0^o and 45^o skews and 8-ft and 10-ft beam spacings were constructed to test the IBTS and UTSE details. Test results showed that at design load levels, skew had no significant effect on the behavior of the two details. All test areas failed in shear, predominantly punching shear. The UTSE detail failed at slightly lower load levels than the IBTS detail due to a 2-in. difference in section depth. However, both details had ultimate capacities at loads well above the design load levels.

After test results showed that the UTSE detail performed as well as the IBTS detail at design loads and reached ultimate capacities at load levels well above design load levels, a simpler alternate detail was developed using the stay-in-place precast prestressed concrete in the end detail. The use of precast panels in the end regions would eliminate special formwork construction and reduce safety concerns associated with such formwork construction at heights. This slab end detail is named PCPE detail. The full-scale PCPE specimen, 0^o skew, was built since panels cannot be easily incorporated in bridge decks with a skewed end. In addition to the behavior and capacity of the PCPE detail, the effects of armor (AJ) and sealed expansion joints (SEJ) on slab ends at design and ultimate loads were investigated. Test results showed that all slab end details (IBTS, UTSE and PCPE) had capacities far exceeding design loads. The PCPE details without AJ and SEJ failed at loads somewhat lower than the IBTS detail, but the AJ and SEJ increased the ultimate capacity by 20 to 25%.

8.2 CONCLUSIONS

8.2.1 Slab end details

Based on the results of the tests performed at the slab ends of the three specimens, the following conclusions can be drawn about the general behavior of the end details:

- The load-deflection response of decks with the three details was nearly identical at DT and 1.25DT design load levels.
    - At both DT and 1.25DT load levels, tensile strains in the flexural reinforcement and the deflection-to girder spacing ratio were both extremely small (less than 15% of yield strain and 1/1700 respectively).
    - An increase in applied loads from DT to 1.25DT load levels resulted in a nearly proportional increase in midspan deflection and strain reinforcement.
- At 3.75DT load levels, the maximum strains were less than 50% of yield except for the positive moment section of the 45° skew in the UTSE detail where strains reached about 70% of yield

strain. However, the capacity was controlled by either punching shear or one-way shear failure prior to development of yield lines or a flexural failure mechanism.

- Crack widths were larger for the test areas with 6 in. top reinforcement spacing (IBTS and PCPE details) in negative-moment regions. The 3-7/8 in. top reinforcement spacing (UTSE and PCPE details) provided better control of crack widths at the same load levels.
  - Overall, the IBTS detail had fewer and wider cracks than the UTSE detail. The number of cracks in the PCPE detail was similar to the UTSE end detail, but crack widths were larger.
- All details failed in punching shear or one-way shear at loads greater than 3.8DT. The reduced depth of the UTSE and PCPE details resulted in a lower capacity.
- Effects of skew:
  - Skew did not have a significant effect on slab end behavior, except for increased deflections and reinforcement strains at service load levels in the 10-ft bay under positive bending. However, strains were less than 10% yield strain and deflections were less than (girder spacing)/ 800 for both the IBTS and UTSE details at design load levels.
  - For highly skewed slab ends (45°), forces in the end region were distributed through a combination of flexural bending, torsional bending, and shear. This distribution caused slabs to experience more severe cracking and to fail in punching shear at lower loads than slab ends with 0° skew.
- Effect of AJ or SEJ:
  - Midspan slab end deflections were smaller in spans with AJ or SEJ
  - Failure loads were 20 to 25% higher for the PCPE detail with an AJ or SEJ compared with an end detail without expansion joints.

8.2.2 Overhangs

When designing a customary 3' TxDOT overhang with the AASHTO LRFD bridge specifications, a 10- by 20-in. loading plate would be located over the girder. Since this loading configuration would not be a critical situation, the overhang lengths were increased to 45.5 in. to represent an overhang in a bridge with a 120' beam and horizontal curve of 600 ft. Based on the tests of the overhangs, the following conclusions can be drawn:

- Breakback overhangs in 45º skewed specimens failed in one-way shear at approximately 2.0DT (25 kips), and breakbacks in simulated 0º skewed specimens failed in punching shear at about 2.6DT (33 kips). All PCP overhangs failed in one-way shear at loads greater than 3.75DT (61 kips).
- Cracks in UTSE-detail overhangs were narrower and more closely spaced than those in corresponding IBTS-detail overhangs, a trend also observed in the span tests.
- The use of the IBTS and UTSE end details in spans resulted in slightly different overhang reinforcement arrangements, but these had nearly no effect on the ultimate capacity of a section.
- In PCPE overhangs, the use of different top reinforcement spacing and expansion joints resulted in a 30% difference between the failure loads.
- In the tests performed in overhangs constructed to simulate 0º skewed overhangs, reinforcement was bent over the girder. During testing, the tensile reinforcement attempted to straighten out at the bend, causing severe cracking over the girder and a torsional redistribution of forces. This

probably decreased the capacity of the section, and would not have been observed in a true 0º skewed overhang.

8.3 DESIGN RECOMMENDATIONS

The following recommendations are based on the test data gathered for the three specimens.

8.3.1 Recommendations for Implementation

- Bridge slabs designed with the IBTS, UTSE and PCPE performed well at DT and 1.25DT load levels. The increase in design load from DT to 1.25DT does not result in significant changes in performance.
    - For the PCPE details, crack widths were larger in the negative-moment region with 6 in. top reinforcement spacing. However, crack widths are better controlled when smaller top reinforcement spacing, 3-7/8 in., is used in the end region.
- For bridge slabs constructed with girder spacing less than 10 ft and skews less than 45°, cracking can be assumed to be minimal or non-existent under DT and 1.25DT applied loads. When slab ends are subjected to overloads, cracking was minimal (lengths were less than 24 in. and widths smaller than 0.01 in.) until approximately 2.0DT.
- For bridge slab ends constructed with AJ or SEJ, results showed that expansion joints contribute significantly to the behavior and capacity of slab ends. However, excluding the contribution from the expansion joints is a conservative approach.
- All slab end details performed well under typical design and over loads. Based on the test results it can be concluded that for bridge slabs constructed with girder spacing less than 10 ft and skews less than 45°, any bridge slab detail discussed in this research can be successfully implemented in bridge deck construction.

8.3.2 Recommendations for Further Research

- For skewed slabs, the applicability of the ACI 318-02 eccentric shear model is unproven and requires further investigation.
- One-way shear capacity should be checked using AASHTO LRFD design provisions but may result in predicted capacities that are excessively conservative. This procedure resulted in reasonable predictions for the single test where one-way shear failure occurred, but gave results that were too low in some test areas where punching shear failure occurred. The applicability of the AASHTO one-way shear should be investigated further.
- The adhesion at the interface between PCP and CIP concrete topping was sufficient for the section to act as a unit. The flexural resistance and other properties of the PCPE detail are complex, and further investigation is needed to fully understand the properties of the PCPE detail.
- Cracks due to restrained shrinkage are inevitable in bridge decks using PCP. Although, shrinkage cracking has no detrimental effect on capacity and performance, further investigation is needed to develop procedures to reduce cracking and to improve the durability and service life of the deck.
- Although testing indicated the expansion joints contributed significantly to the performance of slab ends, the testing completed in this study is too limited to provide a complete understanding of the transfer of forces from the concrete to the expansion joints, and requires further investigation.

- Previous research on CIP and PCP decking did not include an evaluation of performance of the deck under static and fatigue loading at slab ends. This research study focused on CIP and PCP decking at slab ends under static loading; therefore, fatigue performance of CIP and PCP decking at slab ends needs to be studied.

APPENDIX A:
EXAMPLE OF ECCENTRIC SHEAR CALCULATION

A.1 ACI 318-02 PROVISIONS ON TWO-WAY SHEAR

Nominal punching-shear stress can be calculated using Section 11.12 of ACI 318-02, shown in Equation A.1.

$$v_c = \min\left\{4\sqrt{f_c'};\left(2+\frac{4}{\beta_c}\right)\sqrt{f_c'};\left(\frac{\alpha_s d}{b_o}+2\right)\sqrt{f_c'}\right\} \qquad \textit{Equation A.1}$$

where f_c' is the specified concrete compressive strength in psi; b_o is the length of the critical perimeter; d is the effective depth of the slab; α_s is 40 for interior loading cases and 30 for end loading cases; and β_c is the ratio of the length of the longest side of the loaded area to the shorter side.

The eccentric shear stress model in Section 11.12.6.2 of ACI 318-02 assumes that a portion of the unbalanced moment is carried by the eccentricity of the shear around the loading area. In the case of combined shear and unbalanced moment, occurring due to the eccentricity of the applied load, the shear stress at the critical perimeter located $d/2$ away from the loaded area is computed using the following equation (Figure A.1):

$$v_u = \frac{V_u}{b_o d} + \frac{\gamma_v (V_u e)}{(J / c_{CD})} \qquad \textit{Equation A.2}$$

where V_u is the gravity shear, b_o is the length of the critical perimeter, e is the distance between the centroidal axis of the critical section and the centroidal axis of the loaded area as shown in Figure A.1.

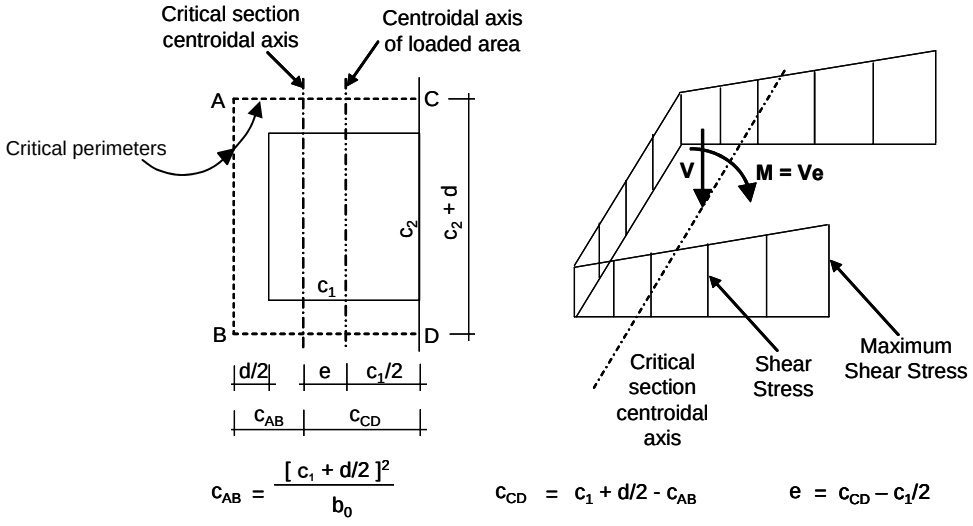

Figure A.1 Shear stress resistance mechanism at end loading areas

The term J is analogous to the polar moment of inertia and is given as follows for end loading areas (Equation (13-27) from MacGregor 1997):

$$J = \frac{d\left(c_1 + d/2\right)^3}{6} + \frac{\left(c_1 + d/2\right)d^3}{6} + 2\left(c_1 + d/2\right)d\left[\frac{\left(c_1 + d/2\right)}{2} - c_{AB}\right]^2 + d\left(c_2 + d\right)c_{AB}^2 \qquad \textit{Equation A.3}$$

in which c_1 is the side length of the loading area perpendicular to the free end, c_2 is the side length of the loading area parallel to the free end, and d is the effective depth of the slab. According to Figure A.1, the critical shear stress occurs at the free end of the loading area and this shear stress needs to be checked against the concrete strength.

The γ_v factor, to compute the portion of the unbalanced moment transferred by eccentricity of shear, is given by the following equation for end loading cases:

$$\gamma_v = 1 - \frac{1}{1 + \left(\frac{2}{3}\right)\sqrt{\frac{(c_1 + d/2)}{(c_2 + d)}}} \qquad \textit{Equation A.4}$$

Punching failure is assumed to occur when the critical stress, v_u, computed from Equation A.2 exceeds the shear strength, v_c, given in Equation A.1. Rearranging Equation A.2, the ultimate punching shear strength of an end loading area can be calculated as follows:

$$V_u = \frac{v_c}{\left(\frac{1}{b_0 d} + \frac{\gamma_v e}{J / c_{CD}}\right)} \qquad \textit{Equation A.5}$$

A.2 EXAMPLE PROBLEM: UTSE WITH PLATE SIZE 20×10

To illustrate the calculation of shear stresses using the eccentric shear model of ACI 318-02, detailed calculations on the shear strength of UTSE slab end detail specimen are provided in this section. The loading configuration through a 20×10 plate and material properties are illustrated in Figure A.2.

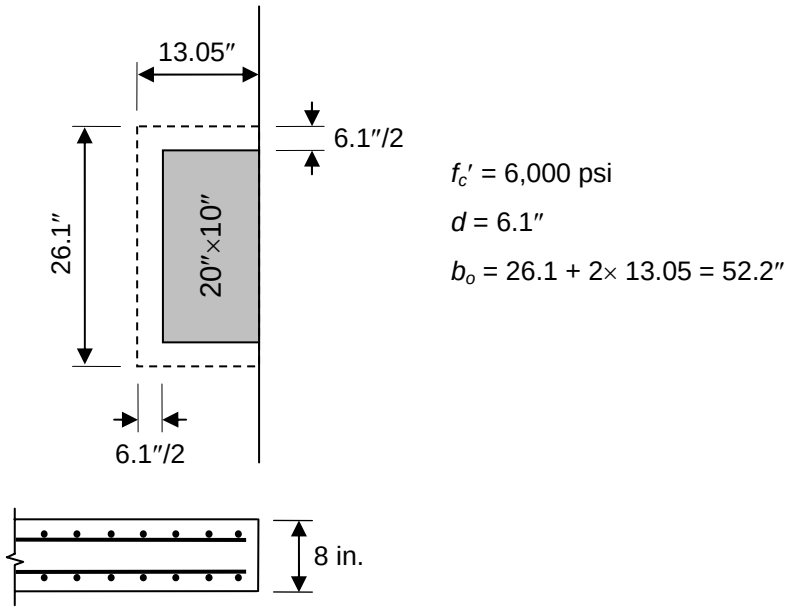

Figure A.2 Punching shear strength of UTSE detail: Eccentric shear model

A.2.1 Nominal punching-shear strength (v_c)

Based on the parameters shown in Figure A.2, the nominal punching-shear strength, v_c, can be estimated from Equation A.1:

$$v_c = \min:\left\{\begin{array}{l}(a)\ 4\sqrt{6{,}000} = 310\,\text{psi}\\ (b)\left(2+\frac{4}{2}\right)\sqrt{6{,}000} = 4\sqrt{6{,}000} = 310\,\text{psi}\\ (c)\left(\frac{30\times 6.1}{52.2}+2\right)\sqrt{6{,}000} = 5.5\sqrt{6{,}000} = 426\,\text{psi}\end{array}\right\}$$

$$\therefore v_c = 310\,\text{psi}$$

A.2.2 Punching shear strength (V_u)

The centroid of the shear perimeter, c_{AB}, and the eccentricity of loading, e, can be obtained as shown in Figure A.1.

$$c_{AB} = \frac{\left(10+\frac{6.1}{2}\right)^2}{52.2} = 3.3''$$

$$c_{CD} = 10+\frac{6.1}{2}-3.3 = 9.8''$$

$$e = 9.8-\frac{10}{2} = 4.8''$$

The torsional moment of inertia, J, and the fraction of unbalanced moment transferred by shear, γ_v, can be estimated from Equations A.3 and A.4.

$$J = \frac{6.1\times\left(10+\frac{6.1}{2}\right)^3}{6}+\frac{\left(10+\frac{6.1}{2}\right)\times 6.1^3}{6}+2\times\left(10+\frac{6.1}{2}\right)\times 6.1\times\left[\frac{\left(10+\frac{6.1}{2}\right)}{2}-3.3\right]^2$$

$$+6.1\times(20+6.1)\times 3.3^2 = 6142\,\text{in.}^4$$

$$\gamma_v = 1-\frac{1}{1+\left(\frac{2}{3}\right)\sqrt{\frac{\left(10+\frac{6.1}{2}\right)}{(20+6.1)}}} = 0.32$$

From Equation A.5, the punching shear strength, V_u, can be obtained as follows:

$$V_u = \frac{310\,\text{psi}}{\left(\frac{1}{52.2\,\text{in.}\times 6.1\,\text{in.}}+\frac{0.32\times 4.8\,\text{in.}}{6142\,\text{in.}^4/9.8\,\text{in.}}\right)} = 55.5\,\text{kips}\ ;\ V_{exp} = 77\ \text{kips (Table 6.2)}$$

REFERENCES

1. American Association of State Highway and Transportation Officials (1998), *AASHTO LRFD Bridge Design Specifications, 2nd Edition.*
2. ACI Committee 318 (2002), "Building Code Requirements for Structural Concrete (ACI 318-02) and Commentary (318R-02)," American Concrete Institute, Farmington Hills, Mich., 319 pp.
3. Bazant, Z. and Cao, Z. (1987), "Size Effect in Punching Shear Failure of Slabs," *ACI Structural Journal*, Vol. 84, No. 1, Jan.-Feb., pp. 44-53.
4. Bieschke, L.A. and Klingner, R.E. (1982), "The Effect of Transverse Strand Extensions on the Behavior of Precast Prestressed Panel Bridges," Research Report 303-1F, Center for Transportation Research, The University of Texas at Austin, Austin, Texas, Jun., 106 pp.
5. Buth, E., Furr, H.L., and Jones, H.L. (1972), "Evaluation of a Prestressed Panel, Cast-In-Place Concrete Bridge," Research Report 145-3, Texas Transportation Institute, Texas A&M University, College Station, Texas, Sept., 140 pp.
6. Coselli, (2004), "Behavior of Bridge Decks with Precast Panels at Expansion Joints," Master's Thesis, The University of Texas at Austin, May, 286 pp.
7. Dolan, V. and Frank, K.H. (1994), "Evaluation of Failure in Bridge Expansion Joint Rails," Research Report 1309-1F, Center for Transportation Research, The University of Texas at Austin, Austin, Texas, Oct., 38 pp.
8. Fang, I., Tsui, C., Burns, N., and Klingner, R. (1990), "Fatigue Behavior of Cast-In-Place and Precast Panel Bridge Decks with Isotropic Reinforcement," *PCI Journal*, Vol. 35, No. 3, May-Jun., pp. 28-39.
9. Fang, I., Tsui, C., Burns, N., and Klingner, R. (1990), "Fatigue Behavior of Cast-In-Place and Precast Panel Bridge Decks with Isotropic Reinforcement," *PCI Journal*, Vol. 35, No. 3, May-Jun., pp. 28-39.
10. Graddy, J., Kim, J., Whitt, J., Burns, N. and Klingner, R. (2002), "Punching-Shear Behavior of Bridge Decks under Fatigue Loading," *ACI Structural Journal*, Vol. 99, No. 3, May-Jun., pp. 257-266.
11. Griffith, E. (2003), "Behavior of Bridge Slab Ends at Expansion Joints," Master's Thesis, The University of Texas at Austin, Dec., 282 pp.
12. Ryan, J. (2003), "Zero-skew Bridge Deck Behavior at Expansion Joints," Master's Thesis, The University of Texas at Austin, Texas, Aug., 319 pp.
13. MacGregor, J.G. (1997), "Reinforced Concrete – Mechanics and Design," 3rd Edition, Prentice Hall, 939 pp.